*Journal of Structural Dynamics*, 1, (pp. 49-137) 2021
Contact Modeling Across Scales: From Materials to Structural Dynamics Applications

Journal of Structural Dynamics

# Contact Modeling Across Scales: From Materials to Structural Dynamics Applications

M. R. W. Brake *

*William Marsh Rice University, 6100 Main St., Houston, TX 77005, USA*

## Abstract

The study of contact is an engineering pursuit that spans multiple disciplines and scales. Structural dynamics, as well as aspects of nonlinear dynamics and vibrations, is concerned with contact in systems at the macroscale. At the microscale, tribology is concerned with the evolution of two surfaces in contact in terms of frictional and wear behavior. Between these two scales, solid mechanics investigates the development of stresses within two bodies due to contact through elasticity and plasticity solutions (amongst other methods). Lastly, contact research within material science investigates the interaction of grains and the evolution of a material's structure due to impact and other damaging events. These four fields, structural dynamics, solid mechanics, tribology, and material science, are traditionally separate even though they are each concerned with interfaces and the contact of two bodies. By integrating all four fields, new opportunities for advancing the understanding of contact emerge. In this paper, open challenges and potential paths forward for future directions in contact-based research is discussed.

**Keywords:** Review; Contact; Impact; Nanoindentation; Multi-Scale; Structural Dynamics; Tribology; Tribomechadynamics; Materials; Mechanics

*Received on June 25, 2021, Accepted on November 29, 2021, Published on December 13, 2021*

This paper is dedicated to the memory of Ilinca Stanciulescu, 1972-2021.

*brake@rice.edu

# Contents

# 1 Introduction

Contact mechanics has far reaching applications across multiple industries and length scales. At the nanoscale, the study of contact mechanics has led to new understandings of plasticity and hardness [1, 2, 3, 4, 5], crack nucleation [6, 7], and how to design a material's structure (including coatings) to be more resistant to damage [8, 9, 10, 11]. By contrast, at the macroscale, contact mechanics is used to predict the forces and stresses associated with contact [12, 13, 14, 15, 16, 17, 18, 19, 20, 21, 22, 23] and impact events [24, 25], including constitutive modeling approaches for structural dynamics applications [26, 27, 28, 29, 30, 31] for both industrial applications [32, 33, 34, 35, 36, 37, 38], robotics [39, 40, 41], biological applications [42, 43, 44, 45, 46], and design applications [47, 48, 49]. Thus, while contact research spans many length scales, the ultimate questions are the same: how does a material or structure respond to contact – in terms of dynamics, damage, and failure. To fully answer this question, though, it is necessary to have an understanding of how contact mechanics at one length scale affects the response of the material or structure at a different length scale.

One impediment to bridging these length scales successfully has been the seemingly disparate set of skills required to understand the context in which contact mechanics research is conducted at each scale. For example, from the nano- to macroscale, the terminology, experimental techniques, solution methods, and output metrics change dramatically. Even within one of these length scales, the research communities can be disjoint. As an example, consider macroscale research on the contact within jointed structures: there are (at least) two different subcommunities – solid mechanics and structural dynamics. From the solid mechanics perspective, researchers are concerned with stress states, predictions of failure, and use static or quasi-static solution techniques [50, 51, 13, 52]. Structural dynamics, by contrast, is concerned with predicting natural frequencies, frequency or time domain response to shock and vibration, and use time integration schemes [53, 54, 26], frequency domain solvers (such as the harmonic balance technique) [55, 56, 57, 58, 59], and quasi-static modal analysis methods [60, 61, 62, 63]. While these two communities typically do not collaborate, both are necessary for advancing the understanding of joint mechanics. Further, this paper argues that by ignoring the research of one of these communities, the design solutions from the other community will prematurely fail. As an example, in the solid mechanics community, interfaces for aeroturbines were traditionally designed to exhibit minimal relative motion, as any amount of slip can lead to wear and failure. However, this results in structures that are significantly under-damped, resulting in large amplitude vibration that causes fatigue failure sooner than expected.

The premise of this paper is that a mutual understanding of terminology, techniques, and perspectives will facilitate the bridging of scales in order to make meaningful predictions of a structure's response (including wear) using principles based on the physics of the nanoscale and tribological interactions. This paper originated in a discussion of open challenges in the area of contact mechanics following a workshop held in May, 2017 at Rice University. The workshop was organized around three principle themes: nanoscale research in contact mechanics, multiscale research in contact mechanics and tribology, and macroscale research in contact mechanics and dynamics. The workshop brought researchers from three traditionally separate but related fields together for two days to discuss recent progress at each of the three scales embodied by the themes as well as to discuss potential paths forward for future directions in contact-based research. In what follows, this paper first presents overviews of recent research at the nanoscale (§2), at the mesoscale (§3), and at the macroscale (§4), and highlights active areas for collaboration to simultaneously advance all three areas.

# 2 Nanoscale Research in Contact Mechanics

In the context of this paper, nanoscale research in contact mechanics spans material science and elements of tribology[1]. The fundamental tool for studying contact at these scales is nano-indentation [1, 2, 4], though other approaches have been used too, such as atomic force microscopy (AFM) [64, 65], in situ scanning electron microscope (SEM) indentation tools [66, 67], and the laser induced projectile impact test (LIPIT) [68, 69] amongst other methods [70, 71]. In general, many nanoscale measurement techniques study contact in a regime (i.e., 10s of nN [72]) where adhesion has significant contributions to the contact behavior [73, 74, 75, 76]. For instance, for a 1 $\mu$m radius nanoindentation tip pressed against a smooth plane, the regime in which indentation is controlled by adhesive forces is below 1 $\mu$N [77] (for an adhesion energy relevant to micro electro-mechanical systems (MEMS)). Further, the effect of adhesion is greater in compliant materials (i.e., those with a low elastic modulus) than those with a high elastic modulus [78, 79]. In macroscale applications (e.g., in bolted joints where the contact forces can be in the kN range [80, 81]), adhesion is viewed as, at most, a modification to the pressure distribution due to contact, resulting in larger

[1] This could, of course, be broadly thought of as including other fields such as applied physics too.

contact areas, higher yield stresses, and lower contact stiffnesses [82, 83]. In what follows, the discussion of adhesion is expanded in §3; however, it is assumed that in structural applications adhesion is not a significant portion of the contact characteristics.

## 2.1 Nano-Indentation

Nanoindentation measurement techniques, as described by Oliver and Pharr, 1992 [1], continuously measure the load-displacement behavior of an indenter being pressed against a material specimen. The key advance introduced by [1] was a new analytical approach to measure the material characteristics based on the force-displacement data from indenting then unloading a sample, which did not need to image the resulting impression in the sample. The material properties are calculated from the unloading data, which behaves elastically and is fit to a power law relation. This technique, thus, provides several key sets of data: the load-displacement curve, the elastic modulus, the material hardness, and the contact area. Nanoindentation techniques have been improved in multiple ways over the last thirty years [2, 4, 84, 85], but the essential aspects of the technique remains the same.

In Oliver and Pharr, 1992 [1], the preferred test method was to indent a sample to a peak load, unload to 10% of the peak load, then to repeat this procedure a total of three times before loading to the peak load, holding it constant for several minutes, then unloading. This procedure addressed several challenges. First, the process of holding the load constant at the peak load for several minutes allows for any time dependent deformations to occur such that the unloading portion of the test is purely elastic and has (hopefully) negligible time dependent components. Thermal drift (i.e., small fluctuations in temperature that cause the instrument components to expand, which is of particular concern for very small displacement measurements) is then assessed by holding the indentation at the point of being 90% unloaded; this lower load and contact pressure helps to assure that any time dependence in the material response is due to thermal drift and not creep or other inelastic recovery mechanisms. Second, by loading and unloading multiple times, the response during the final unloading is (mostly) elastic as time-dependent plastic effects have had a chance to diminish. This method has since been improved as the continuous stiffness measurement technique [2, 85]. In order to calculate the elastic properties of a material accurately, without errors associated with plastic deformations, the continuous stiffness measurement technique superimposes an oscillation onto the indentation profile. In this manner, the contact is continuously alternating between loading and unloading as the indentation depth is increased, allowing for many measurements of the elastic properties at multiple indentation depths. Errors due to plasticity during continuous stiffness measurement indentations can be minimized by keeping a fixed ratio of the alternating load to the mean applied load during indentation [85, 86, 87].

Common types of indenters for nanoindentation include both spherical and, more widely used, a pyramidal indenter known as a Berkovich indenter [88]. The Berkovich indenter is a geometrically self-similar three-sided pyramid that has a similar area to depth function as the Vickers indenter (see [89] for a discussion of indenter geometries). The profile of the Berkovich indenter is relatively blunt, with an included angle of 142.3 degrees (i.e., between an edge and the opposite face), and is relatively easy to machine to a sharp edge due to its three sides. Thus, it is often preferred for nanoindentation tests. The different indenter geometries do result in different measurements (and predictions) of force-displacement relationships. As the indenter radius transitions from a sharp Berkovich indenter (which could be approximated as a sphere with a small radius, such as of 5 nm) to a sphere with a much larger radius, the measurements become more stiff [90]. From the Hertz model for elastic contact [91, 21], this makes sense as the contact force $F$ is related to indentation depth $\delta$ via

$$F = \frac{4}{3} E^* \sqrt{r^*} \delta^{3/2}. \tag{1}$$

The effective modulus $E^*$ and radius $r^*$ are given by

$$E^* = \left( \frac{1-\nu_1^2}{E_1} + \frac{1-\nu_2^2}{E_2} \right)^{-1} \tag{2}$$

$$r^* = \left( \frac{1}{r_1} + \frac{1}{r_2} \right)^{-1}, \tag{3}$$

where subscripts indicate properties belonging to one of the two objects in contact, and $\nu$ is Poisson's ratio.

## 2.2 Hardness

The fundamental measurement of nanoindentation is the load-displacement curve for a given specimen-indenter pair. From this load-displacement curve (an example of which is shown in Fig. 1 for copper indented with a Berkovich indenter), both the elastic and plastic properties of a specimen can be calculated [4]. In particular, plasticity is often described in terms of the yield strength and the hardness of a material. There are many definitions for hardness [89] (e.g., Brinell, Vickers, Rockwell, Knoop, etc., which can be related through hardness conversion tables [92]), but here the definition for hardness commonly used throughout the nanoindentation community is used [4]

$$H = \frac{P}{A}. \tag{4}$$

Hardness, $H$, is defined in terms of the load from an indentation experiment, $P$, and the projected contact area, $A$, at that load. The total contact area measured from the residual indentation (which is commonly used for hardness measurements at larger length scales, such as by the Vickers hardness measurement) is different than $A$, which is calculated at the maximum load by means of a precise measurement of the indenter shape and is a projection of the indenter into the initial, flat surface. This difference between the total contact area and the projected contact area is most pronounced for materials with small values of $E/H$ [93, 4]. For materials with large values of $E/H$, this effect is reduced. Thus, one crucial aspect of nanoindentation is the characterization of the indenter itself. As the tip of the indenter can blunt, deviations from the ideal geometry of the indenter can result in errors in the estimation of the contact area at low loads. Thus, $H$ is more reliably measured at (relatively) large loads[2]. From the continuum mechanics perspective (as embodied in the definition of Eq. 4), $H$ is independent of length scale, but 70 years of research on size-scale effects on $H$ indicate that $H$ is significantly dependent upon the depth of the indentation [94].

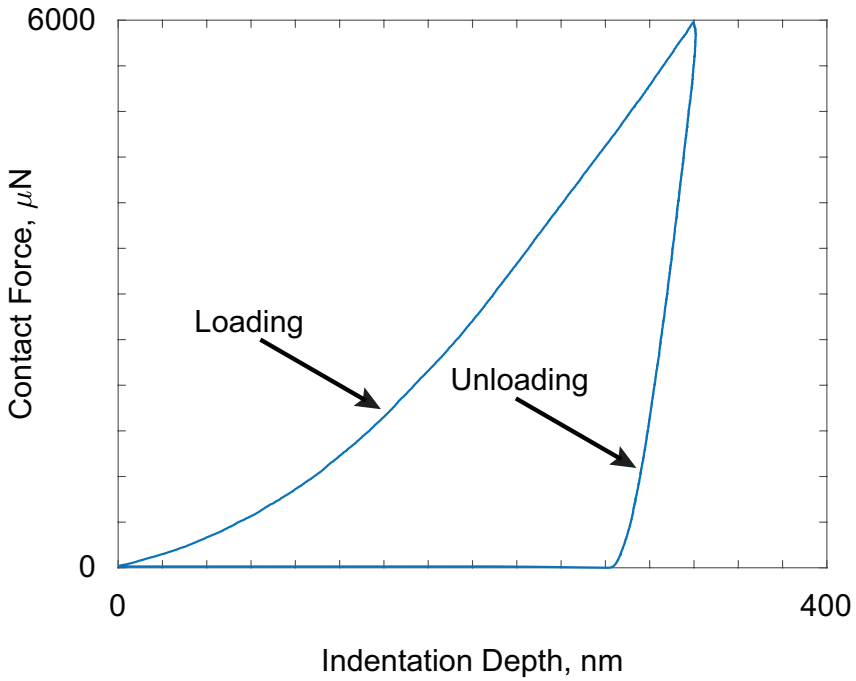


**Fig. 1:** Examples of a nanoindentation measurement.

In theory, hardness should be a characteristic that describes the plastic properties of a material. The concept behind Eq. 4 is that once a material has been loaded such that its response is fully plastic, the average contact pressure under the indenter is constant. Thus, hardness should be constant above a critical load threshold that indicates that a fully plastic response has been achieved [95]. In practice, though, this is not the case as materials harden and the measurements convolute both plastic and elastic responses. In particular, Eq. 4 is sometimes referred to as the Martens, or universal hardness, as it characterizes materials that exhibit combined elastic and plastic deformation [96]. Consequently, as the hardness of a material is dependent upon the load, indentation depth, indenter

[2] A relatively large load for a nanoindenter may be, for instance, in the mN range.

geometry, and indenter material, there are several open questions related to describing hardness and plasticity relating to scale and indenter geometry. Specifically, an open challenge in the research community is:

> **Challenge 1**: How does the hardness measured at one scale with a specific geometry relate to the hardness measured at a different scale and/or geometry?

The origins of hardness, and other plastic properties of a material, lay in the material structure [97]. Most metals are polycrystalline (i.e., composed of many crystals, or grains). Thus, at small length scales, the material exhibits a high degree of inhomogeneity as each crystal (grain) can have its own orientation, size, and imperfections. As discussed further in §2.3.1, the size of a grain is strongly related to its hardness and yield strength [98, 99] (which, in turn, affect the stiffness of an interface), among other properties such as those related to corrosion [100]. Typically, due to manufacturing processes or surface polishing, the grains near a surface are smaller than the grains within the bulk of the material. Consequently, the hardness and material strength vary throughout a specimen. The fabrication of structures with a consistent, nanocrystalline grain size throughout is still an open challenge within materials science [101, 102, 99, 103].

There has been some success in developing a scaling relationship for hardness measurements, particularly [104, 105]. In [104], a model for $H$ as a function of depth, $\delta$, is proposed

$$\frac{H}{H_\infty} = \sqrt{1 + \frac{\delta^*}{\delta}}. \tag{5}$$

In the limit of an infinitely deep indentation, hardness is bound by $H_\infty$. The dependency of $H$ on the depth of indentation is captured in the characteristic depth of penetration $\delta^*$, which is a property of the indentation material and is dependent upon the statistically stored dislocation density throughout the material. This model, however, best fits data in the micro-indentation range and significantly over-predicts $H$ in the nano-indentation range [106, 107]. More recent work has extended this modeling concept to nano-indentation [105] by defining multiple length scales to describe both the nano- and micro-regimes.

In [104], Eq. 5 is developed for geometrically self-similar indenters (e.g., the Berkovich indenter). For spherical indentation, indentation scale effects take on a different form [106, 94]. Because spheres are not geometrically self-similar, the indentation scale effects are driven by the sphere's radius. This results in indentation scale effects being present for both nano- and macro-indentation experiments as the strain induced in the material increases with indentation depth, thus increasing the hardness due to work hardening[3] [94]. Consequently, as the radius of the spherical indenter is reduced, the hardness of the material is observed to increase.

Complicating the comparison of hardness across scales is the fact that the definition of hardness used at different scales is often incompatible. While Eq. 4 treats $H$ as a continuum property that is scale independent, the macro-indentation tests convolute multiple scale dependent issues [108, 89]. For instance, Brinell hardness is defined as the peak load divided by the residual surface contact area, $A_r$. The Meyer's hardness test, much like the continuum definition of hardness, uses the projected contact area for a given load. One notable difference between these tests and the nanoindentation tests is that both the Meyer's hardness test and Brinell hardness test assume a spherical indenter. For Meyer's hardness, the indentation shape function is empirically determined, which results in the Meyer's strain hardening exponent $n$ [89, 109]. By contrast, the definition of Rockwell hardness is based on the difference of deformations ($\Delta\delta$) at two different loads, based on the concepts of [110]. Depending on which Rockwell test is used, the indenter is either a sphere or the Brale indenter [89], which is a cone truncated by a small sphere. For many of the hardness scales described in Table 1, the hardness measurement is conducted at a fixed load (e.g., 3000 kgf for the standard Brinell hardness test[4]), and the contact area is estimated with varying degrees of precision. For a more extensive list and discussion of hardness scales, refer to [89].

To illustrate some of these differences, Fig. 2 shows hardness values measured at the nanoscale for annealed oxygen-free copper using a Berkovich indenter [116, 117]. As the indentation depth varies from 1 nm to 300 nm, the hardness reduces from approximately 1000 GPa to 2 GPa. At even larger scales, Berkovich indentations of a similar species of annealed, oxygen-free copper yielded hardness values of 1.25 GPa for indentations of 200 nm

[3] One difference between the communities that study the mechanics of materials and the communities that study nonlinear dynamics is the use of 'hardening'. In mechanics, hardening is used to refer to as the ability of a material to support greater stresses after yielding (as opposed to an elastic, perfectly plastic material that cannot support stresses greater than the yield stress). In the nonlinear dynamics community, on the other hand, hardening is used to refer to a system that stiffens with increases in excitation, and is most commonly associated with the system's frequency response function. Throughout the rest of this text, hardening will refer to the plastic behavior of a system, and not the term used throughout nonlinear dynamics to mean increases in stiffness in the frequency response function.

[4] While kgf is a non-standard unit, it is the units used by the Brinell hardness test. To convert to a standard SI quantity, multiply by gravity to calculate the corresponding force in N.

| Name | Definition | Geometry |
|---|---|---|
| Universal (Eq. 4) | $P/A$ | Spherical or Pyramidal typically |
| Brinell [111, 112] | $P/A_r$ | Spherical |
| Knoop [113] | $P/A$ | Rhombic Pyramidal |
| Meyers [109] | $P/A$ | Spherical |
| Rockwell [114, 89] | $N - 500\Delta\delta$ | Spherical ($N = 130$) or Brale ($N = 100$) |
| Vickers [115] | $P/A_r$ | Pyramidal |

**Table 1:** Summary of several of the definitions of hardness from measurements. Note that $A$ refers to the projected contact area, $A_r$ refers to the residual surface contact area, and $\Delta\delta$ is the difference in deformation at two different prescribed loads.

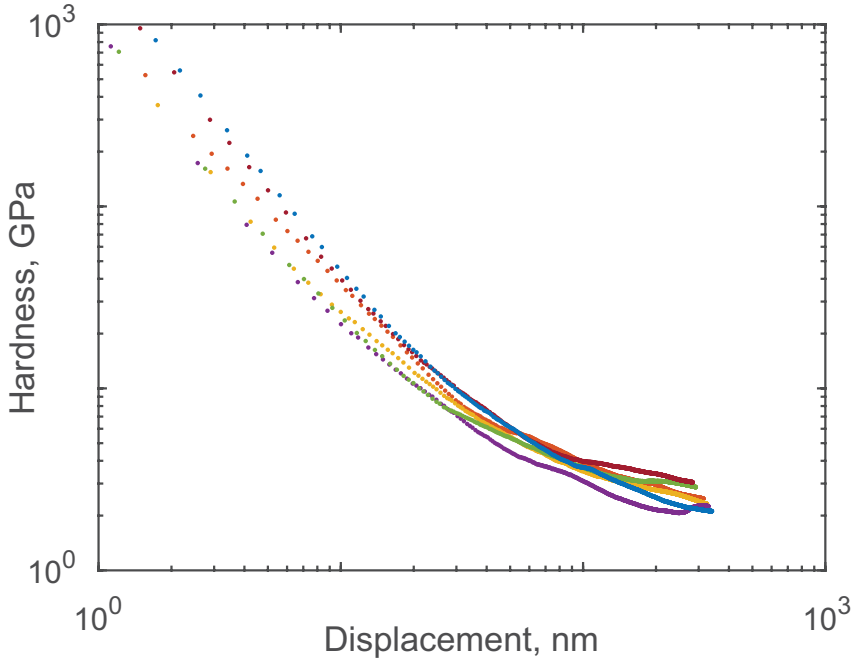


**Fig. 2:** Hardness values from nano-indentation measurements of annealed, oxygen-free copper using a Berkovich indenter [116, 117]. Each color represents a different repetition of the same measurement.

that reduced further to 0.7 GPa for 3 μm indentations. At the same time, indentations via a Vickers indenter yielded hardnesses of 0.5 GPa at displacements as large as 14 μm [118]. Thus, there is a strong scale dependency for hardness as the plastic zone of indentation grows [119, 120].

In comparing nano-indentation measurements with microhardness measurements, deviations of up to 40% in measured values of hardness at the same load are observed across a range of metals [121]. For spherical indentations, measurements of hardness show lower values for small indentations as compared to moderate indentations (e.g., indentations of 10s of nm compared to 100s of μm) due to the lack of geometric self-similarity of the spherical indenter, then decrease again for even larger indentations, which is supported by high fidelity finite element modeling of indentation [122, 123, 124]. These measurements of hardness are complicated by both scale dependent issues as well as material dependent issues. For larger indenters (specifically spheres), more of the material response under the sphere is elastic than plastic, as compared to an indentation at the same load by a smaller sphere due to the influence of contact radius on contact pressure (i.e., Eq. 1). The measured hardness is also sensitive to the method in which the contact area is measured and the discrepancy between projected contact area and total contact area. For instance, the projected contact area at a peak load can yield one hardness value; if, instead, the measured residual contact area is used, then this will result in a different hardness value. For an entirely elastic contact, the residual contact area is zero, which yields an infinite hardness if the residual contact area is used. Thus, while measurements of hardness from the same experimental technique are useful in comparing the plastic properties of materials, a more fundamental understanding is needed to compare hardness across scales and geometries adequately. From a

structural dynamics perspective, hardness is important as it is directly related to wear resistance. Depending on the nanostructure of the material, wear resistance can improve linearly or super-linearly with hardness [125, 126, 127], which is discussed further in §3.3.

## 2.3 The Evolution of Nanostructures

To better understand hardness and the plastic deformation of materials, much of the recent nanoscale research has focused on understanding how the nanostructure of a material changes in response to deformation. In particular, this field has been driven by efforts to find extremely hard materials (i.e., with hardness similar to or greater than that of diamond) [128, 129, 96, 130] for use in contact and wear protection applications, such as machining, manufacturing, drilling, and jet turbines [131]. As an aside, note that from a tribological perspective, simply optimizing the hardness of a material is insufficient for wear applications as optimal materials are able to either self-lubricate or have extremely low frictional properties [132]. That is, hardening one surface is a wear mitigation strategy that is best employed when only one surface needs to be protected; if, on the other hand, all surfaces in a tribosystem need to be protected from wear, then the prevailing strategies are to mitigate wear by either reducing the coefficient of friction, or by exploiting the tribochemistry of surface interactions to establish a self-lubricating tribolayer[5].

Before discussing the nanostructure of a material, it is important to highlight the difference between the nanoscale view of a material and the view of a material from a tribological or higher scale. At higher length scales (i.e., some tribology research, contact mechanics, and dynamics), the material is viewed from the continuum perspective - that is, it is homogeneous. In actuality, though, the material is polycrystalline (usually), which results in a heterogeneous material structure. For fine grained materials, this heterogeneity is clearly evident at the nanoscale, particularly near surfaces. This heterogeneity (i.e., in terms of grain size, lattice structure and orientation, dislocation density, and defects) can lead to dramatically different local properties[6] [138, 139] that are difficult to characterize due to the size scale of the structures (even coarse-grained polycrystalline materials are difficult to fully characterize, thus nanocrystalline materials present a significantly greater challenge) [140].

### 2.3.1 Dislocations and the Hall-Petch Effect

There are multiple competing mechanisms that interact to change the nanostructure of a material during indentation. Rather than discussing in depth the nanoscale material science research, such as reviewed in [141, 142, 139, 98, 143, 144, 99], several specific properties and phenomena are discussed here, specifically in light of their ramifications for constitutive properties observed at larger scales.

When a material is deformed, one of the lowest energy means of achieving the plastic deformation (from the perspective of the material scale) is through a dislocation, or movement of one set of atoms relative to another at a low stress level. In indentation experiments, two types of dislocations are observed: geometrically necessary dislocations that must be present near an indentation to accommodate the material being displaced, and the statistically stored dislocations throughout a material (i.e., internal to a grain) that result from uniform straining of a material resulting in a hardening behavior [94]. Dislocations that accumulate at a grain boundary can result in the grain breaking into two separate grains if the dislocation energy is sufficiently high enough to generate a new dislocation path; however, for smaller grain sizes the energy for dislocations to move along the grain boundary is significantly lower than to generate a new dislocation path [142]. As the grain size of a material becomes larger, the strength of the material typically decreases as the stress necessary to move a dislocation across a grain boundary is decreased (in a simpler view of it, having smaller grains means that there are more boundaries relative to the volume of the grains for dislocations to accumulate at, which results in a larger stress being necessary to cause the material to yield). This concept of increasing the yield strength, $\sigma_y$, of a material by reducing the grain size, $d$, is referred to as the Hall-Petch effect [145, 146, 139], which in its simplest form is described as

$$\sigma_y = \sigma_\infty + kd^{-n},$$

and is based on the yield stress of a single crystal, $\sigma_\infty$, and a constant, $k$, with the exponent $0.3 \leq n \leq 0.7$ [145, 147]. At grain sizes below (approximately) 10 nm, the Hall-Petch effect is limited by the dominant mode of deformation becoming the sliding of grain boundaries relative to each other instead of dislocations accumulating along a grain

[5] As an example of a wear mitigation strategy in engines, zinc dialkyl-dithiophosphate (ZDDP) is a common additive for lubrication that grows a protective, wear resistant tribofilm on the surface of contacting components [133, 134, 135, 136, 137].

[6] Both different from other grains as well as from the bulk material properties.

boundary [148][7]. The critical grain boundary size is typically where the maximum yield strength of a material occurs [145], as illustrated in Fig. 3. The Hall-Petch effect also applies to the hardness of a material. The reason for this can be observed in the empirical model of hardness observed by Tabor [150], in which hardness is related to the yield strength as $H = 2.8\sigma_y$[8]. Physically, as the grain size is reduced towards the critical limit, hardness increases due to a decrease in the number of dislocations that occur in pile-ups at grain boundaries [151]. From the definition of hardness, (4), hardness is the load that a plastically deformed material is able to support. Thus, it is directly related to the yield strength of the material as the yield stress is the stress at which plastic deformation initiates. The phenomenon of work hardening results from an accumulation of dislocations such that their corresponding strain field begins to overlap. As a result, the material develops a resistance to the formation of new dislocations, and thus increases the yield strength of a work hardened material [102].

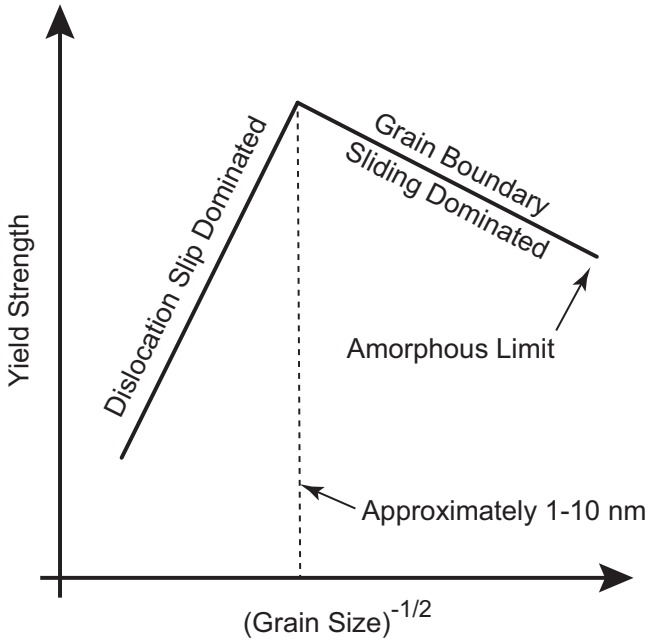


**Fig. 3:** Illustration of the Hall-Petch effect.

Through the processes of heat treatment or wear (either intentional via processes such as friction stir welding [152], or unavoidably through the designed use of a surface), the size of grains change [153]. For materials with very fine grains (e.g., 1-5 nm in size), wear can cause grains to grow [154, 155, 156]. This results in a hardening of the material (as the grain size is increased towards the optimal size for the Hall-Petch effect), and an apparent breakdown of Archard's wear model [154, 157, 158][9]. This change in grain size is not driven by localized heating, but rather through plasticity. Conversely, for materials with large grains (e.g., 100-1000 nm), wear can lead to a refinement of the grain sizes [159, 160].

For both coarse and fine grained surfaces, when the structure of the material near the surface evolves to be (or persists as) a thin layer of very fine grains (below 10 nm), the coefficient of friction tends to be lower than if the surface evolves to have a very thick region of small grains (which can lead to an increase in friction due to delamination of the grains) [159, 155]. Physically, this phenomenon is due to surfaces with very fine grain structures having plastic processes that are dominated by grain boundary-mediated plasticity [155, 161]. Because the grains are small enough such that the ratio of surface area to volume becomes large, the grains slide and rotate relative to each other rather than accumulating dislocations along the boundary [162].

If the initial grain size is above a critical threshold, then the grain structure is thought to coarsen, and the coefficient of friction increases, due to plasticity being driven by dislocations primarily [155]. This implies that there is a relationship between yield strength and frictional behavior as well since the yield strength is directly related to the

[7] This is termed the inverse Hall-Petch effect, which has found mixed support in experiments. One explanation for the mixed support is due to the role of grain-boundary relaxation [5], and another explanation attributes it to the emergence of inhomogeneous flow at grain sizes below the critical limit [149].

[8] Implicit in this model is the assumption that the material exhibits little to no work hardening

[9] Archard's wear model is discussed further in §3.3.2

grain size. Thus, a major take-away for structural applications is that the long term frictional behavior of an interface is governed by not just the bulk material properties [153], but also the design of the material's nanostructure [163]. Further, the material's nanostructure, if designed appropriately, can improve wear performance to the point that it outperforms expected limits set by a material's mechanical properties [157].

This consideration of a material's nanostructure and material properties for designing the wear-related performance of a system frames the second open challenge. Often, application engineers and designers are faced with the challenge of determining what materials should be used for an interface. Very often, decisions are made with scant information about the wear and tribological properties of the system, let alone the long term characteristics. One approach to solving this problem would be a series of wear evolution maps that link the wear properties over time with a material's microstructure and the applied loads. This concept of a wear evolution map is similar to Ashby's wear mechanism maps [164], which have elucidated the type of wear that occurs for different species of materials under different loading conditions. A missing link in traditional wear maps is the relationship between the properties detailed in the wear map and the frictional behavior of a system. Additionally, what other parameters drive similar processes (e.g., temperature).

> **Challenge 2**: More, and more accessible wear evolution maps are needed to facilitate designers and application engineers selecting materials and their structure for interfaces.

From a design engineer's perspective, there are many questions related to how to choose a material and surface finish for different applications. Unfortunately, at least in the US, appreciation and engagement of tribology is often an after thought in the design process for most industries (excluding several major industries such as drilling). As a result, the present wear mechanisms maps are not widely known about by design engineers, and are incomplete for the design process. Perhaps one approach to Challenge 2 would be a wear encyclopedia for a given tribosystem to compliment the present handbooks and textbooks that design engineers rely upon (such as Shigley's [80]). This summarized information would need to incorporate data about how both bulk and interfacial grain sizes relate to manufacturing processes, and how the material is expected to wear in different loading regimes and environments. Thus, an entry describing the tribosystem formed by two materials would need to include the manufacturing parameters that a designer can vary (i.e., heat treatment and surface finish), how these relate to the surface and bulk properties, what wear mechanisms (i.e., adhesive wear, abrasive wear, etc.) are dominant in different environments (in terms of load, displacement/velocity, lubrication, etc.), and both what the wear rate might be and how it might evolve due to wear.

### 2.3.2 Designing Interfaces via Coatings

The design and fabrication of engineered nanostructured materials is an active area of research [165, 166, 11]. One approach for customizing the material properties and structure of a surface is through the use of coatings. Due to the small scale nature of nano-indentation, it is well suited for measuring the properties of thin films and coatings, provided that they are smooth[10] [167, 8, 10]. In particular, thermal spray coatings often provide significant resistance to wear and corrosion [168]; however, without sufficient polishing, it is often difficult to measure the hardness of thermal spray coatings by nanoindentation due to their surface roughness. In measuring the mechanical properties of coatings, there are a number of size-dependent effects on mechanical properties [169, 105], though, driven by dislocation mechanisms associated with grain and crystal size [104, 170, 171, 172]. This is partly observable in the stochastic bursts sometimes observed in very small scale nanoindentation measurements [173], which are hypothesized to be due to homogeneous nucleation that initiate dislocations within regions of the grains that were previously devoid of dislocations. From the review [174], this is best explained by indentations at low loads resulting in dislocations along a single slip system; as the load is increased, however, dislocations become constrained as multiple slip systems begin to participate, until the increasing number of dislocations begin to reform in low-energy configurations (e.g., recrystallization). This results in the hardness value first increasing (for very small loads), then decreasing until an asymptotic limit is reached [175, 176, 177]. In the search for superhard materials that are even harder than diamond, researchers make use of the Hall-Petch effect in which decreasing the size of crystals (down to approximately 1 to 10 nm) in a randomly oriented polycrystalline material increases the hardness [178]. Consequently, as the thickness of a nanostructured coating is decreased, the hardness increases [179].

There are multiple challenges in selecting or designing coatings for macroscale applications, which stem from both an incomplete understanding of the physics of contact as well as having accessible tools readily available for

[10] For surfaces with relatively large roughness values, topological variations in the surface can significantly change the measured response curves as the indenter tip could be contacting the top of an asperity, the valley between two asperities, or the edge of an asperity.

designers. In particular, due to the uncertainty introduced with bonding a coating to a substrate, one source of challenges stem from the interaction between coatings and substrates. If a coating's elastic properties are significantly different from the substrate's, then this can restrict the practical utility of a coating and lead to degraded performance [8]. This challenge is further exacerbated when considering lubrication, conductivity, or other environmental effects. Thus, an open challenge is how to select the right coating for a specific application:

> **Challenge 3**: When considering the properties of a substrate, what are the optimal properties for a coating for a given application and environment?

### 2.3.3 Fracture Toughness

In the two previous sections, the properties of a material observed in nanoindentation experiments have been driven by dislocation and grain boundary-mediated plasticity. These two phenomena have been directly related to a material's yield strength and hardness. A third property describing the plastic behavior of a material that is observed in nanoindentation experiments is its fracture toughness, which is particularly relevant for brittle materials [180, 181, 182] as it describes the plastic behavior at a crack tip. It is common to observe radial cracks in nanoindentation experiments of brittle materials. Based on [183] and subsequent work (such as [180]), the fracture toughness, $K_c$, is experimentally measured from indentation experiments in terms of the observed crack lengths, $c$, (shown in Fig. 4) via

$$K_c = \alpha \left(\frac{E}{H}\right)^{1/2} \left(\frac{P}{c^{3/2}}\right), \tag{6}$$

in terms of the elastic modulus, $E$, and hardness, $H$, for a given load, $P$, with the empirical coefficient, $\alpha$, specific to the indenter geometry (e.g., for the Vickers indenter, $\alpha \approx 0.016$) [180]. Above a critical threshold of approximately $E/H = 30$, the Lawn-Evans-Marshall model (Eq. 6) breaks down, and the fracture toughness is better characterized by the Palmqvist model [184]

$$K_c = C(\nu)\frac{P}{c^{3/2}}, \tag{7}$$

where $C(\nu)$ is a fit that is dependent upon Poisson's ratio, $\nu$. The physical difference between the Lawn-Evans-Marshall model and the Palmqvist model is the assumed form of sub-surface cracks (illustrated in Fig. 4). In the Lawn-Evans-Marshall model, subsurface cracks are assumed to be median or 'half-penny' cracks, which resemble a semi-circular shape that is bisected by a crack extending from the indentation tip straight down into the material [180]. These half-penny cracks, as shown in Fig. 4, extend from the edge of one crack tip, across the indentation location, to the extreme edge of the opposite crack tip - that is, they span both the radial cracks on the surface and the indentation location. In the Palmqvist model, on the other hand, subsurface cracks are assumed to extend only underneath the surface radial cracks and not the indentation location. These cracks (referred to as Palmqvist cracks and sometimes as radial cracks [180]) are also semi-circular like the half-penny cracks, as illustrated in Fig. 4, with the defining characteristic being that the Palmqvist cracks do not span the indentation location. One reason why these fits, which are based upon the observed lengths of surface cracks, are successful is that brittle materials during nanoindentation will not contain any sub-surface cracks if there are no surface cracks [185]. Further, due to the nature of nanoindentation, cracking is not due to pre-existing flaws and defects, but rather it is due to the plastic deformation beneath the indenter tip [185][11].

Active challenges still persist in understanding the relationship between fracture toughness and observable quantities in nanoindentation experiments. In particular, three areas stand out: influences of the crack length to the contact size, the influence of Poisson's ratio, and the role of the crack shape, as characterized by $E/H$. Many of these challenges can be addressed numerically through high fidelity cohesive zone modeling [180], but work still remains to implement observations from these simulations into improved experimental practices for deducing $K_c$ as well as $E$ and $H$. As much of the utility of nanoindentation experiments for structural applications is in the characterization of material properties, understanding the fundamental relationship between measurable quantities and the properties that govern the compliance of an interface are paramount.

> **Challenge 4**: What is the fundamental relationship between indentation measurements and the plastic properties of hardness and fracture toughness?

[11] As an interesting aside, models of indentation cracking have shed light on a discrepancy in constitutive relationships between measurements and simulations – by including hydrostatic pressure-based criterion in the yield criterion (such as the Drucker-Prager Cap model), simulations more closely match the unloading portions of measured force-displacement curves [186].

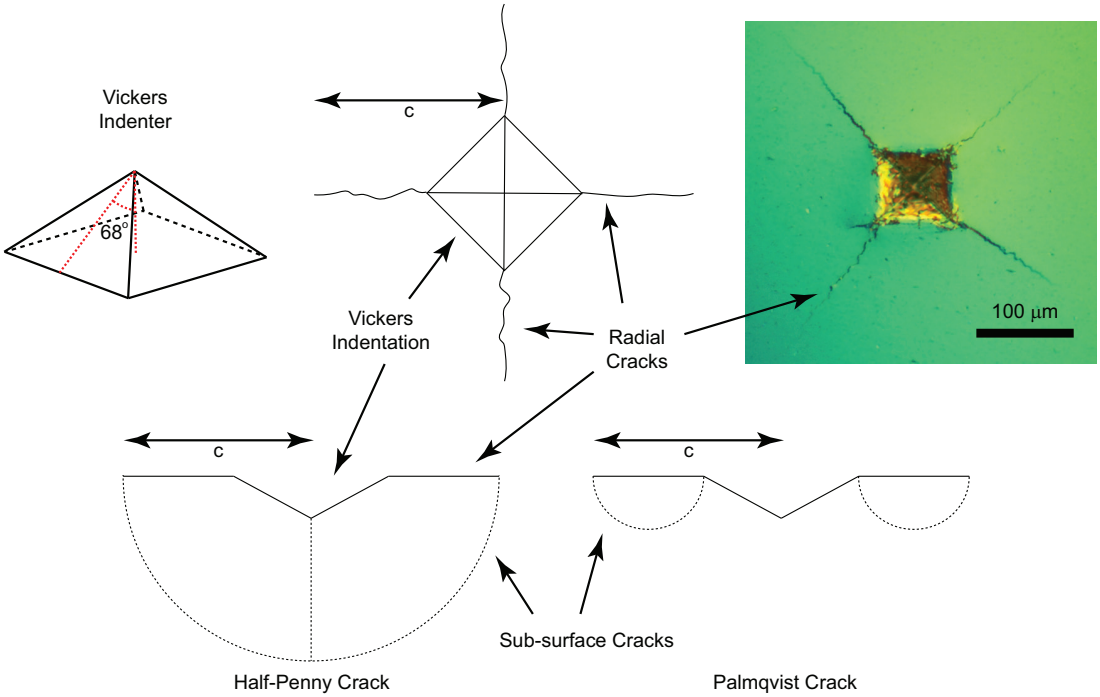


**Fig. 4:** (Left, top) Geometry of a Vickers indenter. (Middle, top) Sketch of an indentation of a Vickers indenter into a brittle material. (Right, top) Image of a nanoindentation of SiC via a Vickers indenter (image courtesy of George Pharr). (Bottom) Illustration of both half-penny and Palmqvist sub-surface cracks.

## 2.4 Frontier Applications within Additive Manufacturing

Understanding the mechanical properties and contact mechanics of conventionally manufactured materials, as discussed in the previous sections, is an ongoing area of research. With the advent of additive manufacturing (AM), many challenges are further exacerbated. For instance, typical metallic parts fabricated via AM have non-ideal material structures – voids, debonding, and sub-optimal grain sizes amongst other challenges. At the same time, the microstructure of additively manufactured metals has unique and, potentially, advantageous properties [187]. Thus, the benefits that the novel material structures and component designs that AM enables far outweigh the disadvantages. Shown in Fig. 5 is the stress-strain curve for two tensile test specimens with identical geometry. One is conventionally fabricated from A356 steel, while the other is fabricated via an AM process using A356 steel and 39% volume 316L steel. The material structure, which can only be achieved through AM, allows for the material to have a significantly higher yield strain before failure. Physically, this is possible due to the material exhibiting multiple microfractures before it fails completely, as the photos of the tested specimen show.

A second area of potential is to change the material structure to significantly alter the damping characteristics of a structure. In [188], the internal structure of a beam structure was modified to increase the damping capacity of the system by a factor of four. As the damping mechanism was due to internal vibration absorbers and not the interface, the system was able to maintain that high level of damping while having an approximately constant stiffness, which is significantly different from most jointed structures and is indicative of reduced interfacial wear.

In the context of contact mechanics, these dramatic changes in material structure will significantly change the properties of the materials and surfaces in contact. Further, the potential for metal composites will require different approaches for modeling materials at a continuum scale. Characterization data from nano-indentation experiments will likely not be relevant for most systems (both due to the poor tribological properties of AM components and the material heterogeneity); however, larger scale indentation experiments may still be able to offer meaningful data. Ultimately, the questions of what are the contact stresses in an AM component and how will an AM component wear must be answered. As can be seen in the materials literature, the answers to the questions are dependent upon both the surface and bulk properties of the material, and thus an understanding of how the material is formed is paramount.

There are many different technologies that compose the category of AM. The fundamental differences in these technologies can result in a diverse set of material structures and properties for the same base material. For

instance, polymer assisted binding (e.g., Binder Jetting) glues powder together into a green body that is later sintered; laser and electron beam-based techniques (e.g., Selective Laser Melting, Electron Beam Melting, and Direct Metal Laser Sintering) melt the powder as part of the printing process, thus requiring no further sintering after the print is finished; and sheet lamination techniques (e.g., Ultrasonic Additive Manufacturing) can preserve a very fine material microstructure as the bonding process is driven by ultrasonic welding instead of melting or glue/sintering. For a review of the different technologies that fall under the category of AM, the reader is referred to [189, 190]. Each of these technologies has its own characteristics and challenges (including issues related to the feedstock as well). For instance, Binder Jetting produces green bodies that typically shrink significantly during the sintering process, making dimensional tolerancing challenging; whereas laser-based techniques can include defects such as pores and inclusions. Further, based on current technologies, an active challenge is ensuring that a part printed on one machine will have the same microstructure and material properties as an identical part printed on the same machine or a different machine using the same technology. There are many (more than 50 for Selective Laser Melting) process parameters that can either be controlled or measured during the AM process that each influence the resulting microstructure of the part [191]. As the material structure is directly related to the yield strength, hardness, friction parameters, and other tribological qualities, this heterogeneity in material structure from part-to-part has significant ramifications for performance [192, 193, 194, 191, 195, 196]. Thus, significant characterization work on the mechanical properties of parts made via different AM technologies is still needed to better understand their tribological and strength properties [197, 198, 199].

> **Challenge 5**: Can additive manufacturing processes be qualified to ensure consistent material properties from one part to another (including across different machines)?

## 2.5 Overarching Challenges and Thematic Issues

As the challenges facing engineering in the 21st century (e.g., hypersonics, space exploration, efficiency to reduce emissions related to global warming) require stronger and lighter materials to be used in extreme environments, these will motivate the advances to come. It could be daunting to think about accounting for the influence of nanoscale features in macroscale simulations. Afterall, if there is such strong dependence on the grain size, how is it possible to conduct design studies for a component that has yet to be fabricated? Fortunately, consistency in manufacturing processes has led to a consistent material structure in fabricated parts. This removes some amount of uncertainty from design; however, it also suggests that material specimens used to deduce the properties of the material being used should be put through as similar of a manufacturing process as the eventual parts as possible in order to maintain a consistent grain structure, heat treatment, and residual stresses from manufacturing. Further, it also suggests that changes in stock material, heat treatment, or manufacturing processes could be intentionally exploited to improve the grain structure of a material, and thus beneficially change its properties. In summary of the discussion

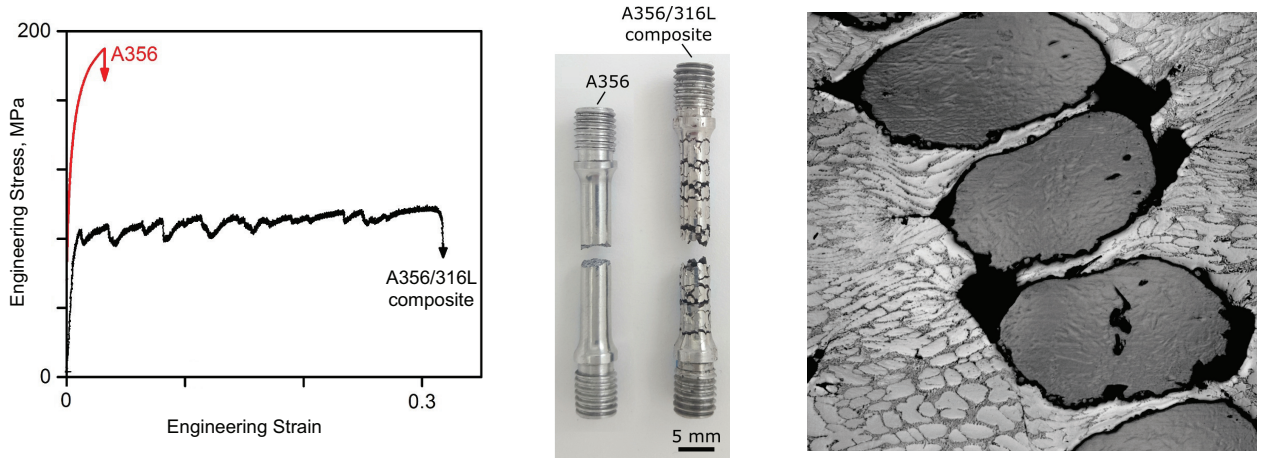


**Fig. 5:** (Left) Stress-strain curve for conventionally manufactured A356 specimen and an additively manufactured A356/316L composite specimen. (Middle) Fractured specimens after testing. (Right) Image of the microstructure of the A356/316L composite. Images courtesy of Zachary Cordero.

of this section, there are several questions that must be addressed in order to overcome the engineering challenges facing society today.

- New insights into hardness are needed that can physically explain the relationship between hardness measured across different scales and different geometries. For instance, how much of the discrepancy is due to statistical variation as compared to variation in grain sizes? Current approaches are somewhat empirical in nature and exhibit a high degree of variability. Further, it is not clear how pertinent a given hardness value is to a new application. Thus, a more fundamental analysis and theory is needed.
- A new generation of Ashby maps is needed [164]. Several open questions exist for how to go about this challenge: what parameters should be considered? How extensive of a round robin should be employed? What distribution of experimental and numerical efforts should be employed? The ramifications on other scales must be assessed too. Protocols must be established to allow for a large scale effort that can successfully blend data from multiple scales and for multiple parameters.
- Grains have been observed to evolve to a stable grain size during repeated wear tests. How does this microstructural evolution affect contact at the macroscale? Does it manifest itself in terms of frictional or plastic behavior that can be controlled? From a macroscale perspective, the smallest feature of interest is the distribution of asperities; thus, how can the gap be bridged to account for the effect of nanoscale features on design and analysis?
- Additive manufacturing will disrupt many aspects of mechanical engineering. The chief question is: how do the microstructures of additively manufactured materials differ from conventional manufacturing techniques? Can the uncertainty in these microstructures be controlled through improved processes? How can multi-material blends be designed and optimized (taking into consideration the voids and debonding that will occur)?

As mentioned throughout, understanding the physics germane to these challenges and moving forward to applying this knowledge to mechanical design is a multi-scale issue: from the material structure itself at the nanoscale to the tribological and contact properties at the mesoscale to the structural performance at the macroscale. In fact, one of the most challenging research goals within the study of contact is connecting the macroscale responses to the physical phenomena at the nanoscale and atomic levels [200].

# 3 Mesoscale Research in Contact Mechanics and Tribology

Tribological research has far reaching applications – coatings or surface texturing to reduce wear and improve frictional performance [132, 201, 202, 203, 204, 205], drilling (both for manufacturing [206, 207] and in oil and gas exploration [208]), artificial joints and other biomedical applications [209, 45, 210, 211], power generation [212, 213, 214, 215], and many other industries that contain moving parts in contact [216]. It is estimated that 23% of the world's energy consumption is due to tribological contacts (of this 23%, it is estimated that 86.5% is due to overcoming friction, and 13.5% is due to replacing worn parts) [217, 218], and that by advancing technologies to improve wear and frictional performance, it would be possible to save 1.39% of the gross world product (estimated as $87.5 trillion in 2019 yielding a savings of $1.22 trillion annually). Many of the challenges that exist, though, rely upon rigid, multibody dynamics modeling of the constituent parts in a system, allowing simulations or measurements to focus purely upon the interface. From a structural dynamics perspective, this approach is oversimplified as the dynamic loading of an interface is strongly influenced by both the support structure surrounding it and the flexible body (i.e., vibration) motion of the system [219, 220, 221].

Tribology research, conceptually, can be divided into four categories: wear and damage, friction, contact forces, and lubrication (e.g., [222, 223, 224]; though the largest of these categories, the lubrication literature is outside of the scope of the present review). In what follows, an overview of contact is first presented, followed by recent research on friction, wear, and some comments on lubrication. As this field has been quite prolific in publications (e.g., there are more than 20,000 publications on modeling rough contact with over 300 papers published per year [225]), the reader is referred to the in-depth reviews of [226, 227, 228, 132, 229, 230, 223, 83, 231] for more information. As well, the subsequent discussion is mainly focused on metals; refer to [232] for considerations related to ceramics or [233] for polymers.

## 3.1 Elastic-Plastic Contact Modeling

The contact between two bodies, whether large, curved surfaces or single, microscopic asperities, is often idealized as contact between two spheres (in the limit of a sphere contacting a semi-infinite plane, this is represented as a sphere in contact with a second sphere that has an infinite radius). As mentioned in §2.1, modern research on the constitutive forces between these two bodies originated with Hertz's stress-based solution [91, 21]. By approximating the two spheres in contact as paraboloids [234, 21, 124], Hertz derived an explicit relationship between the contact force, $F$, and interference (i.e., indentation depth in Fig. 7), $\delta$, which scaled with $\delta^{3/2}$ (see Eq. 1). The assumption that the spheres can be represented as paraboloids is valid for small deformations. In metals, the extent of the elastic response of the material ends (i.e., transitions to an elastic-plastic response) well before this assumption breaks down; for rubber and other elastomers, this assumption becomes invalid for large (but realistic) loads [235, 236, 237, 238, 239, 240]. Corrections for this effect have been recently proposed [241, 124], which have been shown to improve the accuracy of elastic-plastic models even after yield as the elastic portion of the solution is still often based on Hertz's solution.

For other geometries, such as cylindrical contact, there is a lack of available closed-form general solutions. As an example, cylindrical (line-wise) contact can be described by [21]:

$$\delta = \frac{a^2}{2r^*}(2\ln(4r^*/a) - 1), \tag{8}$$

and is defined in terms of the width of the contact patch, $2a$, which depends on the load and out-of-plane stresses, and if the cylinder is tilted or flush with the surface. For instance, under plane strain assumptions for modeling finite geometries,

$$a = \frac{2p_0 r^*}{E^*}. \tag{9}$$

The total contact force, $F$, is found from integrating the contact pressure distribution (with maximum pressure $p_0$) over the entire contact area, which can then be substituted back into Eq. 8 to find an explicit force-displacement relationship. This process, though, requires prescribing values to one of the unknown variables (such as $a$, the shape of the pressure distribution, etc.). Additionally, this relationship also assumes that the contact pressure (and thus deformation) is uniform over the length of the cylinder, resulting in two perfectly aligned cylinders with no relative tilt due to uneven loading. Consequently, general solutions for cylindrical contact, due to end effects, misalignments (including the relative tilt of the cylinders), and other challenges, do not exist.

### 3.1.1 Elliptical Contact

For asperity scale models, the assumption of spherical shapes is commonly employed; however, this assumption is typically invalid. Real surfaces usually have ellipsoidal asperities, and thus need to be characterized in terms of both a major and minor axis [242, 243]. The geometric difference between spherical and ellipsoidal contact significantly changes the stress distribution in the contact patch [244], with the material at the contacting surface being dominated by plasticity at much lower loads for ellipsoidal contact than spherical. This is apparent in the Hertzian model of contact for ellipses [21, 245, 246, 247][12]. For major and minor principal curvatures $\kappa_{ia}$ and $\kappa_{ib}$ on body $i$ with inclination angle $\alpha$, the contact force is modified as [21, 245]

$$F = \frac{4}{3}E^*\sqrt{R_e}\delta^{3/2}f_2^{-3/2}, \tag{10}$$

where the effective radius

$$R_e = \sqrt{R_1 R_2}, \tag{11}$$

is defined in terms of the relative radii via

$$R_1 = \frac{1}{(B+A)-(B-A)} \tag{12}$$

$$R_2 = \frac{1}{(B+A)+(B-A)} \tag{13}$$

$$B + A = \frac{1}{2}(\kappa_{1a} + \kappa_{1b} + \kappa_{2a} + \kappa_{2b}) \tag{14}$$

$$B - A = \frac{1}{2}\left((\kappa_{1a} - \kappa_{1b})^2 + (\kappa_{2a} - \kappa_{2b})^2 + (\kappa_{1a} - \kappa_{1b})(\kappa_{2a} - \kappa_{2b})\cos(2\alpha)\right)^{1/2}, \tag{15}$$

[12] Note that [247] has typos in the definition of the following quantitites.

with $R_1 \geq R_2$. The full solution for the modifying function $f_2$ in Eq. 10 is derived from the elliptical geometry of the contact patch, which has semi-axes $a$ and $b$ (with $a > b$). The eccentricity of the ellipse is defined

$$e = \sqrt{1 - \left(\frac{b}{a}\right)^2}, \tag{16}$$

which leads to the solution for $f_2$ in terms of $e$ as [21]

$$f_2 = \frac{\left(\frac{2e^2}{\pi^2}\right)^{1/3} \mathbf{K}(e)}{\left(\left(\left(\frac{1}{1-e^2}\mathbf{E}(e) - \mathbf{K}(e)\right)\left(\mathbf{K}(e) - \mathbf{E}(e)\right)\right)^{1/2}\right)^{1/3}}. \tag{17}$$

Here, $\mathbf{K}$ and $\mathbf{E}$ are the elliptic integrals of the first and second kind[13]. To complete the formulation, the geometry of the contact patch is related to the eccentricity by

$$\frac{R_1}{R_2} = \frac{\frac{1}{1-e^2}\mathbf{E}(e) - \mathbf{K}(e)}{\mathbf{K}(e) - \mathbf{E}(e)}. \tag{18}$$

These relationships are approximated in [245] via

$$f_2 \approx 1 - \left(\left(\frac{R_1}{R_2}\right)^{0.0684} - 1\right)^{1.531}, \tag{19}$$

and

$$e \approx 1 - \left(\frac{R_2}{R_1}\right)^{4/3}. \tag{20}$$

The asymptotic limits of $f_2$ (Eq. 17) approach 1 for $e = 0$, and 0 for $e = 1$, which results in the Hertzian contact model (Eq. 1) for $e = 0$, and a contact force that increases with $e$. The exact and approximate solutions are further compared in Fig. 6. The effect on the contact force is relatively small for most values of $e$; however, from the definition of Eq. 16, a factor of four difference between the semi-axes (i.e., $a/b = 4$) results in a 10% increase in contact force, and a factor of 23 difference (which is a realistic number for some polishing methods) results in a 50% increase in contact force. Further increasing $a/b$ to 66 results in a force multiplier of 2. For ratios above 100, the relationship between $a/b$ and the force multiplier is approximately linear on a log-log scale.

### 3.1.2 Elastic-Plastic Contact

One limitation in both the Hertzian and elliptical contact model is that they are both for purely elastic contact. Contact of metals, however, rarely is purely elastic. As illustrated in Fig. 7, the purely-elastic regime only spans the first 10-20 nm (depending on the materials involved). Deformations above the yield displacement involve some permanent plastic damage, which is observed upon unloading as the residual plastic deformation (i.e., for a sphere indenting a flat, this would be the depth of the indentation left by the sphere). Due to the path-dependent nature of plasticity, there are no general, closed form solutions based on the stress states of the bodies in contact[14] (such as Hertz's solution for elastic bodies) describing the constitutive relationship for elastic-plastic contact. Instead, recent research into modeling the constitutive relationship for contact between two bodies can be categorized as either finite element analysis (FEA)-based or analytically-based modeling.

Analytically-based modeling for elastic-plastic contact often posits a solution form based on observations of experimental behavior [249, 250, 251, 252, 253, 254, 255, 24]. Often, these models are empirical in nature rather than being based on first principles; however, the first principles-based Hertzian solution is typically used to describe the response before the initiation of plasticity. As a result, these models require simplifying assumptions to describe the constitutive behavior post yield. Due to the wealth of experimental data for large indentations (i.e., involving forces or displacements that are many times greater than the force or displacement necessary for yield), the challenge for developing an analytically-based model is largely associated with modeling the transitionary regime from the

[13]Note that in this set of equations, the argument used in Matlab would be "ellipke($e^2$)" due to inconsistency in how [21] and Matlab define the elliptic integrals.

[14]There are, however, several special cases with closed form solutions, but these rarely are germane to contact mechanics [248].

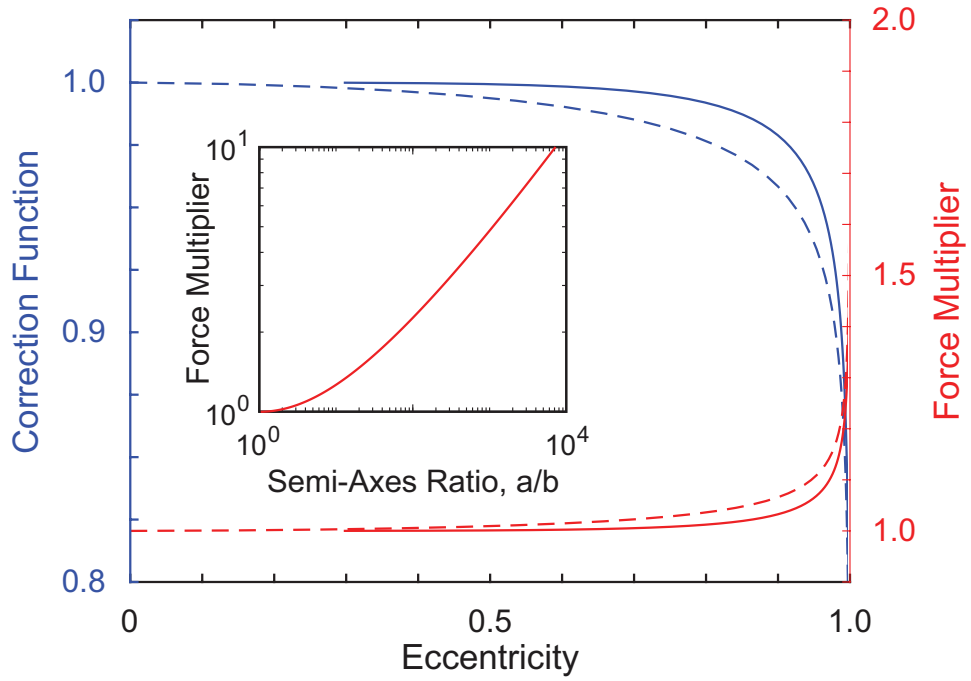


**Fig. 6:** The correction function $f_2$ for elliptical contact (left axis, blue) and its resulting modification of the contact force (right axis, red). Shown are the exact solution [21] from Eq. 17 (solid) and approximate solution [245] from Eq. 19 (dashed). Inset: the force multiplier plotted as a function of the ratio of the semi-axes, $a/b$; note that the axes are log-log.

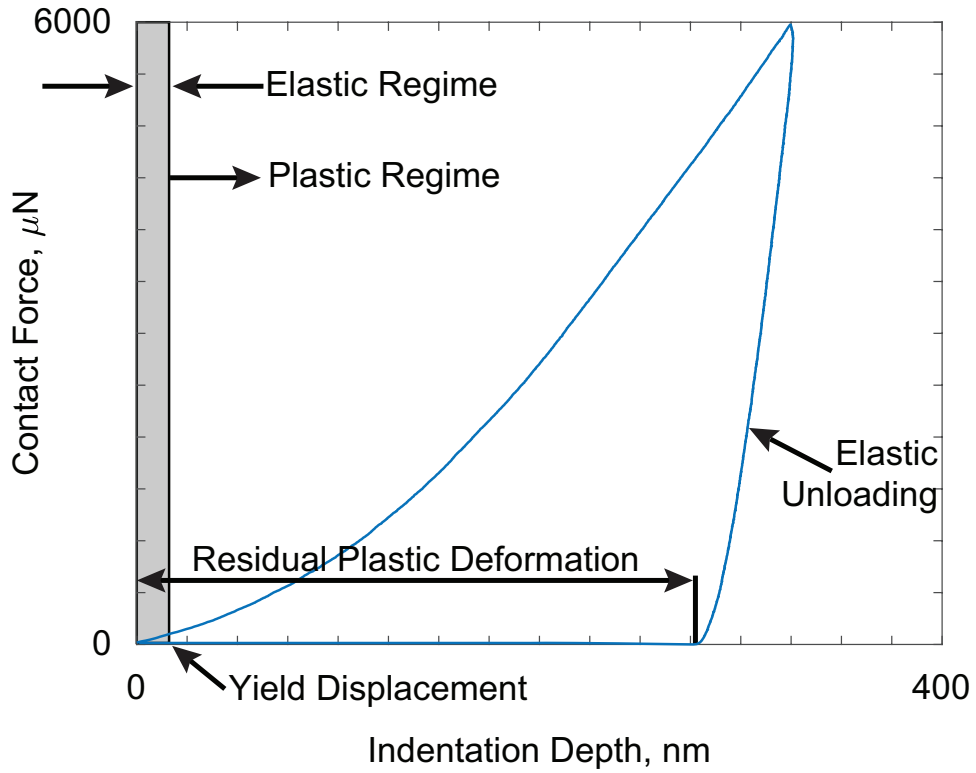


**Fig. 7:** Examples of a nanoindentation measurement, labeled with key features of elastic-plastic indentation.

onset of plasticity to the development of a plasticity-dominated response. After yield is initiated in a pair of contacting specimen, the response is dominated by elasticity at first as most of the material near the point of contact has not yet yielded. Once the plastic zone has expanded to dominate the volume near the point of contact (for at least one of the two objects in contact), the contact transitions into a plasticity-dominated regime in which the contribution of the far-field elastic deformation is small (and eventually negligible at even higher loads) compared to the compliance of the near-field plastic deformation. Due to the scarcity of highly resolved experimental data that spans the transition from purely elastic behavior to plasticity-dominated behavior, analytically-based models must assume a functional form for transitionary functions that govern the behavior of contact in the mixed elastic-plastic regime. As an example, the set of assumptions employed by [24], which uses a set of hyperbolic transitionary functions (based on $\mathrm{sech}(x)$) to span the mixed elastic-plastic regime, include:

1. The transitionary functions must recover the elastic force at the onset of yield.
2. The contact force must always increase with displacement, and the rate at which the contact force increases with displacement cannot decrease (this assumes that the material does not fracture).
3. The Hertzian contact force (Eq. 1) is an upper bound for the elastic-plastic contact force after yield occurs due to plastic behavior being more compliant than elastic behavior.
4. The contribution of the force from a fully plastic response is the lower bound for the elastic-plastic contact force after yield occurs.
5. The contact force and its derivative must be smooth across the inception of yield.

From these and other assumptions, a solution form is posited that satisfies all of the assumptions. This approach has had mixed success due to the scarcity of data in the mixed elastic-plastic regime and due to the more speculative nature of the assumptions governing the behavior in the plasticity-dominated regime. Nonetheless, this modeling approach yields relatively simple models that can work well for certain material pairs.

By contrast, FEA-based models start with a large data set of finite element simulations of contact for a wide range of material properties and contact geometries. A best fit trend line is then fit to the resulting data set, yielding the FEA-based model. Examples of this modeling approach are detailed in [256, 257, 258, 23, 123, 259, 22, 260, 261, 176, 177]. There are several limitations to these modeling approaches as well, chief among which is that they are correlations to FEA simulations. Consequently, the model fits are only as accurate as the underlying material model used in the FEA simulations (often elastic-perfectly plastic material models are used, though more recent models include bilinear strain hardening [176, 177]). Like the analytically-based models, these models are also defined in terms of several different regimes that often correspond to elastic deformation, mixed-elastic plastic deformations, and plasticity-dominated deformations. As well, most of the FEA-based models use the Hertzian solution to describe the elastic regime of the response, with the model fits only being employed for the post-yield behavior.

Thus, there are several commonalities between the FEA-based models and the analytically-based models. Both sets of models usually use the Hertzian solution to describe the elastic regime of the response, and most of these models also use a von Mises yield criterion to determine the onset of plasticity (e.g., see [21, 251, 22, 24, 177]). Using the Hertzian stress distribution, the von Mises yield criterion gives that the deformation at which yield first occurs in the material is

$$\delta_y = \frac{r^*}{\mathcal{F}(\nu)}\left(\frac{\pi\sigma_y}{2E^*}\right)^2, \tag{21}$$

defined in terms of the yield strength, $\sigma_y$, and the maximum of the function describing the shape of the stress field as a function of distance $z$ beneath the contact patch

$$\mathcal{F} = \max_{z\geq 0}\left(-(1+\nu)\left(1-\frac{z}{a}\tan^{-1}\left(\frac{a}{z}\right)\right)+\frac{3}{2}\frac{1}{1+(z/a)^2}\right)^2. \tag{22}$$

As the maximum value is a function of the ratio $z/a$, where $a$ is the contact radius, this quantity only needs to be calculated once per simulation. The ramification of this equation is that the material first yields some distance beneath the contact patch itself. For a numerical approximation of Eq. 22, see [22, 177].

A second set of similarities between these two sets of modeling frameworks is the lack of model validation. Rarely are these models validated against experimental data. Instead, they are often compared with previous models and sometimes against a limited set of data. The FEA-based models are usually verified against a set of simulations

that were excluded from the data used to fit the model; however, this type of verification allows epistemic modeling errors (e.g., simplifications of the material model) to persist. A challenge with validating these models is that often the parameters needed for the models are not included in data sets provided in the literature, which diminishes the effectiveness of a validation effort if a parameter has to be estimated or calibrated to match the data. For this reason, it is recommended that experimental studies should provide as complete data sets as possible, including not only indentation/flattening data, but also tensile test data and very detailed descriptions of the specimen (including surface finish) and methods. See §3.1.6 for more discussion of this.

### 3.1.3 Flattening versus Indentation

An important distinction to be made in these models is the difference between indentation and flattening [261, 176, 177]. For two bodies in contact of different radii of curvature, indentation is defined by the body with the smaller radius of curvature having a higher stiffness (i.e., elastic modulus) than the body with the larger radius of curvature. Upon compressing the two bodies together, typically the larger body is plastically deformed and an indentation is left on it by the smaller body, which may not experience any plastic deformation. Conversely, flattening is defined by the body with the larger radius of curvature having a higher stiffness than the body with the smaller radius of curvature. Upon compressing the two bodies together, typically the smaller body is plastically deformed such that its contacting surface is flattened. These different cases are further illustrated in Fig. 8. Though some models try to span both regimes with a single set of equations, the fundamental physics of the two regimes (particularly in the distribution of stresses and displacement of material in the plasticity-dominated regime) is sufficiently different to warrant two sets of models. In the limit of both bodies being the same size, indentation and flattening models should converge to the same values [124].

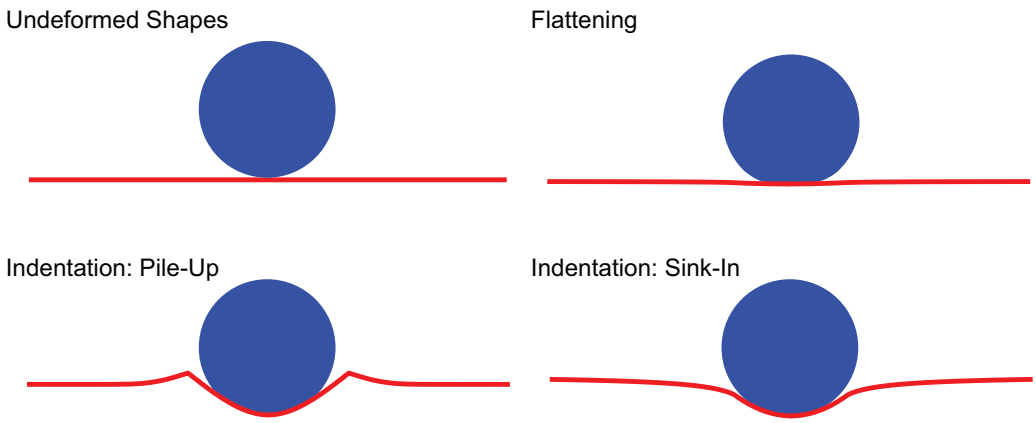


**Fig. 8:** Illustrations of the differences between flattening, indentation with pile-up, and indentation with sink-in. The deformed shapes are taken from the simulation results of [176, 124, 177].

One unique aspect of indentation that further differentiates it from flattening is that material can either pile-up or sink-in at the edge of the contact zone [93, 262, 263, 177]. These two characteristics are determined by how the material outside of the contact region is deformed. In the case of pile-up, a ridge of material is formed around the indentation; sink-in, by contrast, resembles an elastic indentation in which the material around the indentation is pulled down by the indentation too. The mechanisms for pile-up are governed by [263]:

- The strain hardening of the material (the less strain hardening, which is closer to elastic-perfectly plastic, the more pile-up is observed);
- The ratio of the elastic modulus to yield strength (the greater the elastic modulus compared to the yield strength the more plastic behavior is observed and thus more pile-up is observed); and
- The friction coefficient.

As explored in [177], which used a bilinear hardness model for the plastic behavior (with a linear elastic modulus $E_f$ and a stiffness modulus in the plasticity-dominated regime of $E_t$, as used in Fig. 9), pile-up occurred for elastic-perfectly plastic materials, and materials with a bilinear hardness ratio $E_t/E_f < 0.01$. For higher bilinear hardness ratios

(indicating a stiffer plastic response and, in the limit of $E_t/E_f = 1$ an elastic response), only sink-in was observed. The ramifications of pile-up and sink-in are also manifested in the frictional behavior of a sphere indenting a half plane [177]. In the case of pile-up, the ridge of material around the indentation increases the effective coefficient of friction by up to 50% compared to the sink-in case as sliding must push more material out of the way.

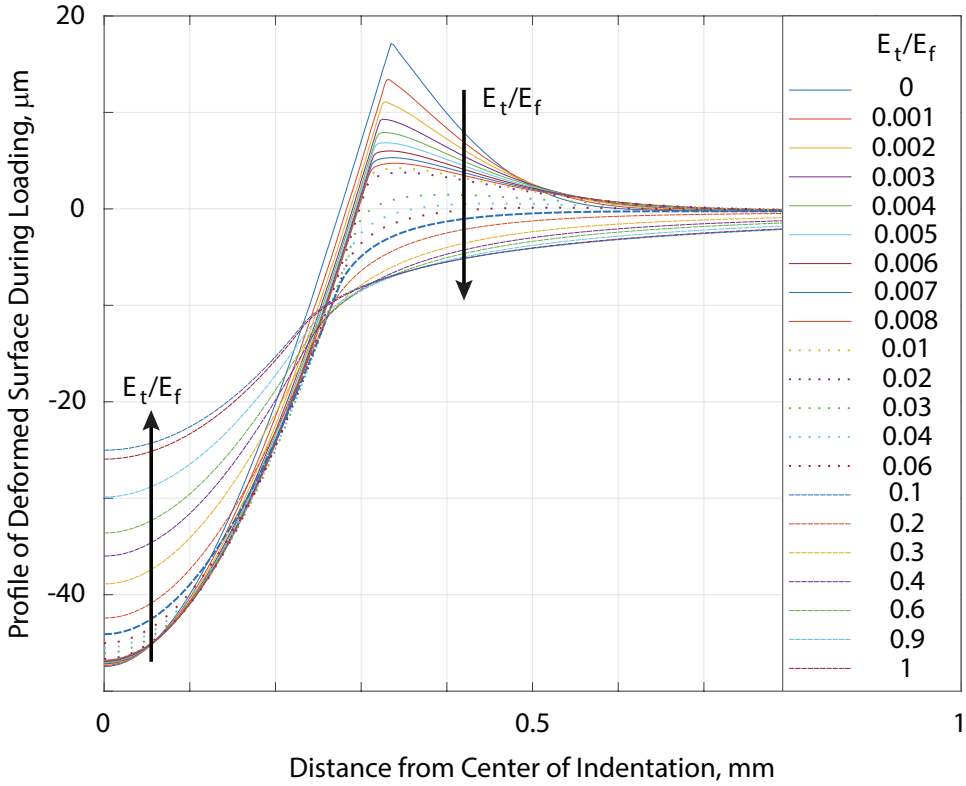


**Fig. 9:** The influence of the bilinear hardness ratio ($E_t/E_f$) on pile-up and sink-in, adapted from the work described by [177].

### 3.1.4 Rough Contact

The wealth of research on the interaction between two round surfaces (e.g., asperities) serves as the foundation for modeling real surfaces. A common feature of real surfaces is that the microscale is described as numerous asperities with heights and descriptions best quantified by statistical measures since there are too many to model in high fidelity. Thus, given a description of the roughness (usually a statistical description) and a contact model governing the behavior of a single asperity, rough contact models determine the contact forces between two real surfaces. This approach to modeling rough surfaces is rooted in [264, 265, 266], and has led to the observation that it is misleading to think that the peaks on a surface profile correspond to the asperities as this gives a false idea of both the number of peaks and the radii of curvature of the asperities [267]. The distribution of asperities on a real surface is fractal in nature [268]. As Archard first proposed: roughness consists of 'protuberances on protuberances on protuberances' [264]. Thus, this brings into question what an asperity actually is – as the contact loads increase, asperities can grow in size and join neighboring asperities (from the perspective of contact at least) [267].

Figure 10 shows the topography of a small segment of a lap joint (for details about the system and similar measurements, see [81]). The asperities, while often visualized as sharp peaks, tend to be smoothly undulating features. As shown in the figure, the radii of the asperities is often several orders of magnitude greater than the heights of the asperities, and the perception of the asperities as sharp peaks is often due to the aspect ratio of how they are displayed (note that in Fig. 10(a), the vertical axis is in µm while the planar axes are in mm). It is worth noting that the instrument used to measure the topography shown in Fig. 10 has resolution on the order of 1 µm, thus it is difficult to evaluate the hypothesized fractal nature of asperities at smaller length scales than this[15]. In general,

[15]Other difficulties in identifying asperities exist as well. Here, an asperity is considered a local peak in the surface profile, and a kernel-integrated approach similar to [81] is used to identify the asperities included in this measurement.

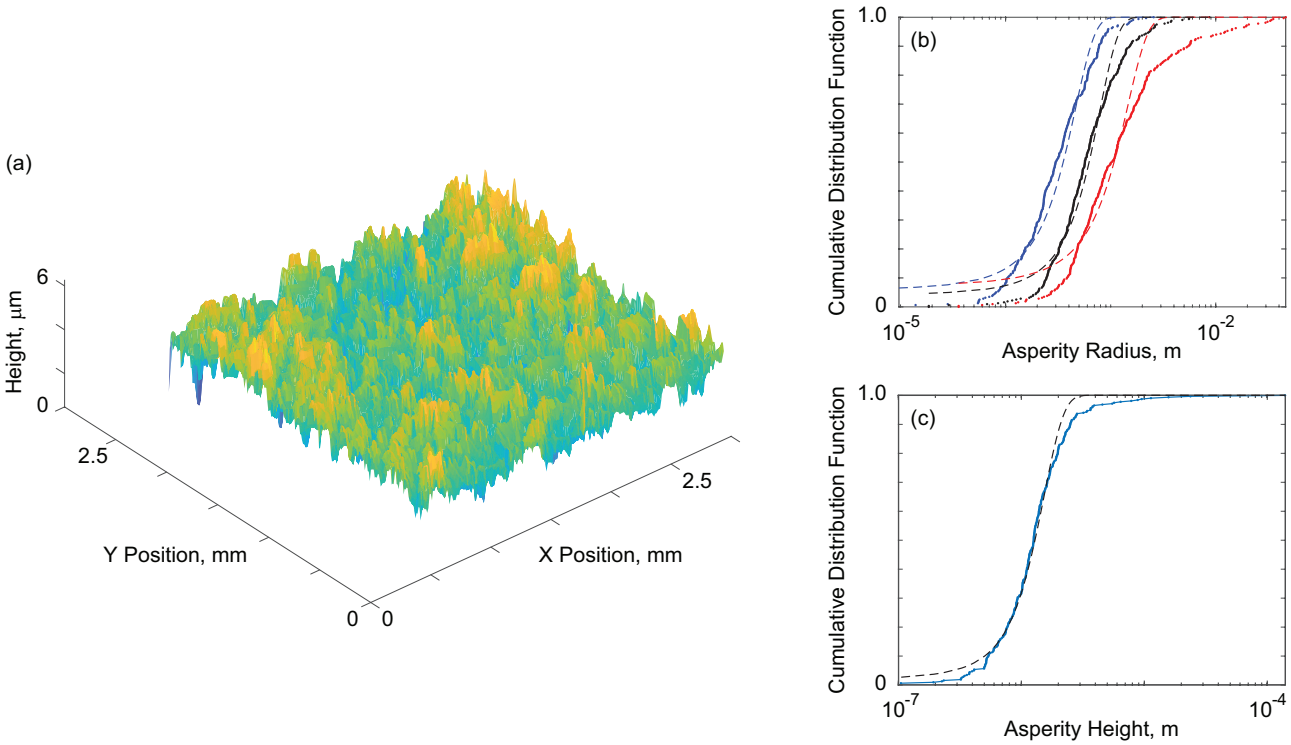


**Fig. 10:** The topography of the surface of a polished lap joint showing (a) the plot of the surface topography over a 2.5 by 2.5 mm patch, (b) the cumulative distribution function of the asperity radii for the semi-minor axes (blue), semi-major axes (red), and geometric mean of the radii (black), and (c) the cumulative distribution function of the asperity heights. In both (b) and (c) a Gaussian distribution (dashed line) of the measured properties (dotted line) is shown.

due to the measurement precision, there is a lower cutoff in the wavelengths of asperities measured; similarly, there is also a higher cutoff that is sometimes imposed to eliminate features that are part of the mesoscale topography, such as waviness from the manufacturing process. To provide further evidence for the notion of asperities being ellipsoidal, Fig. 10(b) shows the measured radii of both the semi-minor and semi-major axes of the asperities. For this measurement, the semi-major radii are consistently a factor of three greater than the semi-minor axes (up until the 75th percentile, where the ratio increases further to, eventually, a factor of 20 by the 98th percentile).

Across both single asperity and rough surface contact, one observation that has motivated much of the modern research in contact mechanics is the linear relationship between contact area and applied normal load. As shown in [269], the contact radius $a$ can be related to the indentation depth via

$$a = \sqrt{2r^*\delta}. \tag{23}$$

This relationship for single asperity contact was observed for rough surfaces too by multiple sources [264, 265]. However, much like measuring the length of a fractal edge, the apparent contact can change with the scale that the contact area is being measured on.

To simplify modeling for rough contact, it is often assumed that two rough surfaces can be modeled as a single rough surface in contact with a perfectly flat surface. This approach, however, can neglect the oblique contact of asperities that may occur in real systems. As shown in Fig. 11, the contact of two rough surfaces can result in conformal contact between asperities that give rise to oblique loads (such as between the two surfaces in contact near a position of 0.4 mm in the figure). These types of features are lost in the simplification of the surfaces as being rough on flat contact; however, it is unclear what the full ramifications of this trade-off are. Early models showed that it is important to capture the elastic coupling between asperities when modeling rough on flat contact [270], but it is still unknown how much contribution oblique contact of asperities has to the macroscale view of contact between rough surfaces. Recent analyses, though, indicate that neglecting the oblique contact asperities likely stiffens models of an interface [271]. More investigation is warranted to determine the relative contribution of oblique contact for real surfaces across a range of materials and geometries.

Rough surface profiles can be modeled either in a statistical or deterministic sense. Multi-scale, deterministic models that attempt to capture the features of a real surface have had some success in showing the importance of capturing the small scale features of asperities in larger simulations [272, 273]. From the statistical modeling standpoint, one of the most popular rough contact models is the CEB model [274], which enhanced the Greenwood model [265] by enforcing volume conservation for the deformed surface. The CEB model has been followed by a number of other approaches [275, 276, 277, 278, 279] that have sought to combine existing single asperity contact models with different statistical distributions (generally Gaussian) of asperities[16]. In parallel, building off of the observations of the fractal quality of asperities [264], a number of models have been posited with the asperity distributions described by different self-affine fractals (e.g., the Weierstrass-Mandelbrot or Cantor sets) [281, 282, 283, 284, 285]. One challenge of these models, however, is that they do not yield unique predictions as multiple sets of parameters describing the fractals can lead to similar results.

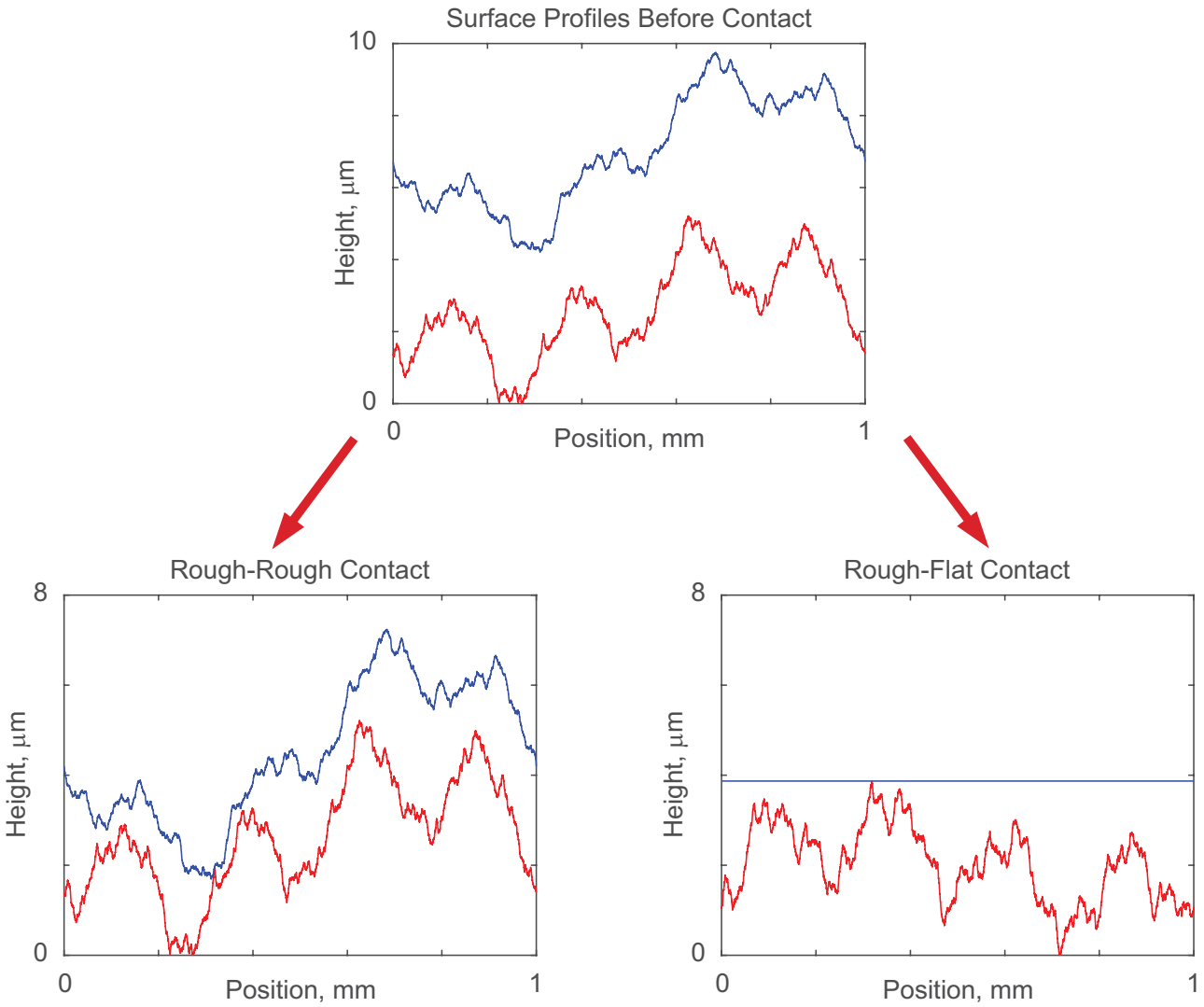


**Fig. 11:** Illustration of two different approaches for modeling contact: left, preserving the surface profiles and modeling contact as between two rough surfaces; right, approximating contact as between a single rough surface and a flat.

A reasonable question to ask is: which approach is more appropriate for real surfaces? As shown in Fig. 10, the measured distributions of asperity heights and radii are well-fit by Gaussian distributions (excluding the tails of the distribution though)[17]. To investigate this question, [286] compared both a Gaussian and a fractal distribution for an

[16] Of note, both [276, 280] consider elliptical asperities.

[17] Note that for surfaces machined by a single point tool, such as a turned surface, a uniform distribution is usually more representative than a Gaussian distribution.

elastic contact model (so as to make the results more clear by excluding the plastic component of the contact model). For both models, the predicted contact parameters (e.g., real contact area) were dependent upon the sampling parameters for the asperity distributions (which can change significantly based on the scale that the statistical parameters are sampled on); however, a clear trend was that fractal surfaces had a different slope for the predicted contact parameters than the statistical model, independent of the specific distribution parameters chosen. Thus, one challenge is to understand how the properties of rough contact scale from the nanoscale to the macroscale [287]. This challenge is further exacerbated when the surface is viewed through the lens of Archard's concept of protuberances upon protuberances. The assumption of a distribution of asperities across scales (e.g., as investigated by [286]) highlights the amount of uncertainty that can be introduced by a statistical or fractal surface model, which was further investigated by the contact mechanics challenge [225].

> **Challenge 6**: What are the effects of modeling simplifications on the prediction of contact between two rough surfaces? Which assumptions (e.g., representing the two surfaces as one rough and one flat, or using a statistical or fractal distribution of asperities) significantly affect the predictions of contact force and contact area, and which assumptions introduce minimal model form error?

### 3.1.5 The Contact Mechanics Challenge

As William Thomson, Lord Kelvin, once said, "if you can not measure it, you can not improve it." For this reason, the pursuit of a predictive contact model for the properties of two rough surfaces in contact is an ongoing research challenge. Because of the scale-dependency of properties (e.g., the real contact area and the hardness), there are many gaps in the available experimental data that limit the advancement of contact models. In order to address this, a contact mechanics challenge was proposed by Müser and Dapp in 2015 as an opportunity for modelers to assess the efficacy of different methods against a truth solution derived from continuum mechanics [225]. The challenge entailed predicting the contact area and geometry (such as gaps) as well as the contact pressures and stresses for a 0.01 $mm^2$ rough surface being pressed against a smooth, elastic flat. The truth solution was calculated using a Green's function molecular dynamics simulation [288] applied to a finely resolved interface with 64,000 by 64,000 discretization points.

Twelve different teams entered solutions into the contact mechanics challenge, with solution methods spanning: a fast Fourier transform (FFT) based boundary value method (BVM) [289, 290, 291], atomistic molecular dynamics [292, 293], and even a scaled-up experiment[18] [294] among other approaches. In order to approach the problem, all of the methods down-sampled the surface to between 1,000 by 1,000 discrete points and 32,000 by 32,000 discrete points. While these numbers would be prohibitively large for macroscale simulations to consider (recall that the interface was 0.01 $mm^2$), the techniques employed by the FFT-BVM method were able to make reasonable predictions with only 1,000 by 1,000 discrete points (which required about one minute of computational time on a laptop). As measuring contact properties internal to an interface for non-transparent materials is largely prohibitively difficult, these high fidelity approaches offer a path forward for advancing knowledge of contact mechanics and improving the existing heuristic models for rough contact.

The utility of the contact mechanics challenge and other similar exercises is that it helps a research community assess both the state of the art techniques as well as the existing gaps in capabilities. Without a periodic, earnest assessment of the methodology being developed, and without intentional efforts to collaborate and fairly compare techniques, it is challenging to do more than incrementally advance the state of the art. The sheer number of papers published on the topic of rough contact (over 20,000 publications since [265] was published) indicates the need for focus through challenges such as the contact mechanics challenge. Thus, one of the challenges going forward is identifying the right challenges to focus the community at appropriate intervals.

> **Challenge 7**: What mechanisms need to be in place to facilitate the periodic assessment of the state-of-the-art through the definition of research challenges for the community to engage in collaboratively?

### 3.1.6 Experimental Validation of Contact Models

Despite the many challenges with interrogating the small scale (and potentially inaccessible) characteristics that are necessary to validate contact models, there has been significant progress over the last century. Validation experiments can be characterized as either direct (e.g., directly comparing measurements and predictions of the

[18] The experiment of [294] used a diffuse light source and the frustrated total internal reflection method to measure the contact area as a function of load resolved across the entire interface, providing extensive and novel experimental insights to the challenge.

constitutive relationships, such as shown in Fig. 7) or indirect (e.g., comparing integrated quantities that are predicted by a simulation involving a contact model, such as the coefficient of restitution) [295]. Both types of experiments are necessary to validate a contact model, especially if there is potential to apply it to a larger range of materials or load cases than spanned by the validation effort. This process is sometimes referred to as orthogonal testing – i.e., testing both the directly predicted quantities as well as a quantity that is dependent upon the model but not predicted directly by the model [296, 24]. In terms of contact mechanics, a challenge faced by using only direct validation data is that not all characteristics can be directly validated. For example, unloading models require a deformed radius of curvature that varies with load; however, this quantity is not accessible. As a result, the unloading models may look qualitatively correct, but small differences can lead to very large errors in the prediction of the coefficient of restitution and thus dissipation characteristics of the system. Vice versa, indirect validation data is insufficient as well as a model could correctly predict the coefficient of restitution but be significantly off in the contact stiffness for both loading and unloading as well as the peak contact forces, which are paramount for understanding damage.

In addition to the wealth of nano-indentation experiments (§2.1), there are a significant number of experiments for direct validation at the mesoscale. These experiments include indentation and flattening measurements as well as optical studies of contact area (using a transparent material pressed against an opaque test specimen such as a metal coupon). Often, these experiments involve custom-built rigs that are designed to measure quantities that commercially available machines are not able to measure (e.g., specific loading regimes or optical measurements of contact area). Much of the mesoscale investigation of contact mechanics dates back to the work conducted by [109, 150], which investigated the relationship between the measured hardness and the plastic response of a material. More recent work has both advanced the precision of the measurements [297, 298, 299, 295], investigated newer materials [300], tested the hypotheses underlying existing models [301], and measured quantities previously inaccessible [302, 303, 304, 294].

A limitation of most of these studies is that the contact radius and area is measured after unloading. This results in a lack of information for how surfaces are deformed during loading, as only the permanent plastic deformations are visible after unloading. An exception to this is [294], in which a scaled up version of the surface used in the contact mechanics challenge was printed in high resolution and pressed against a transparent material. Using a diffuse light source and the frustrated total internal reflection method, the contact area during both loading and unloading was able to be measured across the entire surface. While this methodology was demonstrated on a soft material (PDMS), its potential application to study hard materials could be realized with hard, transparent ceramics such as sapphire.

Indirect validation measurements have largely focused on measuring the energy dissipated across an impact event. The coefficient of restitution can be defined multiple ways [252, 24]: in terms of the change of normal velocity, tangential velocity, velocity magnitude, or energy from before to after the impact event. Coefficient of restitution experiments largely focus on low velocity, normal impact between a sphere and a flat test specimen [305, 235, 306, 295], with a few studies focusing on sphere-on-sphere impact [307, 308]. In some cases, contact duration is also able to be measured by creating a circuit between the impactor (usually a pendulum) and the test specimen [295]. This test data is able to validate contact mechanics models indirectly by establishing a model for the impact event, which is typically of the form of a differential equation similar to

$$\ddot{\delta} = -g + \frac{F(\delta)}{m},$$

where $\delta$ is the contact displacement, $g$ is gravity, $F(\delta)$ is the contact force, and $m$ is the mass of the impactor. Integrating the differential equation across the entire impact event with the initial condition of the velocity of the impactor just before contact yields the rebound velocity after impact, which is used to calculate the predicted coefficient of restitution. See Fig. 12 as an example of a pendulum-based coefficient of restitution test setup.

Significantly less data is available for oblique impacts, which combine both normal and tangential loading[19]. Oblique impact experiments can be categorized as either a sphere impacting an inclined flat specimen [309, 310, 24] or a cylindrical rod with a rounded end being dropped at an angle against a flat specimen [311]. In addition to the previously described coefficients of restitution, oblique impact also involves a change in the rotational energy of the impactor – which is usually included in the energetic coefficient of restitution as a rotational energy term. Using a cylindrical indenter with a rounded end facilitates controlling for the initial rotational energy before impact.

Table 2 provides an overview of coefficient of restitution experiments. The experiments fall into two categories: drop or pendulum. Drop experiments release a sphere (or rod with spherical end caps) from a set height such that it impacts a target plate directly beneath it. In these experiments, the impact velocity is controlled by the height that the spheres are released at. This setup is particularly well-suited to being automated, which was done in [312] where over 5,000 experiments were conducted using a robotic system to pick up and release spheres. Pendulum experiments

[19] Tangential loading can also be of concern when there is a material or geometric dissimilarity between the contacting bodies.

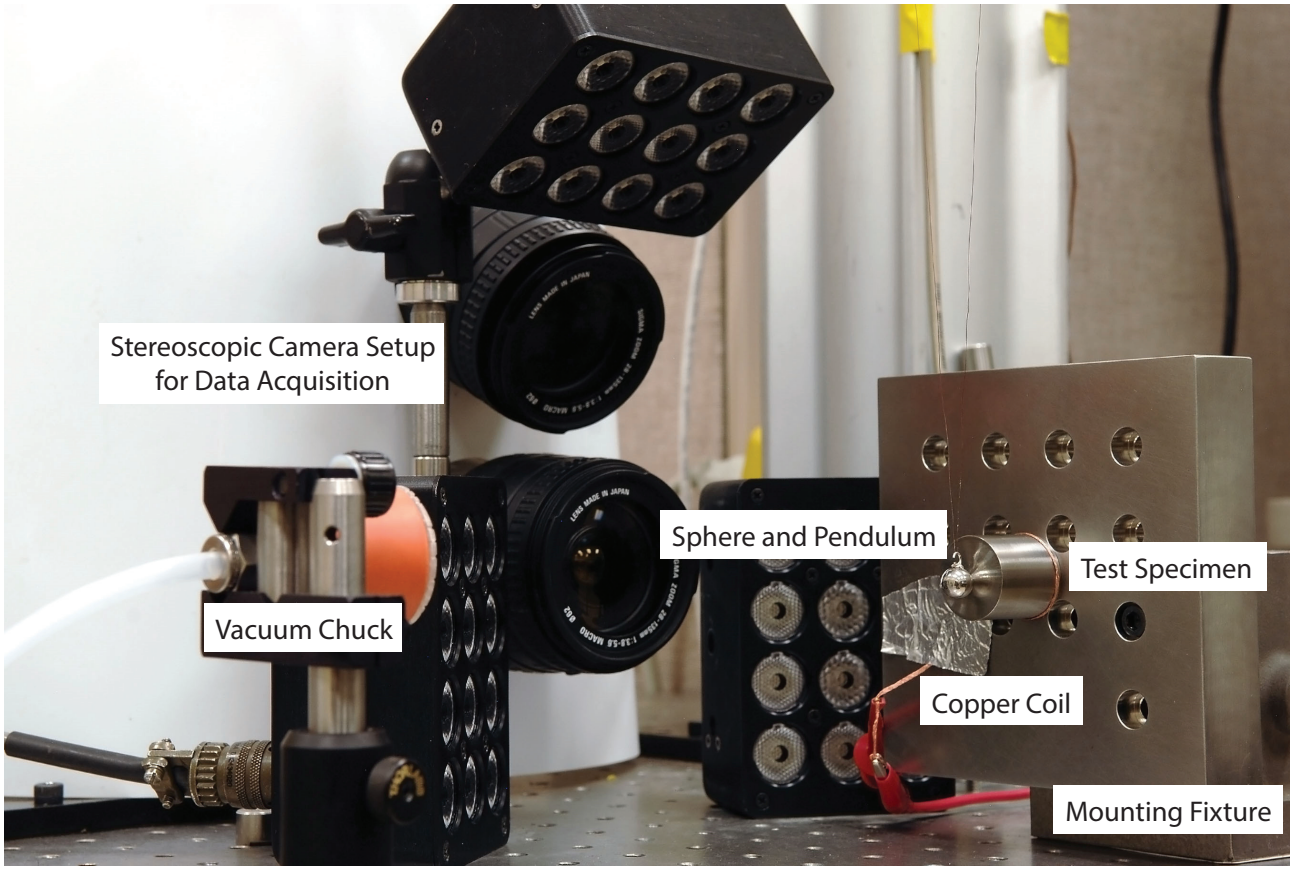


**Fig. 12:** Experimental setup for a coefficient of restitution experiment. Velocities throughout the experiment are recorded via digital image correlation, and impact time is recorded via a circuit that is closed when the sphere is in contact with the test specimen. See [295] for more details.

involve either a sphere on the end of a pendulum arm (typically a bar or a string/wire) impacting a fixed plate, or two spheres, both mounted at the end of pendulum arms, impacting each other. For the experiments with fixed plates, several of these were setup such that the plates could be inclined, allowing for oblique impact experiments. Note that for the oblique impact studies in Table 2, the coefficient of restitution data also includes metrics such as the tangential restitution coefficient. While not detailed here, there is a wealth of papers in the granular flow literature that study the coefficient of restitution of agricultural and industrial materials (such as grains, wood pellets, coal, etc.). For more information, refer to [313, 314, 315]. The modeling of materials in granular flow used for additive manufacturing (i.e., metal or ceramic particles) are typically based on the studies in Table 2 or similar. Most studies in Table 2 report values as a function of impact velocity or drop height unless only a single impact velocity is investigated.

| Study | Setup | Materials | Measured Data |
|---|---|---|---|
| Tatara and Moriwaki, 1982 [305] | Pendulum | Lead, Brass, Porcelain, Agate, Glass | Coefficient of restitution |
| Sondergaard et al., 1990 [316] | Drop, Oblique | Steel, Bronze, Pyrex Glass, Lucite, Aluminum | Coefficient of restitution |
| Nobre et al., 1999 [309] | Pendulum, Oblique | SFNOR 25CD4 Steel, Sintered $\alpha$-Alumina | Coefficient of restitution, indentation profile, impact duration, peak normal and tangential loads, and tensile test summary properties |

**Table 2:** Summary of representative coefficient of restitution studies for elastic-plastic materials.

| Study | Setup | Materials | Measured Data |
|---|---|---|---|
| Kharaz and Gorham, 2000 [306] | Drop | EN9 Plate Steel, Aluminium Alloy, Aluminium Oxide | Coefficient of restitution |
| Gorham and Kharaz, 2000 [310] | Drop, Oblique | Soda-lime Glass, Aluminium Alloy, Aluminium Oxide | Coefficient of restitution, rebound angle, and rotation speed |
| Kharaz et al., 2001 [317] | Drop, Oblique | Soda-lime Glass, Aluminium Oxide | Coefficient of restitution, rebound angle, and rotation speed |
| Dong and Moys, 2003 [318] | Drop, Oblique | Steel, Glass, Malachite, Rubber, Mild Steel, Slate | Coefficient of restitution and angular velocity |
| Stevens and Hrenya, 2005 [319] | Pendulum | 316 Stainless Steel, AISI 52100 Chrome Steel | Coefficient of restitution and contact duration |
| Dong and Moys, 2006 [320] | Drop, Oblique | Steel, Chrome Steel | Coefficient of restitution, rebound angle, angular velocity, and tangential velocity |
| Minamoto and Kawamura, 2009 [307] | Pendulum | SUJ2 Steel | Coefficient of restitution and contact duration |
| Aryaei et al., 2010 [321] | Drop | Steel, Aluminum | Coefficient of restitution |
| Minamoto and Kawamura, 2011 [308] | Air gun[20] | SUJ2 Steel | Coefficient of restitution, contact duration, tensile and compression test data |
| Marinack, Jr. et al., 2013 [322] | Drop | 1100-H16 Aluminum, Borosilicate Glass, Brass Alloy 260, Chrome Steel, Low-Carbon Steel, NiTiNOL 60, Polybutadiene, S2 Tool Steel, S7 Tool Steel, 440C Stainless Steel, Tungsten Carbide | Coefficient of restitution |
| Müller et al., 2013 [312] | Drop | Stainless Steel, Glass | Coefficient of restitution |
| Ghaednia et al., 2015 [311] | Drop, Oblique | AISI 201 Stainless Steel, AISI 1010 Low-Carbon Iron | Coefficient of restitution and rotation speed |
| Brake et al., 2017 [295] | Pendulum | 6061 Aluminum, Aluminum Oxide, Copper, Hiperco, Nitronic 60, Phosphor Bronze, Stainless Steel 304, 440C Work Hardened Steel, Titanium | Coefficient of restitution, contact duration, tensile test summary properties, nanoindentation data |
| Patil et al., 2017 [323] | Drop | NiTi60 | Coefficient of restitution |
| Patil and Higgs III, 2018 [324] | Drop | Brass Alloy 260, Aluminum 1100-H16, Tungsten Carbide, S2 Tool Steel, Low Carbon Steel, Borosilicate Glass, Aluminum 6061 | Coefficient of restitution, surface roughness, and indentation depth |
| Hlosta et al., 2018 [315] | Pendulum | C10E Steel, Wood - Ash, ABS Plastic, Corn Seeds, Spruce Sawdust, Black Coal | Coefficient of restitution |

**Table 2:** Summary of representative coefficient of restitution studies for elastic-plastic materials.

[20]The air gun setup is similar to the drop setup in that it involves one sphere being shot towards a second sphere through a guided channel.

| Study | Setup | Materials | Measured Data |
|---|---|---|---|
| Hashemnia, 2020 [325] | Drop | Steel, Aluminum, Copper | Coefficient of restitution and temperature (but not velocity) |
| Sandeep et al., 2021 [326] | Drop | Glass, Chrome Steel, Leighton Buzzard Sand, Stainless Steel, Granite, Rubber | Coefficient of restitution and surface roughness |

**Table 2:** Summary of representative coefficient of restitution studies for elastic-plastic materials.

A barrier to the widespread use of published experimental data for validation purposes is that models often require more material characterization data than is typically reported. As an example, when it is reported, the hardness is given as a static value from a well defined test (such as Brinell or Rockwell); however, this gives little to no information regarding strain hardening or how the hardness varies with load. While most papers report material properties for the specimen tested, these are typically from the literature or standard tables rather than characterized values of the specific materials tested. Only three of the papers in Table 2 report tensile test data for the specific materials tested [309, 308, 295]. Further, many papers present material data (such as from hardness testing) that may be sufficient for one type of constitutive model, not anticipating the potential needs of future modeling efforts. Complicating validation efforts further, some studies (e.g., see [320] in Table 2) only report a basic description of the material, such as "steel". From a model validation standpoint, this renders the data set useless as it does not contain any of the necessary information to simulate the experiment (such as material properties at the very least). Therefore, experimentalists are challenged to document not just the results of their experiments, but also the characteristics of the test specimen from orthogonal experiments (e.g., tensile test data).

> **Challenge 8**: Papers that report experimental data must include a thorough characterization of the materials being tested in addition to the results from contact experiments for future modeling efforts.

## 3.2 Friction as a System, not as a Constant

The development of the commonly used Coulomb friction model is the embodiment of 500 years of observations, spanning research by Da Vinci in the 1400s, Amontons [327], Coulomb [328], and Bowden and Tabor [329] amongst others. This model has three fundamental assumptions: that the friction forces are independent of the area in contact, that the friction forces are linearly dependent on the normal load, and that the friction forces are independent of sliding velocity. These three assumptions are implicit in the form of Coulomb's model

$$f = \mu N. \tag{24}$$

While these assumptions are appropriate and have found widespread application at the macroscale, they are often inappropriate for describing friction at smaller scales. The friction force, $f$, is dependent upon sliding velocity – as evidenced by stiction, viscous friction, kinetic friction in rubber, and Stribeck effects among other mechanisms [330, 31, 331, 332, 333, 228]. The friction force is also strongly dependent on area[21] [334, 335], and it does not vary linearly with load, $N$ [336, 331, 332, 82, 223, 337] (unless the friction coefficient itself is allowed to vary with load [336]).

The widespread adoption of Coulomb's model overshadows the fact that friction is still poorly understood and that predictive friction models do not exist. As a thought experiment, consider a glass of water sitting on a wooden table during a humid day. At first, the glass might have a coefficient of friction, $\mu$, of about 0.4 (depending on many factors of course). Over time, condensation builds up and the frictional system now contains water as a lubricant between the glass and wood, which significantly reduces the coefficient of friction to 0.2. Several days later, once the humidity has reduced, the coefficient of friction returns to the original value of 0.4. Over time, as the glass is repeatedly rubbed on the wooden surface, a polished groove (a wear scar) develops, further lowering the friction on dry days to 0.25, and on humid days to 0.13. These values are further modified by the temperature of the liquid in the glass. In this manner, friction is a time evolving system that is dependent upon the environmental conditions, the materials in contact, the interfacial conditions, and many other variables [338, 339, 340, 341, 223, 335]. Thus, it is misleading to think of the

[21] Recall from the contact mechanics challenge [225] that the contact area is very different from the surface area.

coefficient of friction as a constant. Instead, each tribosystem – the unique confluence of load conditions, material properties, and environmental characteristics (e.g., temperature, atmospheric pressure, chemical compositions, etc.) where surfaces are in contact – needs to be studied independently in order to determine the frictional characteristics of an interface[22].

A deceptively simple question that must be asked is: what is friction? One answer might be a set of mechanisms that dissipate energy when two surfaces are in contact with relative tangential motion. Though even this definition is insufficient as it neglects some mechanisms that resist motion before sliding begins. Perhaps a better definition might be:

> **Friction**: a set of mechanisms at, or near, an interface that dissipate or store energy when two surfaces are in contact with tangential forces applied that in the absence of these mechanisms would result in unimpeded relative tangential motion.

Through adhesive forces, elastic strain energy, and other mechanisms, friction forces can resist tangential forces before motion occurs. This pre-sliding component of friction is often conceptualized as the linear spring in a Jenkins model (also referred to as an elastic sliding model), which necessitates that the definition of friction include the capacity of friction to be more than just a dissipative mechanism.

Once a critical threshold is exceeded (e.g., the onset of sliding), the dissipative mechanisms dominate the frictional response. There are multiple sources for frictional energy dissipation: elastic strain energy [227, 343, 230], plasticity (dislocations, crystal orientation changes, other changes in the microstructure) [344, 345, 346, 347, 348, 335], fracture (in terms of generating new surfaces, breaking bonds, etc.) [349, 350, 351], interfacial slip (breaking of interfacial bonds and elastic mismatches) [349, 230], adhesion (specifically the hysteretic separation/pull-off behavior) [352, 79, 233, 332, 228, 353], acoustic emissions [354, 355, 356, 357, 358], electrical resistance [359, 360] and the generation of electrical charge[23] (i.e., triboelectricity) [365, 366, 367, 368, 369], electromagnetic radiation [370], heat generation [350, 371, 372, 373, 335, 374], and even X-ray generation [375]. Additionally, the microstructure, roughness, and geometry can facilitate impact events on multiple scales in an interface [376, 377, 378], and the presence of lubrication – both solid [339, 223] and liquid [379, 215] – can add even more mechanisms for energy dissipation.

Unfortunately, all of these mechanisms can contribute simultaneously; however, their relative contributions vary vastly and are highly scale-dependent [345, 380, 333, 351]. In order to study them in isolation, there are some means to control the relative contribution of each mechanism. As an example, the plasticity index, $\psi$, describes the relative importance of plastic deformations in a rough surface contact [381]

$$\psi = \frac{E^*}{H}\sqrt{\sigma\kappa} \tag{25}$$

in terms of the RMS height of the surface, $\sigma$, and curvature, $\kappa$. The plasticity index can also be derived as the ratio of plastic work to total work done during indentation of a surface [382, 341]. This only deconvolutes one pair of mechanisms that contribute to energy dissipation during frictional interaction, though, and more research is needed to further isolate and assess the relative contribution of the dozens of mechanisms that actively dissipate energy during a frictional event.

> **Challenge 9**: What are the mechanisms that contribute to frictional energy loss, and what are their relative contributions in different settings?

At the heart of this challenge is the task of isolating and identifying the relative contribution of different mechanisms to frictional energy loss. This task will require new, multi-scale approaches to both modeling and in situ experiments to study these mechanisms and their relative importance at different scales. With an improved understanding of these mechanisms, this should provide new insights into why Coulomb's model has seen such widespread applicability despite its limitations. Additionally, a remaining open question will be whether it is possible to have a deterministic friction model or if, due to the quantities involved such as surface roughness, friction can only be understood in a statistical sense.

[22] The issue of modeling frictional contact is further exacerbated by many of the models currently employed being non-physical. This is evident in either their derivations, their adoptions from other fields, or their widespread use in other fields to describe general hysteretic behavior instead of friction itself. See, for instance, the models discussed in [342].

[23] As an interesting aside, see the triboelectric nanogenerator [361, 362, 363, 364], which has an output area power density of up to 500 W/m$^2$ and a total energy conversion efficiency of up to 85%.

### 3.2.1 Time-Evolving Effects

With the view of friction as a system, it is natural to conceptualize friction as a time-evolving quantity. The evolution of friction over time is clearly visible in most wear experiments, such as shown in Fig. 13. As the mating surfaces are worn, the coefficient of friction more than doubles over the course of the experiment for this specific system (for other systems, it could exhibit significantly different behavior, such as decreasing to near zero or even increasing to an extremely large value before the system siezed). At the same time, the contact stiffness also increases by more than a factor of two, which has significant ramifications for modeling the normal contact of surfaces with slip (either macro- or micro-). These effects are further exacerbated when the materials themselves exhibit time-dependency; however, the effects due to creep, relaxation, or other viscous behaviors are beyond the scope of this article [383].

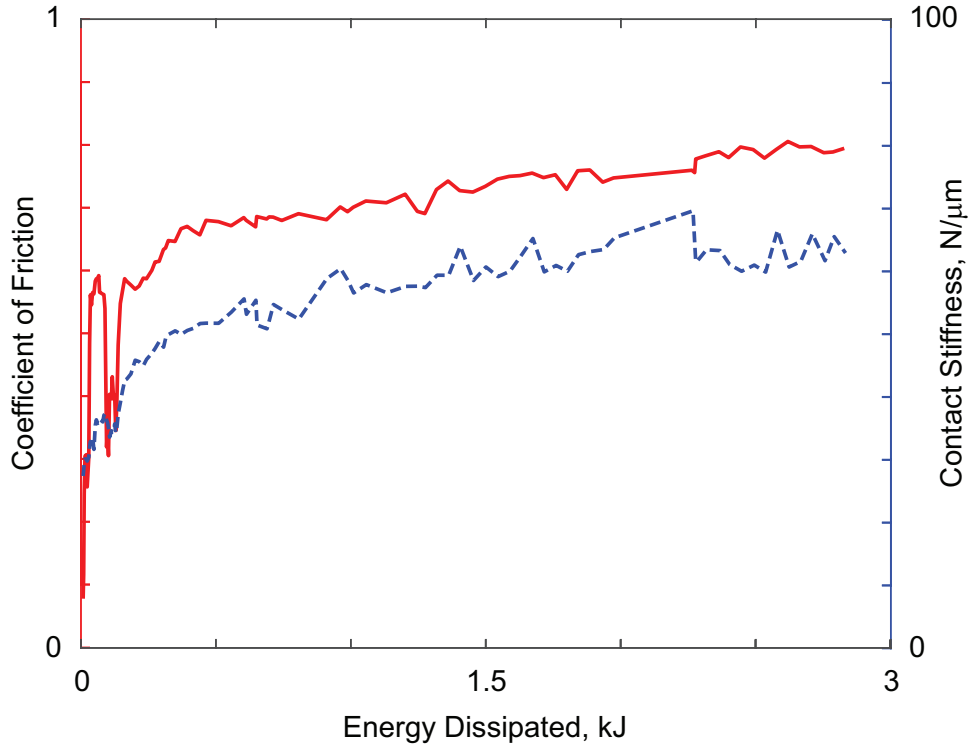


**Fig. 13:** An example of measured friction (red, solid) and contact stiffness (blue, dashed) changing over time (as parameterized by energy dissipated) for a wear experiment based on the data from [384].

One salient example of a model that captures the time evolution of frictional wear within automotive disk brakes is [385, 371, 372, 373, 386]. In this model, a coupled set of partially differentiable equations are derived for the evolution of both friction $\mu$ and temperature $T$ with time $t$

$$\frac{\partial \mu}{\partial t} = \alpha \left( \mu - \mu_{static} \left( N, v, T \right) \right), \tag{26}$$

$$\frac{\partial T}{\partial t} = \beta \left( T - T_{static} \left( N, v, \mu \right) \right). \tag{27}$$

These equations are parameterized in terms of the normal force, $N$, (which is a function of time), sliding velocity, $v$, (which is also a function of time), coefficients determined from high fidelity simulations, $\alpha$ and $\beta$, and the stationary values of $\mu$ and $T$ denoted as $\cdot_{static}$. With the two free coefficients, $\alpha$ and $\beta$, these models are fit to the results from high fidelity simulations of the system of interest. A predictive model for the evolution of friction, along with the wear of a surface, however, is beyond the state of the art [381].

## 3.3 Wear

One of the major sources of energy dissipation during relative sliding between two bodies is wear surfaces[24]. There are many different categories of wear, that each contribute to the damage of a surface under different regimes [387, 388]. In a review from 1995, over 182 different models of wear were found in papers published between 1957 and 1992 in the journals *Wear* and *Wear of Materials* [389]. While there is little consensus on the precise set of categories, they can be generally classified as: adhesive, abrasive, fatigue, and corrosive, of which abrasive wear is the most prevalent accounting for more than half of all industrial wear problems [390]. These different wear mechanisms can occur simultaneously [391]; for instance, fretting is a combination of multiple wear mechanisms as discussed in the next section.

The process of wear is strongly related to the compatibility of the materials in contact. As defined by Rabinowicz [392], the compatibility of metals, with regards to wear rate, can be determined from the binary phase diagrams. Compatible materials exhibit severe wear and are prone to seizing or cold welding (which are related to adhesive wear), while incompatible materials tend to exhibit moderate wear that is driven by non-adhesive mechanisms [393]. An example of a material compatibility chart is provided in Fig. 14. This chart implies that a material pair such as platinum and tin are compatible and likely to be prone to severe adhesive wear, and that a material pair such as lead and nickel are incompatible, resulting in non-adhesive wear mechanisms dominating their interactions. The precise mechanisms in action for a given tribosystem, though, are dependent upon more than just the materials in contact.

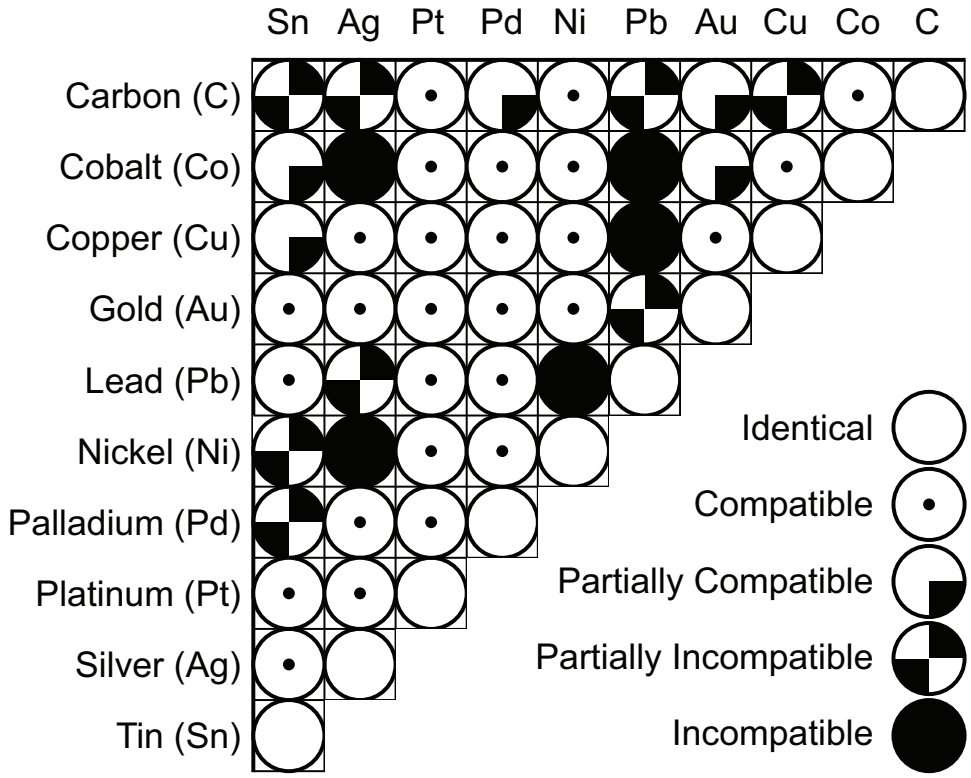


**Fig. 14:** An example of material compatibility charts developed by Rabinowicz. This modified excerpt is based on [336].

**Adhesive wear** occurs in sliding contact of two smooth surfaces when the atomic bond between materials in the interface is greater than the strength of the surrounding area in one of the surfaces [394]. This can be further differentiated as atom-by-atom adhesive wear and fracture-based adhesive wear. Atom-by-atom adhesive wear has a smoothing effect on a surface that can lead to cold welding, galling, or seizing (particularly in materials such as aluminum or titanium). Fracture-based adhesive wear, by contrast, is a roughening phenomena that generate debris and lowers friction forces over time. The transition between these two distinct regimes of adhesive wear is governed

[24]Here, this article focuses on surfaces in contact; however, wear can also be due to electrochemical processes or other mechanisms that do not involve the contact of two solid bodies.

by the elastic energy released by debris generation being greater than the adhesive energy to debond two asperities, creating a new pair of surfaces [395]. At the macroscale, the wear rate is able to be described empirically by the normal load on the surface and cumulative sliding distance via Archard's wear model (§3.3.2) [396]; however, at the asperity level, the tangential load and its effect on the asperity junction size in addition to sliding distance is a better indicator of wear rates [397, 394] as adhesive wear is dependent upon the real contact area of the contacting surfaces [398, 399]. The rate of adhesive wear is significantly affected by the temperature within the interface [400]. During dry sliding, it is possible for the flash temperature to instantaneously exceed 1000°C [401] (even though the bulk temperature of the specimens away from the interface may be close to the original temperature still). This increase in flash temperature significantly increases the adhesive force, which, in turns, exacerbates the adhesive wear in a system [400]. Methods to reduce adhesive wear include changing the microstructure of the surface (e.g., via coatings), modification of alloying elements, or use of lubricants [402, 403, 404, 396].

**Abrasive wear** is defined as the loss of material when a hard surface or particle slides over a softer surface. Abrasive particles can also form through work hardening, which results in cases where two similar materials mated together experience abrasive wear. There are two different classifications of abrasive wear: two-body and three-body wear [405]. Two-body wear refers to two surfaces in contact, and three-body wear [406] refers to a third object, such as particulate or debris, between the two surfaces (this is also referred to as erosive wear sometimes). In three-body abrasive wear, depending on the quantity of debris in the interface, the wear mechanism can transition from rolling to indentation [405]. Generally, abrasive wear is governed by the angularity of the wear features (i.e., surfaces or debris) [406], and the hardness of the surface, with harder surfaces exhibiting less abrasive wear [407]. For this reason, materials such as tungsten cobalt or hard coatings are used for machine tools [408]. Abrasive wear, at least at the nanoscale, is driven by the contact loads and is independent of the relative sliding velocity of the two surfaces [409].

**Fatigue wear** can be characterized as the formation of sub-surface cracks that, over time, grow until they reach the surface and debris is generated [387]. This can also be conceptualized as the gradual degradation of the strength of a surface until it can no longer support the repeated surface loading [410]. After abrasive wear, fatigue wear is considered the second most common type of wear mechanism [388]. Fatigue wear can be categorized by two different regimes – low cycle fatigue, and high cycle fatigue. In low cycle fatigue, wear particles are generated after a low number of cycles as significant plastic damage is accumulated with each cycle of motion. By contrast, high cycle fatigue is initiated by stress concentrations around inhomogeneities or other existing defects within the material that gradually grow over time. Fatigue wear is a common failure mode in rolling contact (e.g., bearings) [411, 412, 413] and prosthetics [42, 414, 415]. The science of fatigue wear, crack initiation, and crack growth is the same as in the study of fracture mechanics [416]. In contrast to abrasive and adhesive wear, fatigue wear tends to generate relatively large debris particles as larger sections of the interface can flake off depending on the size of the subsurface cracks.

**Corrosive wear** (sometimes referred to as erosion corrosion or tribocorrosion) occurs when chemical reactions create a reaction layer on the surface of an interface that is subsequently removed via sliding [417, 418, 419]. When the growth rate of the reaction layer is higher than the removal rate, this results in a protective reaction layer being formed; otherwise, the bulk material is removed as the interface is worn. Corrosion itself is a process that converts a refined material to a more stable form (e.g., an oxide) [168]. The oxides that are formed in metal joints tend to be much harder than the bulk materials of the components. As a result, there is potential for wear mechanisms to exacerbate each other, such as occurs with fretting wear. Corrosive wear is strongly dependent upon the environment that the interface exists in [417, 420]. For instance, lower oxygen levels can potentially inhibit oxidation, whereas salt water can significant increase corrosion rates. Corrosive wear can be greatly exacerbated by the chemical reactions between the solids and any lubricant, particularly in the presence of electrical contact (e.g., lubricated contact pin-receptacle pairs) [421]. As a result, the process of tribo-corrosion is described as the combination of mechanical wear processes (such as abrasion) and chemical or electrochemical corrosion [422]. A persistent challenge in advancing the fundamental understanding of corrosive wear processes is a lack of an adequate, unified approach for measuring wear rates in highly controlled environments (controlling, for instance, quantities such as the concentration of abrasive particles in a fluid) [423].

The four major categories of wear that are germane to contact mechanics as discussed in this review are summarized in Table 3. There are many other categories of wear though. Perhaps the next two distinct categories of wear would be electrochemical wear and cavitation wear [424]. Electrochemical wear is a special case of corrosive wear that is accelerated by an electrical current that drives chemical reactions [425, 426, 100]. This process is often used as a polishing method for metals, which is referred to as electrochemical machining [427, 428], and also as a method to accelerate the study of corrosive wear [429, 421]. Consequently, this is a non-contacting wear method that has limited application in contact mechanics; however, it is widely used in surface polishing. Likewise, cavitation wear is a type of three body wear (the fluid and surface make up the two sides of the interface, and the air bubbles from cavitation create the third body that drives the wear mechanism) that results when cavitation bubbles implode under

| Wear Type | Mechanism | Characteristics | Common Mitigation Strategies |
|---|---|---|---|
| **Adhesive** | Atom-by-atom | Increase in friction; possible seizing/galling/cold welding; smoothing of surfaces and reduction in gap between surfaces | Use of coatings or lubricants |
| | Fracture-based | Decrease in friction; roughening of surfaces; generation of debris | |
| **Abrasive** | Two-body or three-body | Driven by contact loads; ploughing and debris generation | Increase the hardness of the surface or use hard coatings |
| **Fatigue** | Low cycle | Significant plastic damage each cycle resulting in crack nucleation | Increase yield strength or reduce contact loads |
| | High cycle | Crack nucleation at stress concentations or existing defects within the material that gradually grow over time | |
| **Corrosive** | Chemical reactions | Oxidation or other chemical processes that form a reaction layer on a surface that facilitates material removal | Modification of environment or lubrication; coatings to prevent chemical reactions |

**Table 3:** Common types of wear germane to contact mechanics.

high pressures causing shockwaves [430, 417, 431, 432]. These shockwaves result in cyclic stresses and wear if they occur near or on a surface, and is often mitigated by micro- and nanoscale surface texturing [433, 434]. While not germane to metal-on-metal contact, it does establish a fluid/gas/solid contact problem that has many connections to the present review of contact mechanics.

Modeling wear in a predictive manner is a grand challenge within the tribology community. Wear events can be categorized as either mild or severe [401, 435]. In mild wear, the oxide layer that forms as new material is exposed is self-sustaining. That is, the rate of growth of the oxide layer is greater than the rate of material removal during the wear process. In severe wear, the surfaces are significantly deformed with damage beyond the microscale. In focusing modeling efforts on severe wear events, these typically involve multiple competing mechanisms and multiple branches of physics (e.g., to account for fluid-structure interaction) and interacting bodies (whether debris or solid lubrication in solid-solid interaction, or fluid interactions for lubricated interfaces). Modeling of wear becomes even more challenging when considering the heterogeneity of many types of coatings used to mitigate wear (e.g., [414]). Thermal spray coatings [436, 437, 438, 439, 440] and cold spray coatings [441, 442], for instance, are heterogeneous structures that include voids, oxides, unmelted particle, lamellar splats (i.e., the shape formed by molten metal impacting a target surface), and the underlying substrate, which is often textured to improve the bond strength of the coating. As an example, a detailed image of the cross-section of a thermal spray coating is shown in Fig. 15. The substrate is shown in light grey and the sprayed material is shown in dark grey.

There have been many different approaches for modeling severe wear, ranging from Archard's model (§3.3.2), to thermodynamic processes. One interesting view of wear is as a nonequilibrium thermodynamic process [444, 420, 445, 446]. Models have been posited to predict wear rates for different tribosystems that span the erosion-corrosion regime [420, 447], fretting [445], dry sliding [448, 449], and fatigue [447]. The crux of this modeling approach is that wear is a permanent and irreversible degradation process that disorders a system and generates irreversible entropy that must be in accordance with the second law of thermodynamics [445]. The multi-physics nature of these interactions (involving temperature changes, dislocation kinetics, plastic flow, electrochemistry, etc.) makes it particularly well suited to this phenomenological approach, though more work is needed to assess its practical application to predicting wear [447]. In all cases, the precise mechanisms that constitute a wear phenomenon are highly dependent upon the specific tribosystem, which limits the generalizability of any specific experiment or model.

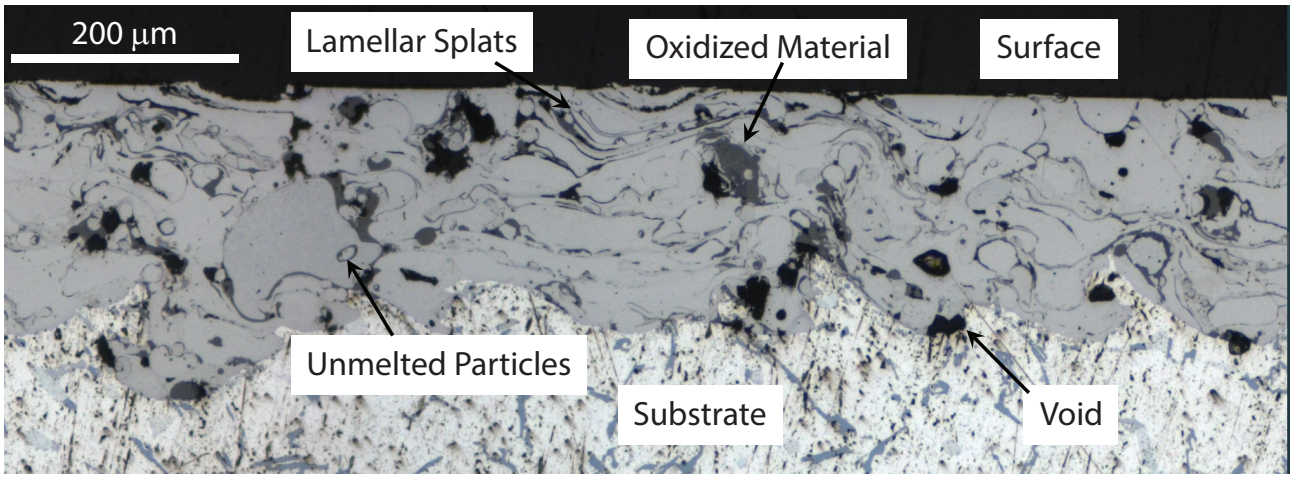


**Fig. 15:** Cross-section image of a thermal spray coating with key features identified. Here, the coating is composed of molten metal that has been sprayed onto a textured substrate. The coating has both voids and inclusions such as unmelted particles or oxides. Away from these features, the coating takes on a lamellar structure as layers are deposited on the surface. Image modified from [443].

### 3.3.1 Fretting Wear

Adhesive, abrasive, and corrosive wear can occur simultaneously in a process known as fretting [450, 451, 452, 18, 453], which is a specific type of wear characterized by high frequency (100s-1000s of Hz) microslip or small amplitude slip (on the order of 10s of μm, though potentially as much as 150 μm) between two bodies. Fretting is a multifaceted phenomenon that involves high stress gradients, multi-axial loading, surface topography and chemistry among other effects [18, 454]. In the context of structural applications, the salient feature of fretting is that there is no (or insufficiently large) gross motion across a jointed surface that could lead to the removal of debris (though fretting can also occur in situations that involve impact or gross slip, which expels debris from the contact patch [455, 456]).

During fretting, adhesive wear gives rise to debris formation that, due to the lack of macroslip across an interface, becomes trapped in the interface. In fretting, this trapped debris can drive abrasive wear. Along the new surfaces that are formed during fretting, corrosive wear increases the wear rate as the debris is oxidized. This is illustratively shown in Fig. 16. The process of fretting, especially in the situation where debris is trapped within the interface, is a non-Coulombic friction that can exhibit dramatic changes (usually reductions) in an effective coefficient of friction [457]. The role of the debris in the interface is highly dependent upon the dominant wear mechanism for the tribosystem: when adhesive wear is the dominant wear mechanism for a triobsystem, the oxidized debris particles can act like a solid lubricant and reduce the potential for fretting damage; conversely, when abrasive wear is the dominant mechanism, the oxidized debris particles exacerbate the wear damage, as described above [458]. Post-mortem inspections of interfaces that have experienced fretting can yield ranges of temperatures that the surfaces were heated to. As different oxides form at different temperatures, an analysis of the oxides (both in terms of chemical composition, size, and shape) in the interface can help determine how hot the surface was (i.e., the flash temperatures) during excitation [459].

A number of factors (as many as 50 different variables [460]) can affect the damage due to fretting:

- Load – higher loads lead to higher damage;
- Amplitude – fretting increases up to the macroslip transition;
- Number of cycles – typically, fretting initiates after a number of cycles has passed, then continuously incurs more damage with each subsequent excitation cycle;
- Temperature – which drives chemical reactions and oxide formation;
- Humidity – which can increase corrosion; and
- Material inertness – which influences a material's ability to be oxidized.

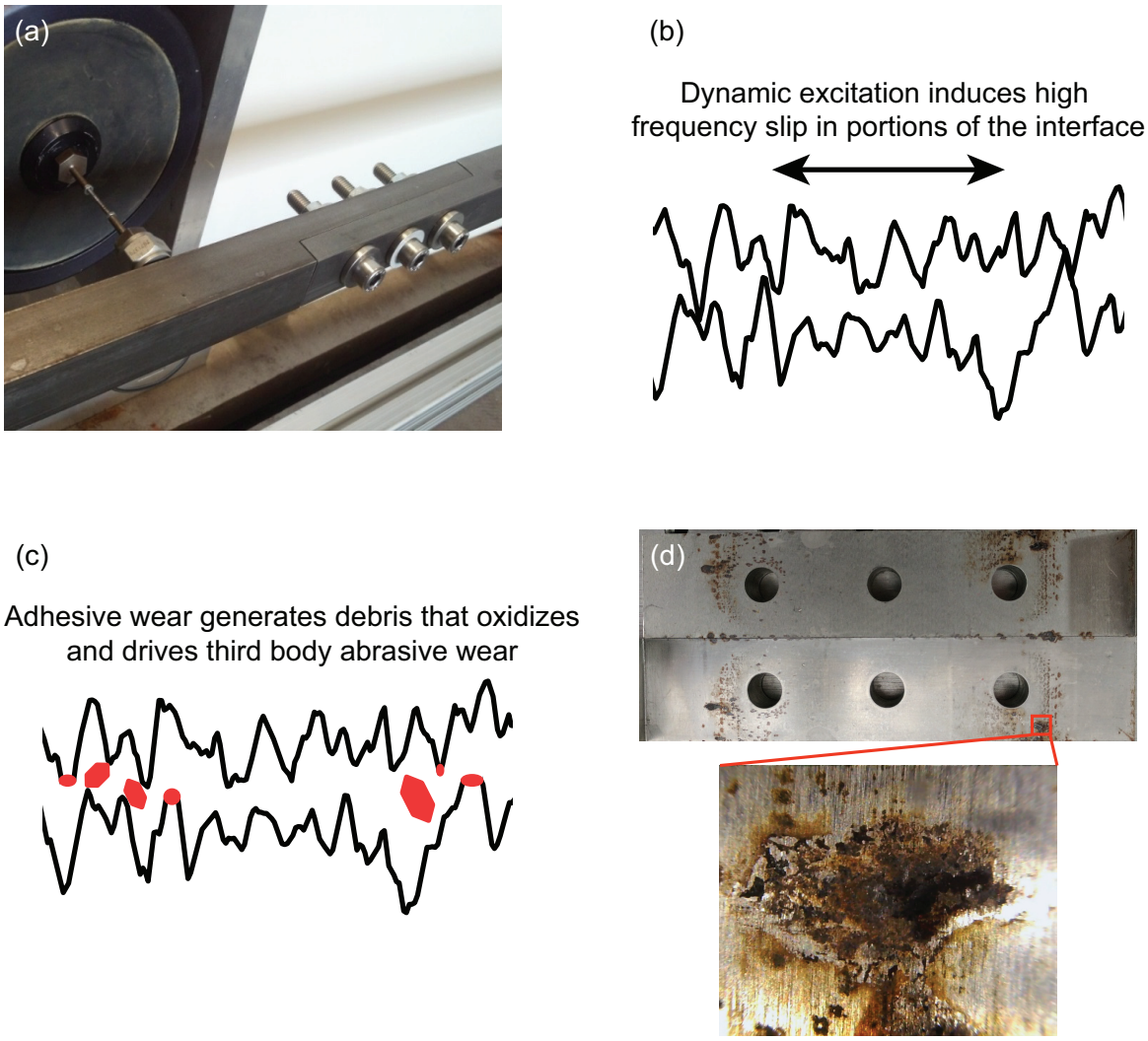


**Fig. 16:** An example of fretting showing (a) the assembled structure and excitation source, (b) illustration of asperity contact prior to adhesive wear, (c) illustration of third body abrasive contact due to oxidized debris trapped in the interface, and (d) photo of the interface showing fretting after excitation.

Often, fretting can result in a significant reduction of a material's fatigue limit (up to 70%) [461]. Fretting can be mitigated through redesign of the joint's geometry, introduction of residual stresses (such as via laser or shot peening, ultrasonic surface rolling, or cold expansion) [462, 463, 464, 465, 466, 467, 468], modification of the surface properties (e.g., through coatings or changes in the surface properties or texture) [469, 458, 470, 471, 453, 472, 473, 474, 475, 476, 205], and lubrication [477, 478]. Recent research has even shown that it is possible to choose metallic alloys that are able to grow a self-sustaining (self-lubricating) tribofilm during excitations within the fretting regime, which significantly reduces the harmfulness of fretting wear [475].

One common approach to understanding the domains where fretting may occur is through the use of a fretting map. There are multiple formulations of fretting maps, but a common theme among them is that they demarcate the loads that may lead to partial slip or gross slip, and within those domains the loads that may cause crack nucleation due to fretting [479, 480, 481, 482], as illustrated in Fig. 17. As indicated by the extensive region in which both fatigue and wear-based damage occur in Fig. 17, different sections of the contact patch can have different dominant damage mechanisms [483, 484]. This mixed regime, generally, is the most damaging regime for structural applications as cracks can easily form and propagate due to the multiple degradation mechanisms [485]. Some recent progress has been made in predicting the fatigue performance of structures exhibiting fretting. In particular, one approach has been through the use of analysis techniques developed to study short cracks [486, 487, 488].

Regardless of the source of wear, the ultimate goal of research within the wear community is a predictive model

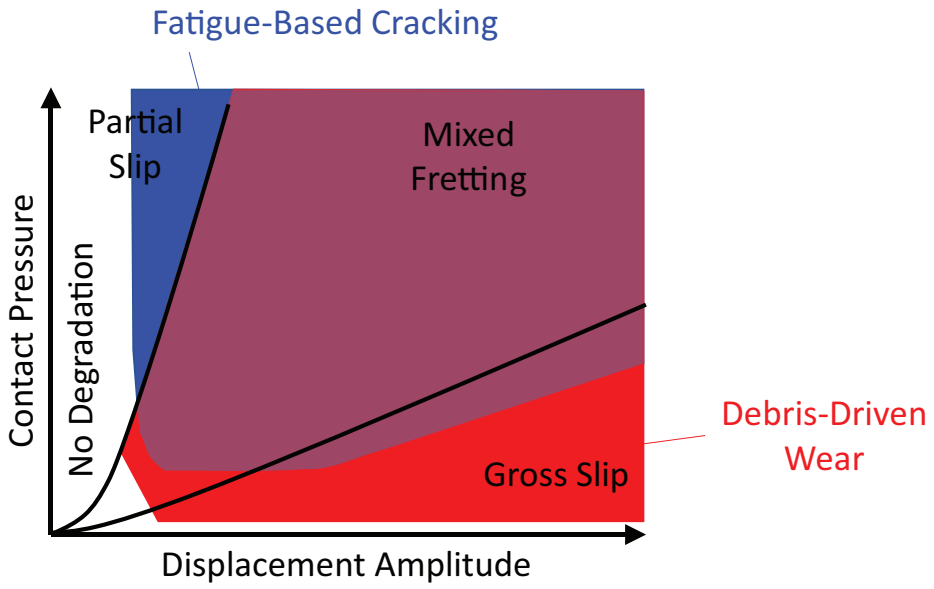


**Fig. 17:** Illustration of a material response fretting map, adapted from [481]. Blue indicates load-displacement regimes where fatigue-based cracking occurs; red indicates regimes where abrasive third body wear occurs; purple indicates regimes where both degradation mechanisms can occur.

of wear rates that is based on the properties of the tribosystem (i.e., materials, loading, and environment for the contacting surfaces). Some recent research even posits wear as being an atom-by-atom removal process that is attributable to stress-assisted chemical reaction kinetics [489]. Given the large number of unknowns due to the statistical (uncertain) nature of the interface, this is an ongoing research challenge [381].

**Challenge 10**: To derive a predictive model of wear rates for a specified tribosystem.

### 3.3.2 Archard's Wear Model and its Permanence

Even though no universal model of wear exists, an empirical formulation, known as Archard's wear model [490], has seen wide-spread use due to its ability to characterize wear throughout a number of different regimes and mechanisms. Archard's wear model was originally developed to study adhesive wear, but many subsequent studies have adapted it to abrasive wear as well. As a brief summary of the model, for two hemispherical asperities in contact with radius $a$, the contact area is $\pi a^2$. For a contact load of $P$, the mean contact pressure acting over this area can be related to the hardness of the softer material via

$$H = \frac{P}{\pi a^2}. \tag{28}$$

When the two asperities are tangentially loaded such that they slip a distance of $2a$, they lose contact. Archard's wear model assumes that there is a probability, $k$, that debris forms from this slip event, and that debris can be assumed to be a hemisphere of radius $a$ and volume $V = 2/3\pi a^3$. Thus, the wear volume per sliding distance traveled is

$$W = \frac{1}{3} k \pi a^2. \tag{29}$$

As $\pi a^2$ can be related to the contact load and hardness via Eq. 28,

$$W = \frac{kP}{3H}. \tag{30}$$

Since $k$ is an assumed constant, without loss of generalizability, $\kappa = k/3$, giving the wear volume for a sliding distance $s$ as

$$V_T = Ws = s\kappa \frac{P}{H}. \tag{31}$$

As Eq. 31 is an empirical formulation, the parameters identified from a given experiment are only applicable to that specific tribosystem. That is, the wear coefficient $\kappa$ measured from a pin-on-disc experiment is not generally applicable to a fretting experiment, even if the same materials and normal loads are used.

Despite its simplicity, Eq. 31 has found widespread support through experiments, particularly those focused on system scale applications (such as fretting in aeroturbines [491, 479]). In particular, the relationship of wear to hardness is strongly supported for plasticity dominated wear (e.g., adhesion and delamination) [164, 492, 493] and also for some regimes of abrasive wear [459]. Further, due to its simplicity, it is widely adopted throughout system modeling [494].

Archard's wear model does, however, break down in several regimes. In cases such as fretting, where oxidation leads to a hardening of the surface or the coefficient of friction significantly changes, it is important to account for this changing hardness in the wear calculations. For these situations, though, modified versions of Archard's wear model can be derived to account for changes in hardness (e.g., [158]), or changes in the coefficient of friction (e.g., [495, 479]) that are observed during fretting. Another area in which Archard's wear equation breaks down is with respect to materials with very fine grain structures. Similar to how the Hall-Petch effect (§2.3.1) shows a significant change in the material behavior around grain sizes of 10 nm, wear experiments show a significant deviation from Archard's equation for very small grain materials [154, 127]. This is partially attributable to a breakdown in the Hall-Petch effect for these grain sizes [496]. Given that even soft materials can have high wear resistance [497] (which contradicts Archard's model that relates wear resistance to hardness), an alternative quantity suggested to predict wear resistance is the ratio of hardness to elastic modulus [8].

Nanoscale wear experiments have elucidated several mechanisms that result in the apparent violation of Archard's equation (i.e., showing that as the hardness increases, the wear rate unexpectedly increases too in some regimes) [154, 489, 127]. One potential mechanism is the chemical mixing of the different layers of material near the wear surface (this is especially prevalent in thin films where the tribolayer, thin film, and bulk material of the substrate could all interact) [489, 127]. A second mechanism comes from the grain sizes evolving during wear. As observed in [154, 161], the grain sizes tend to evolve to a specific size for a given tribosystem (i.e., large grains shrink to a specific size and small grains grow to the same size). As observed in [154, 157, 161], wear could be categorized into different regimes for the same tribosystem – e.g., low cycle wear could be characterized by the mating of the two wear surfaces, medium cycle wear by the development of gradients in the grain sizes, and high cycle wear by the formation of a distinct coarse grain layer. More work is needed to understand the scale-dependence of wear, how it contributes to the prediction of a wear rate for a given tribosystem, and what the ramifications for macroscale applications are.

> **Challenge 11**: What is the scale-dependency of wear, its relationship to the Hall-Petch effect, and its ramifications for macroscale applications?

## 3.4 Lubricated Contact

The domain of lubricated contact is far more extensive than can be covered in this review[25]. However, some concepts are discussed here as a starting point for readers interested in learning more. In general, lubricants are typically an oil-based liquid (though sometimes a water-based liquid is used) with additives designed to affect the tribological properties. Additionally, solid lubricants [499, 223], such as graphene and $MoS_2$, or gaseous bearings (such as air) are also used. In all cases, the lubricants are intended to separate the contacting surfaces, reduce wear, and control friction. Additionally, some lubricants also inhibit corrosion, promote the formation of oxide layers, provide sealing, eliminate heat, remove debris, and reduce noise.

For non-solid lubricants, the frictional properties are described by the Stribeck curve [500, 501, 502], which is illustratively shown in Fig. 18. The Hersey number (also referred to as the Stribeck number)

$$\text{Hersey} = \frac{\eta v}{P}, \tag{32}$$

is parameterized in terms of the fluid viscosity, $\eta$, relative velocity of the two sides of the interface, $v$, and normal load, $P$. Higher Hersey numbers indicate thicker lubrication films and higher damping. For machine components, the vibration characteristics change significantly through the different regimes of the Stribeck curve. As described in [413], common characteristics of each regime (for industrial applications) include:

**Unlubricated** contact consists of relatively high frequency vibration and stress waves that include impact events. This regime is exacerbated by adhesive and fatigue wear that induce surface roughening.

[25] For a detailed review of lubricated contact in revolute joints and journal bearings, see [498].

**Boundary Lubrication** still consists of relatively high frequency vibration and stress waves, and still includes impact events. The vibration in this regime is exacerbated by abrasive wear, with significant surface roughening still. Further, the hydrodynamic forces are insufficient to separate the two surfaces that are in contact, the load is still primarily carried by solid-solid contact as well as boundary lubrication on the asperities, and the fluid lacks thin film damping effects. Boundary lubrication is dependent upon the role of the lubricant and surface chemistry to form a tribofilm.

**Mixed Lubrication** spans both elasto-plastic hydrodynamic lubrication and elasto-hydro-dynamic lubrication. The response of the surface, and its wear, is still significant in this regime, but viscous characteristics begin to emerge. Generally, over time, abrasive and fatigue wear lead to surface smoothing.

**Elasto-Plastic Hydrodynamic Lubrication** is a relatively new field of study in which the deformations of the surface are significant enough to drive both abrasive wear and fatigue wear. This regime can exist for both high loads ($P$) and low velocities ($v$), and can also occur if an interface is starved of lubricant (i.e., the lubricant is not replenished quickly enough during use).

**Elasto-Hydrodynamic Lubrication** still considers the deformation of the surfaces; however, deformation is limited to the elastic regime. The behavior of the lubrication is often described by Reynold's equation for hydrodynamic oil pressure build up. Typically, the film thickness is constant, which results in reduced vibration and friction.

**Hydrodynamic Lubrication** exists when the pressure within the lubrication film is sufficient to separate the two surfaces, resulting in a relatively thick film that exhibits fluid damping effects and minimal vibration. As with other regimes, the contamination of the lubricant with debris can increase abrasive wear.

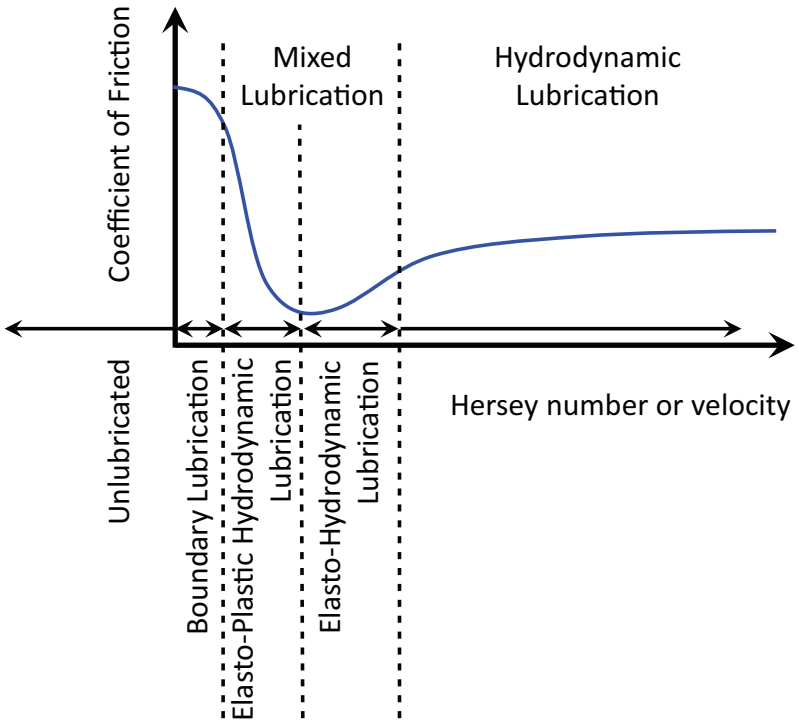


**Fig. 18:** Illustration of a Stribeck curve, with boundaries of dry friction, boundary lubrication, elasto-plastic hydrodynamic lubrication, elasto-hydrodynamic lubrication, and hydrodynamic lubrication indicated.

Across the regimes of both boundary lubrication and mixed lubrication (including elasto-plastic hydrodynamic lubrication [503] and elasto-hydrodynamic lubricaiton [504]), the deformation of the two sides of the interface is significant. At times, especially with boundary lubrication, the interface is insufficiently lubricated and solid-on-solid

contact still occurs. Even small amounts of lubrication, however, can significantly affect the contact properties of an interface – including the adhesion forces, contact area, and gap function – as liquid films can create a tensile force between surfaces [505].

The surface topography for boundary and mixed lubrication regimes is able to attenuate both friction and wear significantly if designed correctly [506, 434]. By patterning a surface with micro dimples, fluid resevoirs are created that can both promote the retention of lubricating film and serve as a trap for wear debris [507, 508]. These advantages hold even for unlubricated interfaces [509]. Due to changes in stiffness and damping in an interface, surface texturing can affect the vibration of a structure [510]. The optimal pattern for a surface texture is dependent upon the application, contact geometries, and operating conditions [434]; however, asymmetric textures, such as ellipsoids and chevrons, seem to offer improved load carrying capacity and friction reduction capabilities compared to spherical dimples[26].

While it has been demonstrated that surface texturing can improve the tribological properties for even unlubricated interfaces, an open research question is whether this will have an effect on fretting fatigue.

> **Challenge 12**: Can surface texturing be used to improve the tribological properties of unlubricated contacts, and if so, in what regimes will it be most successful?

## 3.5 Heuristic Modeling

Tribological models of wear and frictional processes typically result in very computationally intensive simulations (e.g., [511, 512]). In order to make the results of these simulations more tractable and applicable to study more general use cases (as opposed to the specific use case that they are first run on), heuristic modeling techniques are needed. Two exemplary heuristic models are Archard's wear model (§3.3.2) and Coulomb's friction model. These often-applied models have been used to fit the results of both simulations (i.e., as heuristic models) and experiments (i.e., as empirical models). In general, heuristic models are formulated for specific simulations. As an example, in [372] a cellular automata simulation of wear of a brake pad is established, from which a set of coupled differential equations is fit.

Data-driven modeling techniques, such as surrogate-based models [513, 514, 515, 516], have seen recent popularity for representing computationally intensive simulations with a relatively cheap model. In particular, machine learning techniques, which span a broad range of modeling approaches, have seen widespread adoption throughout the physical sciences due to their ability to discerning patterns within large data sets [517]. This widespread adoption has also included extensive research within the materials [518, 519, 520, 521], tribology [522, 523, 524, 525, 526], and structural dynamics [527] communities.

> **Challenge 13**: How can machine learning frameworks be leveraged to advance our understanding of the physics of friction, wear, and contact?

## 3.6 Overarching Challenges and Thematic Issues

The diversity of research areas within the field of tribology gives rise to many challenges for advancing the physical understanding of how surfaces interact. Inherent in many tribology studies are multiple categories of physics (such as solid interactions, fluids, heat transfer, etc.), and multiple damage mechanisms that can and do occur simultaneously. Thus, distinguishing the major contributing factors to the evolution of damage (and thus friction and wear) of an interface is a major challenge and research goal within tribology. In summary of the discussion throughout this section, there are several consistent themes:

- With a view of friction as a system rather than as a static parameter (i.e., $\mu$), several questions must be addressed to advance a new generation of models: What mechanics dominate frictional interactions in different regimes (e.g. acoustics, plasticity, etc.)? What model would be best to represent it? Can anything be learned from black box heuristic models that can advance our physical understanding of friction? What is the boundary of applicability for current models (such as Archard's wear model)? For cases where current models apply, can a predictive model for $\mu$ be developed?

- Many research areas in tribology focus on a specific application (e.g. the wear performance of a particular alloy). Is it possible for these narrowly defined projects to be incorporated into a larger effort by defining a set of best practices in experimental data to be collected such that the results can be directly added to the new

[26] This observation ties in well with the modeling and observations of elliptical contact, which is discussed in §3.1.1.

generation of Ashby maps? Is a new benchmark or reference measurement/system needed? Can data science help identify bridging mechanisms across the studies for more general application?

- The persistence of Archard's work is due to its usability. Instead of focusing on the breakdowns of Archard's work, can a new set of scaling laws motivated by Archard's work be used to explain how newer models could be extended to larger regimes?

Finally, as seen in the scale dependence effects between the nano- and microscales (e.g., the Hall-Petch limit and its influence on hardness), is there an inherent difference between macroslip and microslip? As friction is studied at the macroscale in structural applications, how relevant is data from tribological studies of friction and wear? A danger exists in over-applying the results of one type of wear test that involves gross slip to study the dynamics of a structure that only exhibits microslip. Thus, as friction is considered from the macroscale perspective, a closing challenge for the tribology community is:

> **Challenge 14**: Can new experimental benchmarks and tools be established to measure and assess microslip properties that are relevant to the frictional interactions observed within structures that exhibit no gross slip?

# 4 Macroscale Research in Contact Mechanics and Dynamics

In contrast to the (often) rigorous approach towards contact modeling at the tribological and materials scales, macroscale methods within the dynamics community often approximate contact with simplified functions in order to produce tractable models (e.g., coefficients of restitution or penalty stiffnesses) [528]. This modeling simplification was borne out of necessity in order to model contact within very large structures. Across a range of disciplines including aerospace [529], automotive [530, 531], tires [532, 533, 534, 535], granular materials [536], machine elements [537, 538], gears [539, 540], orthopaedics [541], and other multibody systems [542], design models can exceed millions of elements (often with element sizes kept coarse, such as 1 mm in length, to accommodate the large-scale nature of the structures), which necessitate upwards of 500,000 core hours for a single design study. Given that these models are applied to structures, it is infeasible to model every contact with sufficient resolution for convergence (e.g., in the finite element studies used to deduce the constitutive models for elastic-plastic contact, upwards of 1,000,000 elements have been used for a single contact pair [543, 176, 177]), especially given that there may be hundreds, or even thousands, of contact pairs throughout a structure [26].

## 4.1 Contact Modeling

In macroscale finite element software, there are multiple approaches to simulate contact. The choice of modeling approach can have significant effects on both fidelity and computational time. Some methods are based on physical models of contact (e.g., Hertzian contact), whereas other approaches are mathematical constraints that are imposed to prevent unrealistic penetration of the contact surfaces. Several of the common modeling methods and formulations are:

**Penalty Stiffness,** in which a piecewise linear spring is used to indicate contact. When the surfaces are out of contact, the stiffness is set as zero, and while in contact, a stiffness, $k_P$, that is usually orders of magnitude stiffer than the rest of the system is used as a penalty to prevent large displacements into a surface:

$$F_P = \begin{cases} k_P\delta & \delta > 0 \\ 0 & \delta \leq 0. \end{cases} \tag{33}$$

Dissipation with penalty stiffness models is usually handled by the addition of a linear viscous term of the same form as the contact model. Thus, the dissipative force, $F_D$ can be formulated in terms of a viscous damping constant, $c$, displacement into a surface (i.e., interference), $\delta$, and velocity, $v$, as

$$F_D = \begin{cases} cv & \delta > 0 \\ 0 & \delta \leq 0. \end{cases} \tag{34}$$

This viscous damping model is a modeling simplification (i.e., a linearization of the nonlinear phenomenon of friction) used for convenience and is not based on empirical observations.

**Coefficient of Restitution** is an instantaneous contact model whereby, upon contact, the velocity of the contacting point is instantaneously changed by the restitution rule. There are multiple definitions of the coefficient of restitution [252, 544, 545, 24] that are formulated in terms of the linear momentum, angular momentum, kinetic energy, velocity magnitude, or even the strain energy.

**Hard Contact** is a model used within finite element simulations that prevents any penetration of surfaces during contact events. This model tends to be overly stiff, especially if the underlying material models used do not account for plasticity.

**Lagrange Multipliers** are often used in analytical models as an additional constraint equation. In the context of contact, the Lagrange multipliers are physically interpreted as the contact force between two bodies. In practice, they can result in solutions that fall between a penalty stiffness model and a hard contact model as numerical methods can relax how strictly the constraint equation must be enforced.

**Augmented Lagrangian** methods are related to Lagrange multipliers; however, rather than adding an additional constraint equation, they seek to replace a constrained optimization problem with a series of unconstrained optimization problems (which are the Lagrangian of the original, constrained problem) coupled with a penalty term that resembles a Lagrange multiplier formulation [546].

**Constitutive Models,** such as described in §3.1, are used as point-wise contact models for simulations that do not consider the local deformation due to contact (either rigid body dynamics or flexible body dynamics in which contact is localized and deformations are negligible on the scale of the system).

**Hertzian** or elastic contact (i.e., Eq. 1; see also [21, 547]) is a special case of constitutive modeling that has no dissipation built into it. Some researchers have added dissipative terms either as a linear, viscous damping model or in a similar form to the Hertzian contact model. For example, $F_D$ could be expressed in terms of the loss modulus $\eta$ of the system as

$$F_D = \frac{4}{3}\eta\sqrt{r}\,\mathrm{sign}(v)\,\|v\|^{3/2}. \tag{35}$$

Contact and impact, by their very nature, are dissipative events. The energy dissipated by the different contact models, however, varies considerably. Without a dissipative term built into the contact models (such as for the penalty stiffness, Hertzian, some Lagrange-based methods, or hard contact), contact is reduced to an elastic event. The simplest approach to incorporate damping into a contact model is to add a linear viscous damping term in the same format as for the penalty stiffness model (i.e., Eq. 34). This approach, as shown by the dashed line in Fig. 19, results in a dissipation rate that is constant with velocity, just like a coefficient of restitution model [548, 25, 536]. Contact of real materials, though, often shows increasing levels of dissipation with velocity, and thus a coefficient of restitution model or a linear viscous damping model are non-physical. The Hertzian model with damping (Eq. 35, the solid line in Fig. 19) can be calibrated to nearly match the experimental data; however, the calibration is the tuning of a non-physical parameter and is thus non-predictive.

One further short coming of the coefficient of restitution model is that it assumes that contact is instantaneous [549]. In reality, contact durations extend over finite intervals (the length of which is highly dependent upon the material pairs), and can significantly affect the dynamics of a system that is aperiodic [548]. Early measurements of impacting systems, however, had insufficient resolution to show that impacts look more like a Haversine function than a delta function [550]. Historically, the coefficient of restitution was significantly more efficient than other contact approaches due to the assumption of instantaneous contact; more recently, though, the use of analytical constitutive models coupled with using a more relaxed contact condition (e.g., a penalty or augmented Lagrange method) has rendered the computational time to be equivalent if not faster than coefficient of restitution methods [544].

To address the non-physical nature of an instantaneous contact model, a dissipative force model for the coefficient of restitution was proposed by Hunt and Crossley [551, 552]. In their model, the contact force is composed of a conservative elastic force (e.g., Eq. 1) and a dissipative force (e.g., Eqs. 34 and 35)

$$F = K\delta^n + \eta\delta^n\dot{\delta}, \tag{36}$$

For $K = 4/3E^*\sqrt{r^*}$ and $n = 3/2$, the elastic portion of Eq. 36 reduces to the Hertzian contact model (Eq. 1). This model form has seen widespread adoption, and there have been multiple improvements to this model since it was

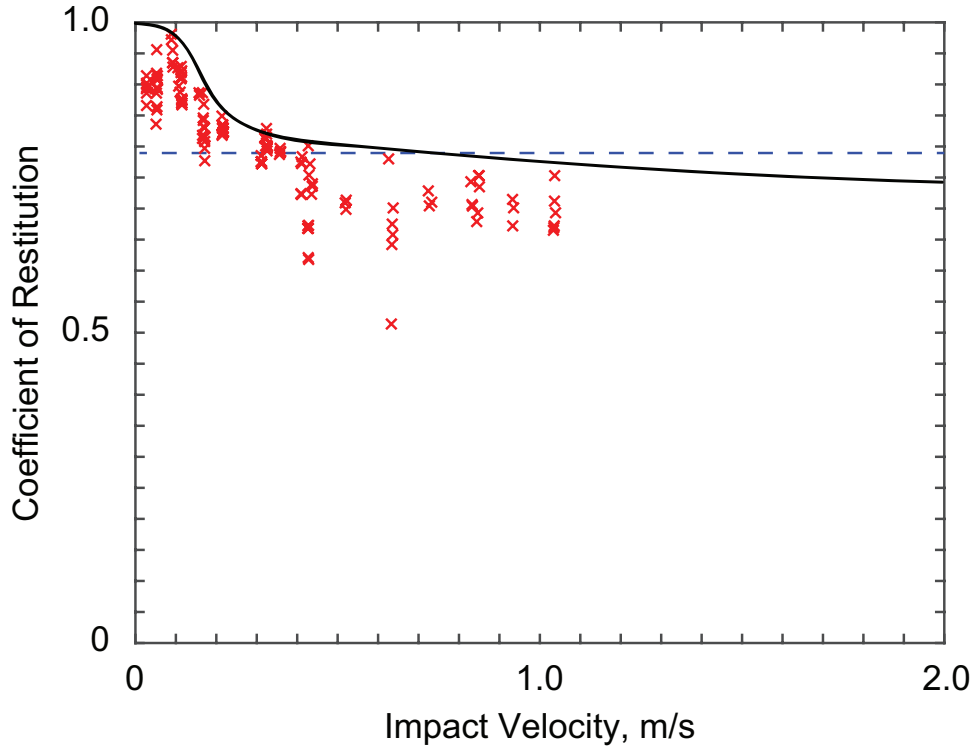


**Fig. 19:** Example of predictions using either a coefficient of restitution or a piecewise linear model (dashed line) and a Hertzian model with damping (solid line, Eq. 35 with $\eta$ tuned to match the experiments) compared to experimental data from [295] for Stainless Steel 304 impacted by work hardened Stainless Steel 440C spheres.

first published (e.g., see the review of [552]). In its original form [551], which gives similar results to the more recent models for low velocity impacts, the viscous coefficient can be expressed as

$$\eta = \frac{3K(1 - C_R)}{2v_0} \tag{37}$$

in terms of a given impact velocity, $v_0$, and prescribed coefficient of restitution $C_R$. That is, this family of contact models require the prescribed coefficient of restitution as an input, rather than being able to predict it like the elastic-plastic constitutive models described in [83]. The difference in these two modeling approaches is highlighted in Fig. 20, which compares the Hunt-Crossley model (Eqs. 36 and 37) to the elastic-plastic model of [24].

To make the comparison in Fig. 20, in addition to the material properties that are used to describe the elastic-plastic model, the Hunt-Crossley model is also prescribed the coefficient of restitution ($C_R = 0.75$) for the impact velocity of interest ($v_0 = 0.2$ m/s), which is in agreement with the data for oxygen-free copper reported in [295]. The load-displacement measurements for this specific specimen are unavailable at this load level and for this precise geometry, but measurements at lower loads and a smaller indenter (Fig. 20(b)) are similar to the shape of the elastic-plastic model. The contact forces predicted by the Hunt-Crossley (and similar) models are in stark disagreement with measured contact forces for metals and ceramics. While Eq. 36 may be appropriate for polymers and other visocelastic materials, this simplified modeling approach is inappropriate for metals, ceramics, and elastomers (e.g., see [240]).

To highlight the differences between several of the other contact models (in terms of the stiffness and satisfying the displacement constraint), a one degree of freedom (DoF) oscillator with a rigid stop located at a displacement of 4.0 from the equilibrium position was modeled. A static force was applied to the oscillator, which was initially at rest, and the contact with the rigid stop was modeled using a penalty stiffness, Lagrange multiplier, and an augmented Lagrange formulation, as shown in Fig. 21. In the penalty stiffness model, the parameter $\alpha$ was defined as the ratio between the penalty stiffness and the stiffness of the oscillator's spring. For values of $\alpha$ that are not significantly greater than the system's stiffness, excessive penetration of the rigid stop is observed. However, in order for the solution to converge in the stiffest cases, up to 149 iterations were needed. For the Lagrange multiplier (Fig. 21(b)), only nine iterations were needed for convergence, and none of the force levels exhibited penetration into the rigid stop

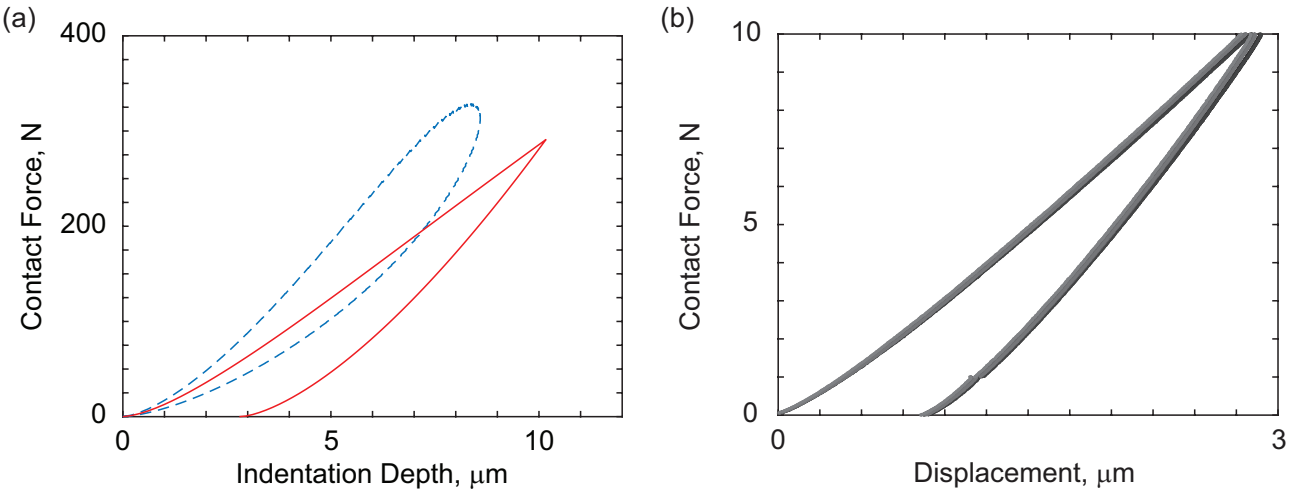


**Fig. 20:** For an Oxygen-free Copper puck being indented by a 440C work hardened Stainless Steel grade 100 sphere: (a) Comparison of the Hunt-Crossley contact model (blue, dashed line, Eq. 36, [551]) with the elastic-plastic contact model of [24] (red, solid line) for an impact velocity of 0.2 m/s (with a sphere radius of 1.1125 cm), based on measured data from [295], and (b) measured force-displacement behavior (also from [295]) for the same specimen indented by a 3.175 mm radius 440c work hardened Stainless Steel grade 100 sphere.

like the penalty stiffness model did. Lastly, the augmented Lagrange method is formulated with the same penalty parameter $\alpha$ as the penalty stiffness model. However, the additional constraint imposed for convergence of the method requires that $\alpha < 1$. As shown in Fig. 21(c), the method converges the fastest for values of $\alpha$ just less than 1.

In static implementations of these contact models, the penalty stiffness model is able to be solved with the fewest steps as it is equivalent to fixing a linear stiffness with magnitude controlled by $\alpha$. In the Lagrange multiplier formulation, the Lagrange multipliers appear as a linear multiplier for the constraint equations. The system of Euler-Lagrange equations will always contain the constraint equations and thus the minimizer will always satisfy the constraint. In this formulation, the Lagrange multipliers are additional unknowns in the system. Although this is a computational disadvantage in comparison to the penalty approach, the final solution, i.e. the minimizer of the Lagrangian, will exactly satisfy the constraints. Further, physical interpretations may be obtained for the Lagrange multipliers. Lastly, the augmented Lagrangian approach can be modeled using an inequality for the constraint condition. As shown in Fig. 21(c), this can result in numerical chatter for values of $\alpha \geq 1$. Finally, regarding the precise value for the stiffness, one commonality with these models is that the constraint equations can be rewritten in terms of a higher fidelity constitutive model (e.g., §3.1).

As an alternative to hard contact models (e.g., Lagrange multipliers) or penalty models (e.g., penalty stiffness or the augmented Lagrange method), constitutive models (§3.1) offer a higher fidelity, physics-based approach for modeling contact. These force-displacement constitutive models are often implemented using the same numerical methods as for other contact models (particularly the augmented Lagrange method). For example, constitutive models can directly replace the penalty term in a penalty model, allowing for a nonlinear model for the interfacial stiffness. The validation studies for these models (see §3.1.6) are typically conducted on stiff solids where the deformation due to contact is highly localized (e.g., a sphere, large block, etc.), and usually involve the contact between a sphere and a flat, or two spheres. In these situations, unlike for contact of a slender beam, the far-field deformation due to contact is negligible, and validation studies model the test specimen as rigid bodies with localized deformation described by the constitutive models.

## 4.2 Contact Taxonomy

Though many of the fore-mentioned studies model contact as between two spheres (or ellipsoids), the nature of contact varies dramatically based on the geometry of the contact interfaces [553]. Several different types of contact geometries are illustrated in Fig. 22, and the characteristics of these types of contact are summarized in Table 4.

Each of the different geometries discussed in Fig. 22 and Table 4 have very different contact properties. For instance, in Hertzian contact, the contact area increases with the load; whereas for receding contact, the contact area decreases with the load, and for complete and common edged contact, the contact area is independent of the load.

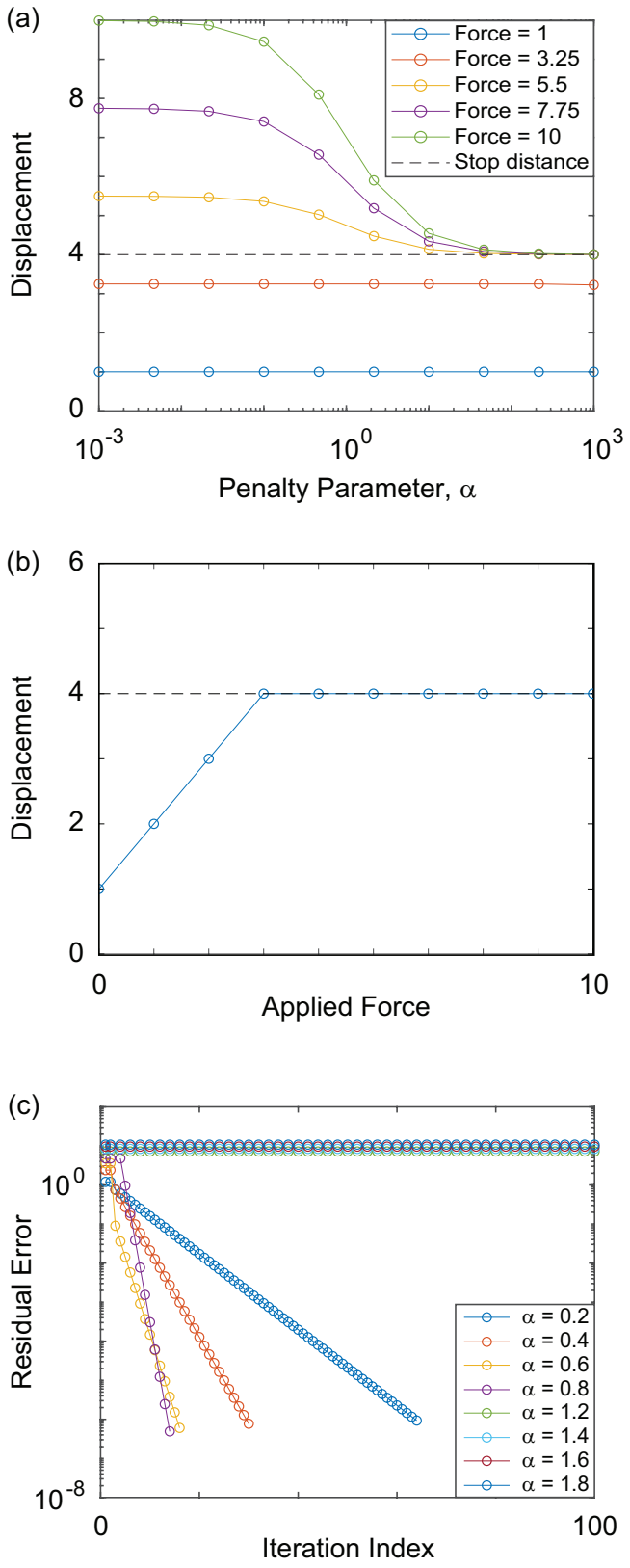


**Fig. 21:** Example of convergence for three different contact models: (a) penalty stiffness, (b) Lagrange multipliers, and (c) augmented Lagrange, showing the influence of the penalty parameter $\alpha$.

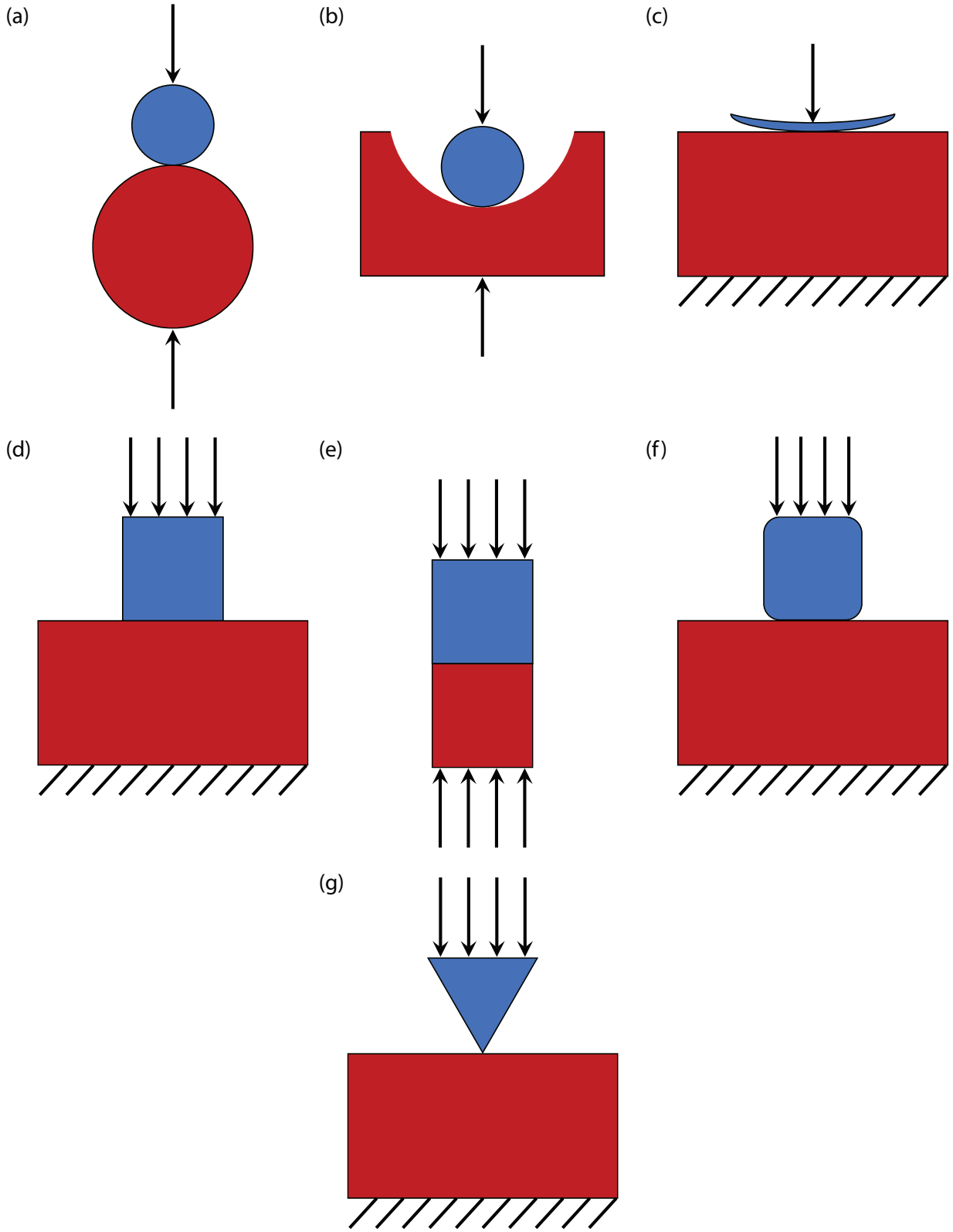


**Fig. 22:** Example of different types of common contact, showing (a) Hertzian (i.e., between two round or a round and flat surface), (b) pin-in-hole, (c) receding, (d) complete, (e) common edge, (f) flat and rounded, and (g) blunt wedges and cones. Figure based on Fig. 1.1 of [488].

| Contact Type | Load, Deflection, and Contact Area Characteristics | Pressure at Edge of Contact |
|---|---|---|
| **Hertzian [91, 21]** | As discussed in §2.1, the contact radius for spherical contact is related to the applied load via $a = (3/4Fr^*/E^*)^{1/3}$, which is often reformulated as $a = \sqrt{2r^*\delta}$; similarly, the displacement could be expressed as $\delta = a^2/r^*$; for elliptical or cylindrical contact, these relationships no longer hold, but the contact area does still increase with force | Zero |
| **Pin-in-Hole [554, 555]** | Similar to Hertz for small loads and contact angles; contact patch defined by geometry primarily | Zero |
| **Receding [556, 557, 558]** | Dependent upon the thickness of the thinner body, width of the applied load, and material properties; contact area is independent of applied load magnitude in most theoretical examples, but for more realistic loading cases may decrease with load magnitude | Zero |
| **Complete [13, 487, 559, 488]** | Contact area is independent of normal load; stress singularity at edges of contact is dependent upon material dissimilarity and angle of corner in contact (shown is a 90° corner in Fig. 22(d)); shear loading can cause separation | Infinite/Singular |
| **Common Edge [560, 561]** | A unique type of contact that has a finite and nonzero stress field at its edges; unlikely to occur in practice as small misalignments between the two bodies results in complete contacts | Finite, but nonzero |
| **Flat and Rounded [562, 563, 564]** | Contact area is weakly dependent upon the normal load; contact pressure tends to have high values near the edge of contact, but tends to zero at the contact edge itself | Zero |
| **Blunt Wedges and Cones [90, 4, 89]** | Load is related to contact radius via $F = 1/2\pi a^2 E^* \cot\alpha$. This incomplete contact has very high pressure at the tip, exhibiting a logarithmic singularity, and is very common in hardness testing. | Zero |

**Table 4:** Characteristics of different types of common contact.

Further, the stress state at the edge of the contact patch for complete contacts is singular in nature; while for Hertzian and receding contact it tends to zero, and for common edge contacts it is finite and non-zero. From the mechanics community, a contact is defined as complete if the contact area is independent of the applied normal load [488]. When complete contacts are subjected to shear loads, the contact area can decrease, but it can never increase. Incomplete contacts (specifically, Hertzian, pin-in-hole, and blunt wedges and cones) are non-conforming, with contact pressures at their edges going to zero, and contact area that increases with load. Receding contact typically occurs when the loads acting on the contact bodies do not fully span the length of the contact patch (as denoted in Fig. 22(c) by the point load on the top body; this is especially common in thin coatings [565] and contact of wires [566]).

## 4.3 Contact in Flexible Body Dynamics

Much of the previous research that has been highlighted here focused on the static or quasi-static contact between two bodies that are sufficiently large that the far-field of their domains can be described as fixed in some sense (e.g., clamped or fixed displacement). Within the vibro-impact community, though, contact between bodies can excite many vibration modes of a structure. In these cases, the bodies themselves are more likely to be deformed in their mode shapes than to be deformed locally by the contact event. In this sense, contact is considered elastic or a point force described by a pre-existing constitutive model. One challenge with structures subjected to vibro-impact is that they are nonlinear systems by definition, and can thus exhibit strongly nonlinear or even chaotic behavior [567, 568, 569].

Consequently, well-designed validation studies are a necessity for assessing models of vibro-impacting systems.

As discussed in §3.1.6, validation experiments can be categorically classified as direct or indirect. In direct studies ([297, 300, 302, 303, 304, 298, 301, 299, 295]), the force-displacement curve of the constitutive model is directly measured from a quasi-static indentation/flattening experiment; whereas for indirect studies ([305, 235, 306, 570, 318, 307, 308, 322, 295]), the coefficient of restitution from an impact event is measured. As a third category, an extensive set of validation data exists within the vibrations and multi-body dynamics community for looking at flexible systems with impact [550, 544]. Since these data sets convolute the material and structural response, they are not applicable to formulating constitutive models; however, they are essential for understanding how contact influences a structure's nonlinear response. Thus, they are paramount for the large range of applications that span both rigid body dynamics [544, 542, 41] as well as vibro-impact or flexible body dynamics [571, 550, 572, 573, 574, 548, 25, 575].

Since the publication of the seminal works of the early 1980s [576, 577, 578, 579, 580, 581, 582, 583, 584, 585, 586, 587, 588], there have been thousands of papers spanning the fields of vibro-impact and impact dynamics. Thus, for reviews of this topic, the reader is referred to [589, 567, 590, 591, 592, 569, 593, 594] for more information on impact oscillators. Notable papers during this time include:

- An investigation of the subharmonic and chaotic responses of impact oscillators [588];
- A critical assessment of the influence of preload and damping on vibro-impact [595, 596];
- The conditions for strange attractors, Hopf bifurcations, and invariant manifolds in impact dynamics [597, 598, 599, 600];
- The emergence of grazing impacts and chatter in flexible systems [601, 602];
- The application of nonlinear normal modes for studying piecewise systems [603];
- The use of random vibration to study jump phenomena [604]; and
- The influence of smoothing piecewise nonlinearities on the dynamics of vibro-impact systems [605].

More recent research has sought to integrate the constitutive modeling from the tribology community with flexible and rigid body simulations [606, 544, 548, 25, 607, 41].

## 4.4 Jointed Structures and Interface Discretizations

Recent efforts to develop more accurate, or even predictive, models of jointed structures have led to an increased emphasis of modeling contact across relatively large interfaces [26]. As a result, the state-of-the-art modeling of jointed interfaces has rapidly evolved from using a small number of large contact patches (often modeled with an Iwan model [30, 608, 609] for the tangential forces, and a hard contact or penalty contact model for the normal forces) to higher resolution models that are more consistent with physics [81, 610, 611]. Two primary sets of considerations for modeling jointed structures include the level of interface discretization and the salient physics included in a model [612].

There are four common, phenomenologically different approaches for discretizing a jointed interface: patch-wise models, point-wise models, thin-layer models, and modal models. These four modeling approaches are summarized in Table 5. For both patch-wise and point-wise models, the interface is typically modeled with a penalty stiffness. The major difference between these two classes of interface discretizations is the number of contact points between each surface. In the patch-wise discretization [219], typically a small number of patches (e.g., five) are defined on each surface. Patches that are opposite each other when the joint is mated together are connected via a virtual node with a spider or similar element (e.g., Fig. 23(c) and (d), see [614] for a derivation of a spider/RBE3 element specifically for jointed interfaces). By contrast, a point-wise model [36, 613, 55, 616, 617, 612, 618] requires a conformal set of nodes on both sides of the interface that are directly tied to each other, such as shown in Fig. 23(b). One consequence of requiring a conformal set of nodes is that often these models break down (at least in terms of accuracy if not more) once a node has displaced an entire element's length relative to its matching node on the opposite surface. As a hybrid between these two methods, another approach is the use of a coarsened interface that contains zero thickness elements (e.g., Fig. 23(e)). The zero thickness elements connect the two surfaces together with a set of elements that are superimposed on top of an existing mesh [32, 58, 81, 614, 610]. Forces from the zero thickness elements are transferred to the corresponding surfaces via a set of tractions, which are formulated to not require a set of coincident nodes on either surface. The constitutive model for both normal and tangential contact is implemented internally to

| Discretization | Description | Typical DoF | Example |
|---|---|---|---|
| Point-wise | Node-to-node contact in which conformal sets of nodes on two surfaces are tied together with a set of constitutive models to describe each DoF. Typically the normal DoFs are linear springs and the tangential are either Coulomb or Jenkins elements. The rotational DoFs are often ignored or not included in the model formulation. | 100s-1000s | Bograd et al., 2011 [613] |
| Patch-wise | A patch-to-patch formulation in which node sets from one side of the itnerface are connected to node sets on the opposite interface via a spider or RBE3 element (e.g., [614]). The constitutive formulations for the tangential displacements typically use hysteretic models as discussed in [342], and the normal DoFs typically use linear springs. | <100 | Lacayo et al., 2019 [609] |
| Thin-layer of elements | A separate, non-conformal mesh of thin (often infinitesimally thin) elements is introduced between the mating surfaces. Hysteretic or more advanced friction models are directly implemented in the constitutive behavior of the elements, and the normal behavior often includes a nonlinear contact model (e.g., Hertzian). | 100s-1000s | Balaji et al., 2021 [614] |
| Modal | The modal equations for the vibration of a structure are augmented with hysteretic elements for each individual mode. In this manner, the characterization of a mode's response is used rather than the response of the contact interface itself. | <10, depending on the number of modes of interest | Roettgen and Allen, 2017 [615] |

**Table 5:** Common types of interface discretization for jointed structures.

the zero thickness elements; in this manner, more sophisticated contact models are being employed for analyzing jointed structures, such as those based on rough contact theory (e.g., §3.1.4 or [619]).

In modal models, the hysteresis of the system is captured via modal hysteresis models that are calibrated for each mode individually [620, 621, 622, 623, 624, 615, 62]. These models are well-suited for modeling structures with weak nonlinearities (as they assume that the mode shapes do not change appreciably and that the modes do not couple), but do require calibration data – rendering them non-predictive. Implementations of modal Iwan models usually linearize the contact interfaces, relegating all nonlinearity to the modal hysteresis model [624]. A separate approach – modal substructuring (both experimental and analytical) – develops linear representations of a jointed system through modal analysis [625, 626, 627]. Like other modal models, the treatment of contact in modal substructuring approaches tends to be linear.

Regarding the salient physics included in a model (or lack thereof), earlier approaches for modeling jointed structures regularized the interface [608]. This typically took the form of a simplification that assumed that there were no normal kinematics, that the nonlinearity could be adequately captured by a hysteretic element, and that only a few hysteretic elements were needed to model the structure accurately[27]. These approaches typically necessitated intensive model updating exercises [609]. From recent experiments on jointed structures, though, it can be concluded that the previous method of regularizing the interface and using a coarse mesh is not feasible for developing a predictive framework. Instead, models of jointed structures must account for:

[27] For a review of hysteretic elements used in joint mechanics, refer to [342].

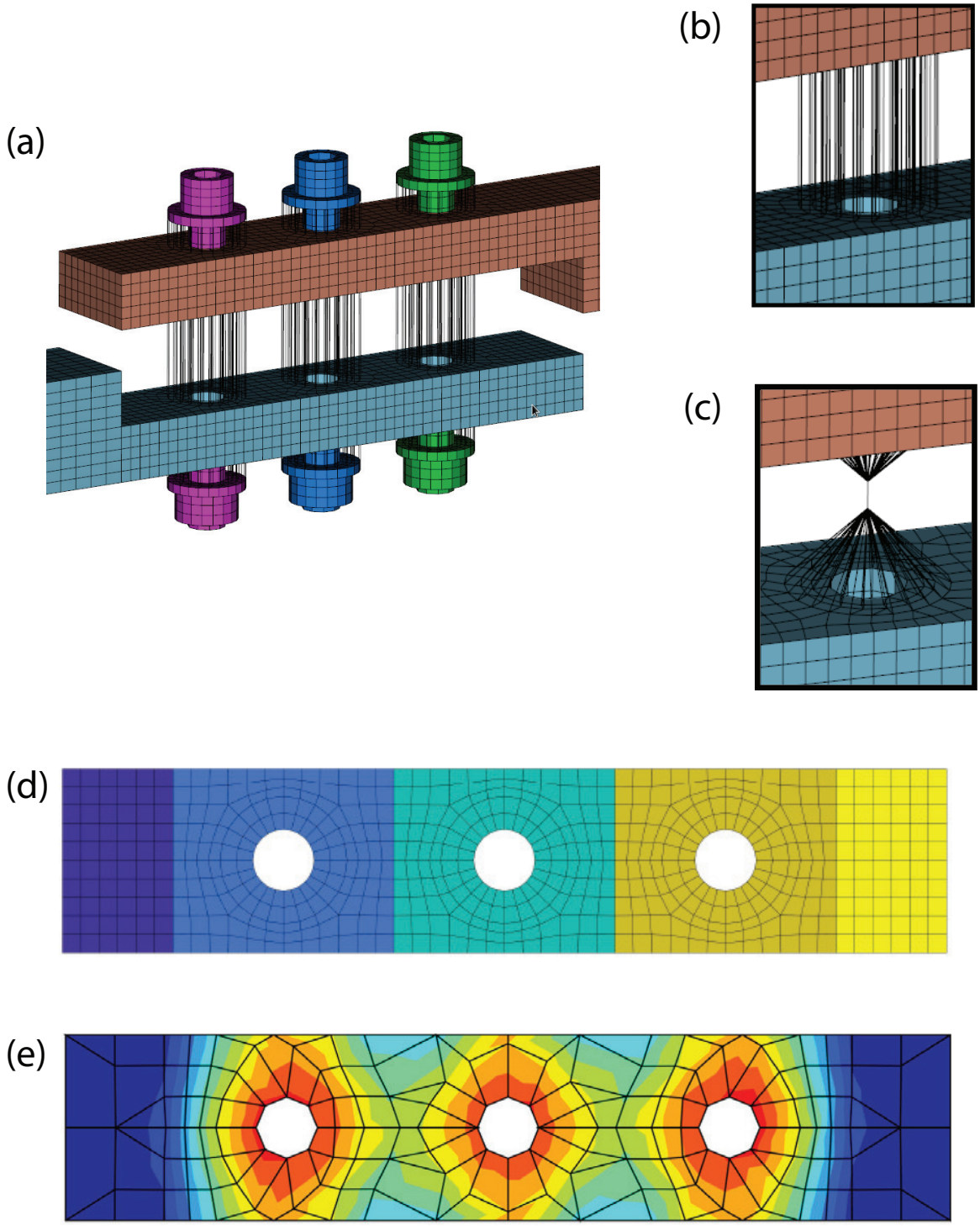


**Fig. 23:** Examples of different discretization methods for a jointed structure, showing: (a) the entire interface, (b) an example of node-to-node contact modeling in which nodes are directly connected to each other (only a subset of the tied together nodes are shown for clarity), (c) an example of a virtual node with a spider element, in which patches are connected to each other, (d) the full mesh on the interface with different patches defined by the different colors (in this case, there are five discrete patches), and (e) a hyper-reduction formulation for a zero thickness element implementation in which a coarse mesh of zero thickness elements is lain atop the original (or reduced order model) interface mesh.

- Contact patches that vary in size and pressure distribution over time [221];

- Separation of the contact interfaces over each period of excitation [378, 628];
- Significant tangential motion, including macroslip, even at low excitation amplitudes [378];
- Energy dissipation due to impact events [378, 628];
- Mode coupling [629, 630];
- Receding contact (i.e., higher bolt torques lead to lower contact areas) [221];
- Asymmetrical behavior across the interface, determined by the mesoscale topography [378, 628, 221]; and
- Pressure cones that are as small as zero degrees [378].

Additionally, the mesoscale and interfacial geometry of the interface significantly influence the contact pressures [631]. Further, new techniques to interrogate the nature of the contact patch using ultrasonic methods are now available [632, 633], which promise to provide even more data for hypothesis testing and model validation. Once these physical observations are reconciled within a modeling framework, it is shown that simulation results have the potential to be predictive in the near future – provided that an accurate normal contact model is used (that accounts for both the microscale topography in which asperities are ellipsoidal and the mesoscale topography that is formed from the manufacturing process and residual stresses) [81, 610, 611], and that the bolt preload is controlled for instead of bolt torque [634, 81][28]

### 4.4.1 Wear of Jointed Structures

Several open questions still exist for modeling contact and the physics of a jointed structure, chiefly the role of wear. Fretting is commonly observed in jointed specimen [635, 636, 26, 384, 637]; however, the extent, necessary conditions, and evolution are still unknown. Further, the role of other types of wear, especially fatigue and those related to plastic damage, are unknown though their effects have been observed [637].

To illustrate the complexity of wear in jointed structures, three nominally identical beams (i.e., fabricated from the same lot of material with the same dimensions, though differences likely existed in terms of the mesoscale topography from machining and surface roughness from polishing) were studied (see Fig. 24 for the measured natural frequencies and Fig. 23 for a model of the interface) [637]. The first beam (dashed black line in Fig. 24) was subjected to only impact hammer testing. Following a high magnitude impact hammer test (approximately 15 kN), a significant and permanent decrease in natural frequency was observed (of approximately 17.5%, corresponding to a 30 Hz decrease). The second beam (dotted blue line in Fig. 24) was subjected to only low amplitude shaker tests, and exhibited no significant changes in its linear natural frequency[29]. The third beam (solid, red line in Fig. 24) was subjected to both impact hammer and shaker testing. Over the lifetime of this beam, its natural frequency was observed to decrease by over 10%. When all three structures were unbolted and the individual beams (i.e., one half of the jointed system) were tested in isolation, the natural frequencies of these linear systems stayed constant throughout the entire test campaign. From studies such as this one, it is clear that wear can significantly influence the contact properties of an interface without modifying the properties of the bulk material. The precise mechanisms for wear, though, vary. In the first beam, wear is driven by extensive yielding across the interface. In the third beam, significant fretting wear was observed.

These observations yield several questions: what are the precise mechanisms of wear in jointed structures? Is it possible to identify and design for mechanisms that can initiate or exacerbate the wear behavior? Additionally, how can these wear mechanisms be incorporated into modeling efforts for jointed structures? One approach was postulated in [384], in which the hysteresis model for the interface was convoluted with a wear function that governed how the contact parameters evolved over time. This approach, though, is a best fit to data and is not suitable for prediction. Since predicting wear is a grand challenge within the tribology community, it will also be a formidable challenge for studying how jointed structures change over time.

> **Challenge 15**: What are the different wear mechanisms that occur in different categories of joints, and what are the conditions necessary to initiate and propagate wear?

[28] The observed variability in strain of bolts torqued to a nominal level is considered one of the greatest sources of experimental error in existing measurements.

[29] Here, linear natural frequency refers to the natural frequency measured at very low excitation levels where the joint is assumed to be inert.

## 4.5 Tribomechadynamics

The majority of macroscale modeling approaches are based in either solid mechanics or structural dynamics. These approaches, though, neglect the effect of wear and the bulk of tribology-based research on friction and contact at small length scales. The field of tribomechadynamics [26, 638] was defined to bridge this gap and to emphasize the need for modeling approaches that combine tribology, mechanics, and dynamics. Early tribomechadynamic modeling approaches [639, 640] originated as members of the tribology community including elements of structural dynamics in models used to study the health of machine elements. Since the term tribomechadynamics was first used [638, 631], it has become a new approach for structural dynamicists to enhance their model fidelity by incorporating elements of tribology and contact mechanics. This has led to multi-scale models spanning applications as diverse as joint mechanics [641, 631, 384, 188, 81, 637, 618, 642, 643, 644, 614, 221, 610], belt drives [645, 646, 647, 648, 649], aeroturbines (and underplatform dampers in particular) [650, 617, 651, 652, 653, 654, 655, 656, 657, 633, 658, 659, 660, 661, 662, 663, 664], rigid body dynamics for robotics [41], biomedical applications [49], and violin bow-string interaction [665].

In particular, the use of tribomechadynamic modeling frameworks for jointed structures has led to a drastic improvement in predictive capability for jointed structures. Before the deliberate integration of tribomechadynamic modeling strategies, the benchmark for blind predictions of the nonlinear dynamics of a jointed structure was 25% error in predictions of stiffness and predictions of damping within two orders of magnitude [608]. Due in part to improvements in reducing experimental error for measuring the properties of jointed structures [631, 637], tribomechadynamics-based models of jointed structures have been demonstrated to predict the behavior of a jointed structure blindly (i.e., without calibration data) to within 1% for stiffness and damping [81, 611]. This improvement in modeling is largely due to the insights gained from the recent experimental observations (§4.4) [378, 628, 221, 629, 630], and the reconciliation of both an improved treatment of the local kinematics of the joint as well as improved contact and hysteresis models (such as accounting for both plasticity and that asperities are elliptical instead of spherical).

The ultimate goal of tribomechadynamic analyses is to model (and optimize) an entire structure in a predictive

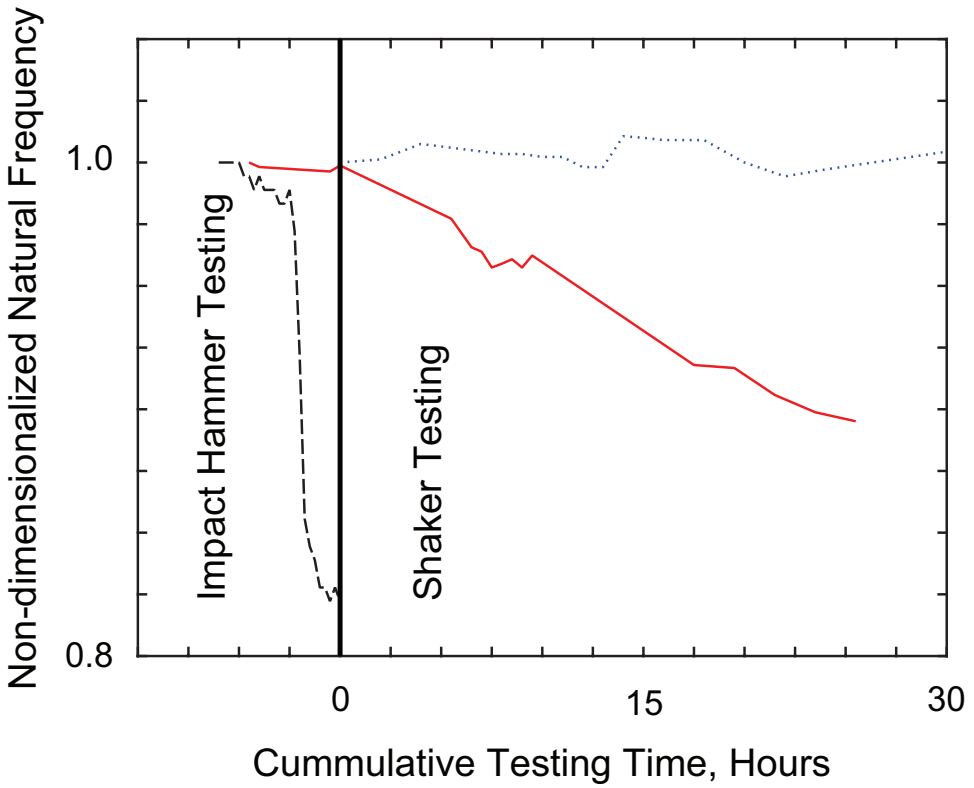


**Fig. 24:** Degradation of the linear frequency of three nominally identical jointed beams. The beam with frequency reported by the black dashed line only experienced impact hammer tests. The beam with frequency reported by the red solid line experienced both impact hammer and shaker testing. The beam with frequency reported by the blue dotted line only experienced shaker testing. Adopted from [637].

manner (i.e., without calibration data). To accomplish this goal, several challenges exist. First, in order to assess the lifetime performance of a structure, and how it degrades with wear, a rigorous treatment of wear in tribomechadynamical models is needed (see Challenge 15). Second, new techniques to scale tribomechadynamic models up to study an entire assembly are needed. To date, the majority of tribomechadynamic analyses have focused on relatively small systems that contain only a few joints at most. As these analyses typically have 100s to 1000s of DoFs per interface, this is not a tractable solution for structures with 100s or 1000s of interfaces.

> **Challenge 16**: What types of mutli-fidelity analyses will be necessary to scale tribomechadynamic models to study large assemblies?

In order to address this challenge, the author proposes that a multi-fidelity modeling approach is needed. For typical structures, there only exists a small number of unique types of joints. Based on the concepts of the surrogate system hypothesis [219], each of the different types of joints can be modeled via a predictive modeling framework to generate data that a calibrated model could be fit to [610]. These calibrated models could then be used to to simulate the dynamics of an entire structure in an efficient method, as summarized graphically in Fig. 25.

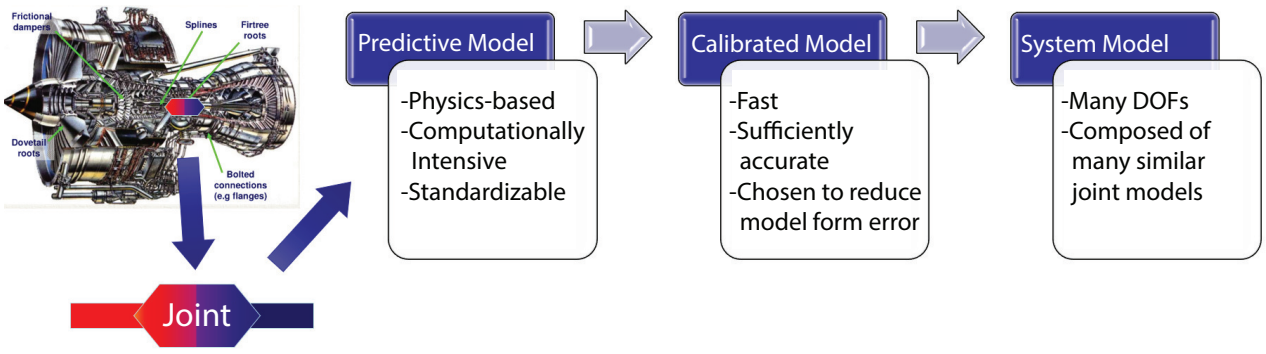


**Fig. 25:** Proposed multi-fidelity approach for applying tribomechadynamics to an entire structure. Engine image courtesy of Rolls Royce.

What still must be addressed, though, is the efficient simulation of large structures. This will necessitate further advances in reduced order models. There are a number of promising techniques already available: hyper reduction [666, 614, 667], modal derivatives [668, 669], and dictionary-based machine learning strategies (i.e., to preserve the physical interpretability of the results) [670, 671, 672]. Additionally, transient and random vibration simulations of these structures necessitate multi-scale simulations in time as typical applications (e.g., launching a satellite) necessitate minutes of excitation to be simulated. Some recent progress to extend existing transient methods has been made [673], but the efficacy of this and other approaches for studying the random vibration of a large, assembled structure with many joints has yet to be demonstrated.

Time integration methods, in particular, are significant limitations for modeling jointed structures. As a result, most of the recent modeling efforts have focused on steady-state [55, 56, 57, 58, 59] or quasi-static [60, 61, 62, 63] modeling methods as these are more efficient approaches to studying the hysteretic properties of a jointed structure. To assess the effects of random vibration, shock, or other transient events, time domain methods are paramount. Most existing joint models rely upon standard integration schemes, such as detailed in [674]. There have been many recent improvements to these algorithms, such as IMEX schemes [675, 54], which combine implicit and explicit methods into a single algorithm, adaptive time stepping for non-smooth dynamics (including contact and friction) [676], contact detection algorithms to allow for an expanded use of large time steps away from contact [677], combination of the time integration scheme with the augmented Lagrangian method for the contact model [678, 679], and applications of energy conservation to formulate more efficient schemes [680, 681, 682]. Much of the recent work has focused on multibody dynamics, which often consider rigid bodies instead of flexible bodies. This raises the question: if time integration methods were developed specifically for the contact of deformable bodies, would these algorithms be able to benefit from the knowledge of the nonlinear mode shapes of the assembled structures?

> **Challenge 17**: Can knowledge of the nonlinear mode shapes of jointed structures be used to devise a more efficient time integration strategy that is suitable for transient and random vibration analysis?

The next major challenge to be addressed is the influence of multi-physics. It is well known that the hysteretic and wear behavior of a joint changes dramatically with temperature [683, 684, 685, 686, 687]. Further, structures themselves also exhibit significant dependency on temperature [688, 689]. However, it is unknown how these effects couple.

**Challenge 18**: How do the effects of temperature on joint mechanics and structural dynamics couple?

These problems are further exacerbated by the existing studies on how friction and wear evolve with temperature being out of context. For instance, measurements of the wear properties is typically done with a sphere-on-flat or a flat-on-flat contact patch without consideration for the dynamics of the structure that it is attached to. Consequently, the measured hysteretic properties for materials going into an interface are significantly different than the hysteresis measured in the context of the actual application.

To demonstrate this, Fig. 26 shows the measured hysteresis for the Brake-Reuß beam (detailed in [26, 631]), and from a fretting rig (detailed in [384]) for test specimens fabricated from the same lot of material. While these two data sets are not directly comparable, due to the excitations being significantly different and the quantities measured not being the same (e.g., the acceleration and force measured for the jointed beam are from the impedance head where the shaker is attached to the system, whereas the quantities for the fretting rig are more direct measurements of the force and acceleration across the interface), their qualitative comparison highlights several significant differences in the measurements of hysteresis.

Even though the materials are identical in the two experiments, the measured hysteretic properties differ significantly. Over the first four hours of testing for the Brake-Reuß beam (Fig. 26(a)), the evolution of the system-level hysteresis is shown; as the system incurs wear, the natural frequencies of all of the modes *decrease* as the system softens [30], and higher harmonics are evident in the hysteretic measurements (Fig. 26(b) for hours seven and eight of testing). As the system wears further (Fig. 26(c)), these higher harmonics go away as the conditions necessary for modal coupling are no longer present (e.g., see [629, 630]). By contrast, the hysteresis measured by the fretting rig (Fig. 26(d)) *stiffened* with wear and exhibits a much simpler hysteretic behavior that can be adequately captured by a Bouc-Wen or Iwan model [384, 342].

Inherent in the measurement of Fig. 26(d) is that the tribosystem of the fretting rig experiment consists of an (approximately) constant normal pressure and gross sliding sufficient to expel debris from the interface. In the wear studies of the in context behavior of a jointed structure (i.e., the hysteretic behavior of Fig. 26(a)-(c)), the contact pressure across the interface varied significantly with time (going to zero at the edges, and varying by up to 20% in the center of the contact patch [221]), and there was insufficient motion to expel any debris from the interface. As a result, the wear mechanisms present in the two different experiments are not the same. It is possible that the hysteresis of the system (i.e., Fig. 26(a)-(c)) could be expressed as a combination of hysteretic elements similar to those measured in Fig. 26(d) that are implemented discretely across many patches within the interface (e.g., Fig. 23(e)). In this framework, each subsection of the interface would have a time varying contact pressure and locally evaluated hysteretic properties due to the mesoscale topography, distribution of asperities, residual stresses, and residual damage. It is unclear, though, if the hysteresis of the tribosystem measured in [384] (i.e., Fig. 26(d)) will be relevant to this type of modeling approach though.

**Challenge 19**: How can the hysteretic measurements of (out-of-context) fretting test rigs be related to the hysteresis measured in built-up structures?

## 4.6 Shakedown and its Relationship with Fretting

Often in systems that exhibit fretting, the effective coefficient of friction for the system can dramatically decrease over time until a stable value is achieved [457]. This process is often referred to as frictional shakedown [488]. Related to the concept of plastic shakedown [691, 692, 693, 694], which states that if a set of self-equilibrating residual stresses exists that prevent yielding for a body under cyclic loading, then the body will always settle into this stress state regardless of the initial conditions [488], frictional shakedown is defined as an interface achieving a steady-state condition in which no frictional dissipation occurs. For general frictional interactions, frictional shakedown is not as robust as plastic shakedown – i.e., it is not guaranteed that if a system can shakedown it will; however, it has been demonstrated that for uncoupled contacts (in which the tangential/slip displacements do not modify the contact pressure), shakedown will occur if it is possible [695, 50, 51, 696, 488]. Many parallels exist between fretting fatigue

[30] Here, softens is used in accordance with the nonlinear dynamics terminology, and is used to mean that the frequency, and consequently stiffness, of the system is decreasing as the excitation amplitude increases.

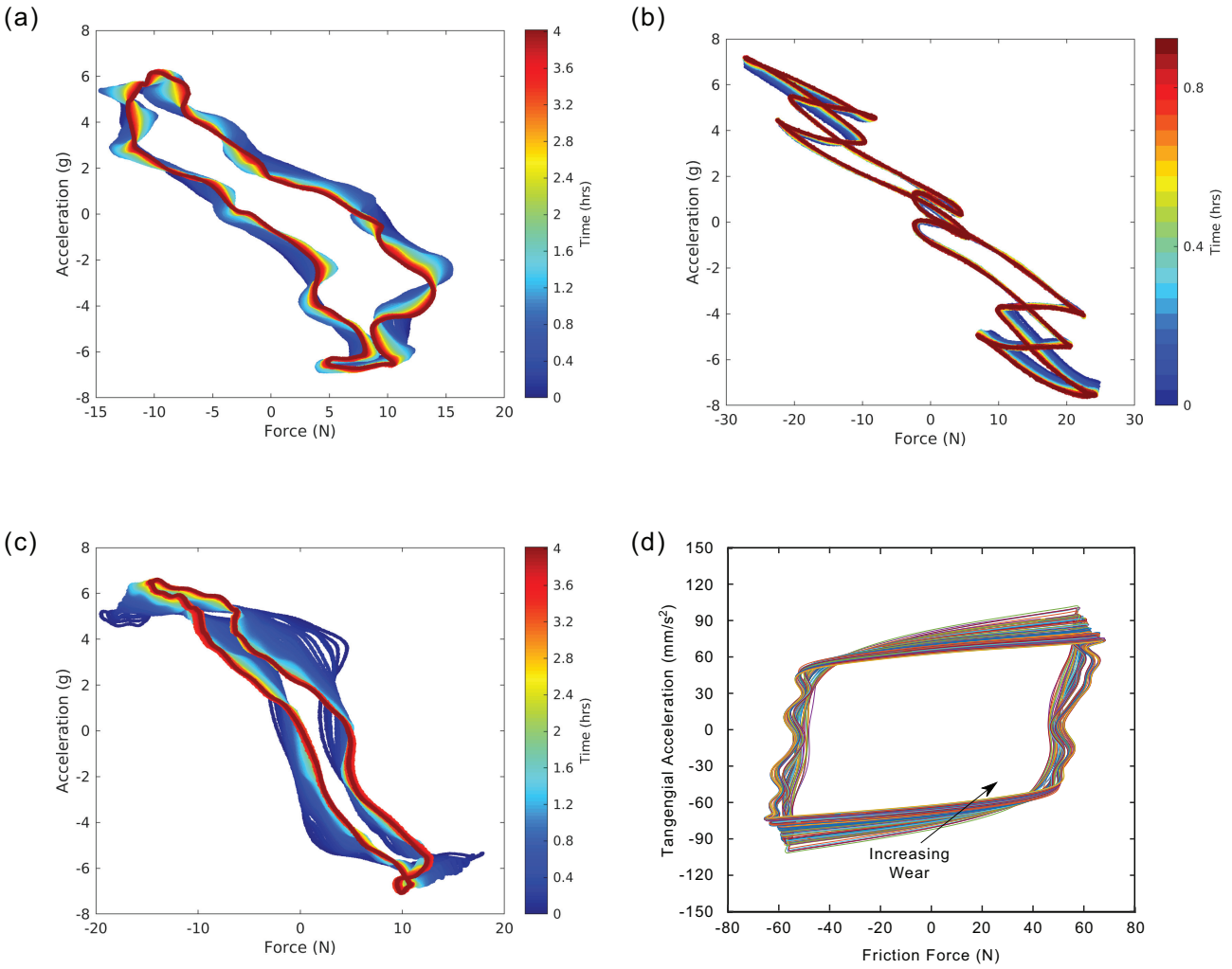


**Fig. 26:** Measured hysteretic behavior for the Brake-Reuß beam (a)-(c) [690] (the system is described further in [631], with excitation frequency near 150 Hz), and for a fretting test specimen that had a 1 mm$^2$ contact patch (d). All specimen were fabricated from the same lot of material. In (a), the measured hysteresis over the first four hours of fixed frequency shaker testing is shown, in (b) the measured hysteresis from the seventh and eighth hours are shown, and in (c) the measured hysteresis from hours nine through twelve are shown. In (d), the hysteresis loops from five hours of testing on a fretting rig (described in [384], with excitation frequency of 100 Hz) are shown.

and notch fatigue, which has enabled the literature related to plastic shakedown to be applied directly to understanding frictional shakedown and fretting [450, 697, 698, 699, 486, 13, 51].

Much like the hysteretic models used to study frictional interactions, frictional shakedown studies the role of the system's memory of previous frictional states [696] (e.g., such as the interactions between different asperities or, in the context of an Iwan model, the state of stretch and slip of the different springs in the parallel set of sliders used), and how these previous states influence a structure's ability to shakedown to a steady-state in which there is no frictional dissipation. To this end, several discrete states are able to be defined: unconditional shakedown, conditional shakedown, and dissipative [700, 701]. In the unconditional shakedown regime, it is guaranteed that the system will shakedown; whereas, for the conditional shakedown regime, there is no such guarantee, but it is possible for the system to shakedown. In the third regime, here termed dissipative, it is guaranteed that the system will never shakedown and will always dissipate energy over every cycle of cyclic loading. Understanding the bounds of these regimes can be extremely useful for designing a structure to avoid excessive wear. This is particularly important for studying applications that are concerned with fatigue, such as aeroturbines, which are designed to survive billions of cycles of loading.

A challenge in understanding the physics of fretting fatigue and frictional shakedown has been the extreme diversity of experiments. The lack of standardization has prevented insights on common benchmarks from being combined into a more comprehensive understanding of the physics of fretting [702, 485]. With the increased standardization of fretting rigs and improvements in experimental techniques, significant advances have been observed in the understanding of the physics of fretting [18].

> **Challenge 20**: In order to develop more fundamental insights into the physics of wear and fretting, standardized experiments and benchmarks are needed that will allow for synthesis of insights from across multiple experimental efforts.

### 4.7 Overarching Challenges and Thematic Issues

Much of the recent research at the macroscale involving contact is characterized by relatively simple models of contact. This is in sharp contrast to the recent progress within the materials and tribology communities. Often, piecewise linear contact models or static coefficients of restitution are used, which neglect the multitude of phenomena that can occur during a contact event. Research in the area of tribomechadynamics has shown that it is both possible and computationally feasible to include higher fidelity contact models for analysis of built-up systems. To summarize the discussion of this section, and to look forward at upcoming challenges, several themes are highlighted:

- One of the greatest areas for immediate improvement of macroscale modeling is the utilization of more accurate contact models. The second greatest area for improvement is in increasing the fidelity of modeling local kinematics in a reduced sense. This could be both in the form of model reduction theory or in terms of intelligent definition of contact patches in an interface.
- Many of the assumptions used in modeling jointed structures are incorrect. In order for a predictive modeling framework to be developed, more realistic assumptions are necessary. Modeling simplifications, though, are still suitable for calibrated modeling frameworks.
- The frontier of macroscale research, now that numerical methods have caught up with modeling, is to involve wear calculations in structural models. Thus, the next challenge is developing time (wear) evolving constitutive models for friction and contact. Once heterogeneous materials, such as from AM or the application of coatings, are considered, this problem becomes even less tractable.
- The multiphysics of contact in frontier applications (e.g., aerospace) involve several competing mechanisms interacting in manners that are unknown. Both experimental and modeling efforts are needed to better understand the effects of temperature and other deviations from ground-based experiments (e.g., the propensity for galling in space to be assessed) on the response of jointed structures.

To study elements of contact mechanics for a jointed structure in isolation, such as fretting in isolation, or, more specifically, the contact mechanics of a jointed interface, neglects the dynamics of the structure. While removing frictional dissipation from a system can improve the wear life of an interface, it results in an underdamped structure that will experience more severe vibration-related issues throughout. Consequently, this can unintentionally lead to shorter interface lives due to fatigue and wear driven by the increased system vibration. This highlights the importance of intentionally considering both tribological and dynamic issues simultaneously, which is the expressed purpose of tribomechadynamics.

## 5 Concluding Thoughts

Throughout this review, a number of overarching themes have been pervasive:

- Multi-scale methods (in both space and time), which incorporate the influence of phenomena as small as material structure on the response of macroscale structures, need to advance simultaneously with the improvement of models at all scales.
- A better understanding of plasticity (including the scale and geometry dependence of hardness) is needed and, consequently, of the rough contact of real surfaces.

- Friction is best thought of as a system of phenomena that are simultaneously contributing to the measured response of a structure, not as a (static) parameter.
- Wear is a multi-faceted phenomena that can lead to extremely different effects for a macroscale structure (e.g., galling versus fretting fatigue); while a predictive model does not exist, existing models can provide new insights for macroscale applications.
- The multi-physics of contact in macroscale applications is often neglected due to the challenge of modeling the mechanics of an interface in a predictive manner. With the increased role of frontier applications, though, this approach is not sustainable.
- The design of materials in contact for macroscale applications must include better understanding of both coatings and additively manufactured materials.
- Both consistent experimental methods with well-defined benchmarks and new experimental techniques to gain unprecedented insights into the role of contact are needed.

These themes can be categorized into four different topics: multiscale modeling, contact of real surfaces, extreme environments, and an improved connection between the design of a material and the design effort for macroscale structures. These themes are further expanded in the remainder of this paper.

## 5.1 True Multiscale

Tribology research is motivated by macroscale issues; however, it is inherently a meso- or microscale research area. Experiments that originate within the tribology community often relegate contact to well defined loads (e.g., point loads), not as time and area varying quantities as observed in interfaces measured at the macroscale. Further, when macroscale loads are used to inform the loading of a tribological study, the macroscale loads are often relegated to rigid body analyses that neglect the flexible body effects and local kinematics of interfaces. As a result, a persistent question is: 'how relevant are tribological experiments to structural applications?' As an example, fretting and wear studies are often conducted with a spherical or small contact in gross sliding with a constant normal load. However, fretting in structural applications typical involve a large interface that may have little to no gross motion and significant, time and spatially varying normal contact pressure throughout the interface. As a consequence, either theory to relate the existing experiments to realistic loadings or else improved experiments that consider realistic interface conditions are needed.

More broadly, as detailed models of contact and material behavior at small scales are advanced, new methods are needed to incorporate these into macroscale applications. The review of multiscale modeling techniques is beyond the scope of this article; however, existing techniques are either insufficient or not adopted. The challenge of multiscale modeling is exacerbated when an application such as a rocket launch is considered: for this type of application, the length scales of interest range from nanometers (to study the material's plastic response) to hectometers (e.g., the space launch system for the Artemis program by NASA is over 100 m in height), and the time scales of interest range from nanoseconds (to resolve contacts accurately) to minutes when transient or random vibration environments are considered. To tackle this challenge, there are numerous potential approaches: multi-fidelity modeling (i.e., where models from one scale are deliberately simplified as a modeling assumption), one-way coupled models (e.g., in which models of small scale effects are compiled into a heuristic model that is used to calculate the effects of a smaller length scale on a larger, but not vice versa), or, with significant investment, true multiscale that simultaneously couples the small and large scales permitting both to affect one another.

## 5.2 Modeling Contact of Real Surfaces

Real surfaces are not collections of elastic, hemispherical asperities. Instead, a typical surface contains ellipsoidal asperities that exhibit plastic responses well before plasticity is observed in the bulk of the substrate. Further, the concepts by Archard [264] – that real surfaces consist of protuberances upon protuberances and that the smaller scale asperities will crush and exhibit plastic deformations while the larger scale asperities are still exhibiting elastic responses – have proven true over time [267]. A second set of modeling assumptions that significantly changes the nature of contact is that two rough surfaces can be treated as a rough surface in contact with a smooth surface (i.e., see Fig. 11). This treatment neglects the many oblique contact interactions that occur within a rough interface, and likely stiffens the model of the interface [271].

These observations are further compounded when considering modeling approaches for joint mechanics. Often, normal contact is modeled in an elastic or linear (i.e., a penalty spring) manner. While elastic contact models are stiffer, overall, than elastic plastic (since plasticity softens an interface), the unloading portion of an elastic-plastic response curve is significantly stiffer than an elastic interaction (see Fig. 7), which is the more relevant regime for modeling a preloaded jointed interface. Taken together, these features can account for a significant percentage of an interface's stiffness. Serendipitously, though, a detailed knowledge of the microscale distribution of asperities is not needed as recent research indicates that statistical knowledge of the asperity features should be sufficient for predictive modeling [81, 611].

## 5.3 Extreme Environments

Many current frontier applications involve extreme environments (e.g., space, deep sea, hypersonic flight), which are characterized by extreme values in pressure and/or temperature. For many fields, structures are characterized and modeled at a nominal (room) temperature and pressure. However, the effects of the extreme temperatures and pressures significantly change the response of the material, interface, and structure [688, 689]. New experiments and theories are needed to investigate these extreme conditions. However, this necessitates a high financial burden that is in conflict with the recent industrial push for fewer experiments.

Examples of existing temperature and pressure testing systems are mostly limited to looking only at material or tribology, and often yield data that is out of context (e.g., Fig. 26). As a result, a fundamental understanding of how these out-of-context experiments can be related to the dynamics of a built-up structure must be developed. Extending this understanding to the study of temperature-related effects is paramount for meeting the challenges posed by frontier applications in hypersonics, space, and deep sea exploration, in which significant temperature variations are found throughout the operating life of a structure, both geometric and material nonlinearities can exist, and loadings can be unsteady due to fluid/structural coupling.

## 5.4 Designing Materials for Intended Responses

As discussed in §2.3.2, a wealth of information exists at the nano- and microscales on how coatings and nano-structured materials offer tremendous advantages for improving the contact mechanics and wear of an interface [703, 132, 410, 168]; however, this information is rarely adopted by system designers to design a structure optimally. Too often, questions – such as 'for a given material and application, what type of coating should be used?' – go unanswered. Two issues must be addressed to enable answers to questions like that. First, research must investigate how coatings influence the macroscopic properties of a structure, and second, design guides to select the optimal coating for a given structural application must be developed for (or be adopted by) the macroscale design community. These issues are often further exacerbated by tribologists not being engaged early in the design process, but rather only after things go wrong.

As a more sophisticated understanding of contact at the macroscale is integrated into best modeling and design practices, it is paramount that the vast amount of materials research be accessible. Previous leaps of applying the knowledge from material scales to system level design have resulted in huge, transformative advances. As an example, consider the Wright brothers: by using liners in their engines to prevent galling and seizing, this allowed them to fabricate their engine blocks out of aluminum instead of cast iron [704]. This change enabled their engines to be light enough for them to achieve the necessary lift for flight.

Like for the Wright brothers' plane, personalized manufacturing is becoming tenable for many engineering applications due to additive manufacturing. As highlighted in §2.4, the AM process creates parts with inherent variability in terms of structural properties. These need to be quantified/characterized and understood in order for meaningful design work to be done involving AM processes. The challenges associated with contact of AM parts in macroscale applications are significantly greater than just quantifying their role at the material level as the parts themselves introduce heterogeneity and uncertainty that typical macroscale analyses do not consider.

## 5.5 Summary of Challenges

Throughout this review, 20 challenges for contact modeling and experiments across scales were identified. Accompanying these challenges is the view that the research at each scale discussed needs to be informed of the ramifications of contact at other scales. For instance, a mesoscale analysis focused on improving the wear performance of an aeroturbine blade may result in a structure with significantly less damping that, in turn, increases the vibration amplitude and significantly reduces the life of the structure. These challenges, therefore, should be viewed in the

context of not just how research at each scale can be advanced, but how research from each scale can be used to better understand contact at other scales. The 20 challenges can be broadly grouped into several categories:

- New and accessible tools are needed for system level analysts to design structures with coatings, surface texturing, and surface conditions in mind from the start, not just as an *a posteriori* effort to understand qualification tests.
- Standardized experiments, benchmarks (intentionally spanning a range of different cases), periodic assessments of the state-of-the-art, and data reporting requirements are needed to facilitate the use of experimental results; too often, the data reported does not anticipate the potential needs of the research community.
- New approaches to relate experiments from one scale to models at a different scale are needed, particularly in trying to understand the complex set of phenomena that occur within interfaces of large, assembled structures.
- A more sophisticated understanding of wear in built-up structures, and modeling frameworks that are capable of assessing the degradation of a structure over time, are needed.
- While further research is needed to better understand plasticity and rough contact, the existing models of contact from the materials and tribology communities are more advanced than what is commonly used by the macroscale research community and should be adopted as tribomechadynamics demonstrates that these can be incorporated without incurring significant computational costs.
- The frontier areas of engineering (e.g., space, hypersonics, deep sea exploration) will necessitate significant advances in understanding contact mediated by extreme temperatures, pressures, and novel materials (such as additively manufactured parts).

# Appendix

## A Participants of the 2017 Contact Mechanics Workshop

Special thanks are given to all of the participants of the 2017 workshop, which spurred the critical discussion that served as the foundation for this paper. These participants included:

Alan Bowling, University of Texas Arlington
Ali Kolaini, NASA Jet Propulsion Laboratory
Andreas Polycarpo, Texas A&M University
Andrew Seagraves, Schlumberger
Ashwin Ramakrishnan, University of Houston
Ben Kubichek, GE Oil and Gas
BJ Fregly, Rice University
David Damm, Schlumberger
Fred Higgs, Rice University
Gagan Srivastava, Dow Chemical
Gangbing Song, University of Houston
George Pharr, Texas A&M University
Gocha Chochua, Schlumberger
Greg Davis, NASA Jet Propulsion Laboratory
Greg Sawyer, University of Florida
Hamid Ghaednia, Harvard Medical School
Jeff Rollings, Bruker
Jeffrey Streator, GeorgiaTech
Jesse Riha, GE Oil and Gas
John Bomidi, Baker Hughes
Jonatan Sierra-Suarez, Sandia National Laboratories
Julien Leclerc, University of Houston
Lee Peterson, NASA Jet Propulsion Laboratory
Mark Mcelroy, NASA Johnson Space Center

Matthew Brake, Rice University
Melih Eriten, University of Wisconsin Madison
Mike Nelson, Prepol
Ned Thomas, Texas A&M University
Nick Boechler, University of California, San Diego
Pascal Bellon, University of Illinois Urbana-Champaign
Patrick Sun, Rice University
Rob Flicek, Sandia National Laboratories
Satish Nagarajaiah, Rice University
Sharath Nair, Bruker
Somuri Prasad, Sandia National Laboratories
Tim Rupert, University of California Irvine
Yang Xu, Auburn University
Yu-Lin Shen, University of New Mexico
Zachary Cordero, Massachussets Institute of Technology

# B List of Challenges

The challenges, as defined throughout this review in the text, are repeated here verbatim in order to provide an accessible list:

**Challenge 1**: How does the hardness measured at one scale with a specific geometry relate to the hardness measured at a different scale and/or geometry?

**Challenge 2**: More, and more accessible wear evolution maps are needed to facilitate designers and application engineers selecting materials and their structure for interfaces.

**Challenge 3**: When considering the properties of a substrate, what are the optimal properties for a coating for a given application and environment?

**Challenge 4**: What is the fundamental relationship between indentation measurements and the plastic properties of hardness and fracture toughness?

**Challenge 5**: Can additive manufacturing processes be qualified to ensure consistent material properties from one part to another (including across different machines)?

**Challenge 6**: What are the effects of modeling simplifications on the prediction of contact between two rough surfaces? Which assumptions (e.g., representing the two surfaces as one rough and one flat, or using a statistical or fractal distribution of asperities) significantly affect the predictions of contact force and contact area, and which assumptions introduce minimal model form error?

**Challenge 7**: What mechanisms need to be in place to facilitate the periodic assessment of the state-of-the-art through the definition of research challenges for the community to engage in collaboratively?

**Challenge 8**: Papers that report experimental data must include a thorough characterization of the materials being tested in addition to the results from contact experiments for future modeling efforts.

**Challenge 9**: What are the mechanisms that contribute to frictional energy loss, and what are their relative contributions in different settings?

**Challenge 10**: To derive a predictive model of wear rates for a specified tribosystem.

**Challenge 11**: What is the scale-dependency of wear, its relationship to the Hall-Petch effect, and its ramifications for macroscale applications?

**Challenge 12**: Can surface texturing be used to improve the tribological properties of unlubricated contacts, and if so, in what regimes will it be most successful?

**Challenge 13**: How can machine learning frameworks be leveraged to advance our understanding of the physics of friction, wear, and contact?

**Challenge 14**: Can new experimental benchmarks and tools be established to measure and assess microslip properties that are relevant to the frictional interactions observed within structures that exhibit no gross slip?

**Challenge 15**: What are the different wear mechanisms that occur in different categories of joints, and what are the conditions necessary to initiate and propagate wear?

**Challenge 16**: What types of mutli-fidelity analyses will be necessary to scale tribomechadynamic models to study large assemblies?

**Challenge 17**: Can knowledge of the nonlinear mode shapes of jointed structures be used to devise a more efficient time integration strategy that is suitable for transient and random vibration analysis?

**Challenge 18**: How do the effects of temperature on joint mechanics and structural dynamics couple?

**Challenge 19**: How can the hysteretic measurements of (out-of-context) fretting test rigs be related to the hysteresis measured in built-up structures?

**Challenge 20**: In order to develop more fundamental insights into the physics of wear and fretting, standardized experiments and benchmarks are needed that will allow for synthesis of insights from across multiple experimental efforts.

## Acknowledgements

The author wishes to express his thanks to Zack Cordero, George Pharr, Robert Flicek, Nidish Balaji, and Michael Leamy for conversations about this manuscript and for the contributed images.

## References

[1] W. C. Oliver and G. M. Pharr. An improved technique for determining hardness and elastic modulus using load and displacement sensing indentations. *Journal of Materials Research*, 7:1564–1583, 1992.

[2] X. D. Li and B. Bhushan. A review of nanoindentation continuous stiffness measurement technique and its applications. *Materials Characterization*, 48:11–36, 2002.

[3] K. J. Van Vliet, J. Li, T. Zhu, S. Yip, and S. Suresh. Quantifying the early stages of plasticity through nanoscale experiments and simulations. *Physical Review B*, 67:104105, 2003.

[4] W. C. Oliver and G. M. Pharr. Measurement of hardness and elastic modulus by instrumented indentation: Advances in understanding and refinements to methodology. *Journal of Materials Research*, 19:3–20, 2004.

[5] N. Q. Vo, R. S. Averback, P. Bellon, and A. Caro. Limits of hardness at the nanoscale: Molecular dynamics simulations. *Physical Review B*, 78:241402, 2008.

[6] R. F. Cook and G. M. Pharr. Direct observation and analysis of indentation cracking in glasses and ceramics. *Journal of the American Ceramic Society*, 73:787–817, 1990.

[7] W. W. Gerberich, J. C. Nelson, E. T. Lilleodden, P. Anderson, and J. T. Wyrobek. Indentation induced dislocation nucleation: The initial yield point. *ACTA Materialia*, 44:3585–3598, 1996.

[8] A. Leyland and A. Matthews. On the significance of the H/E ratio in wear control: A nanocomposite coating approach to optimised tribological behaviour. *Wear*, 246:1–11, 2000.

[9] S. Suresh. Graded materials for resistance to contact deformation and damage. *Science*, 292:2447–2451, 2001.

[10] R. Saha and W. D. Nix. Effects of the substrate on the determination of thin film mechanical properties by nanoindentation. *Acta Materialia*, 50:23–38, 2002.

[11] A. Khalajhedayati, Z. Pan, and T. J. Rupert. Manipulating the interfacial structure of nanomaterials to achieve a unique combination of strength and ductility. *Nature Communications*, 7:10802, 2016.

[12] J. R. Barber and M. Ciavarella. Contact mechanics. *International Journal of Solids and Structures*, 37:29–43, 2000.

[13] C. M. Churchman and D. A. Hills. General results for complete contacts subject to oscillatory shear. *Journal of the Mechanics and Physics of Solids*, 54:1186–1205, 2006.

[14] M. Ciavarella. The generalized Cattaneo partial slip plane contact problem. I-theory, II-examples. *International Journal of Solids and Structures*, 35:2349–2378, 1998.

[15] D. A. Hills, R. C. Flicek, and D. Dini. Sharp contact corners, fretting and cracks. *Fracture and Structural Integrity*, 25:27–35, 2013.

[16] D. M. Mulvihill, M. E. Kartal, D. Nowell, and D. A. Hills. An elastic-plastic asperity interaction model for sliding friction. *Tribology International*, 44:1679–1694, 2011.

[17] D. M. Mulvihill, M. E. Kartal, A. V. Olver, and D. Nowell. Investigation of non-Coulomb friction behaviour in reciprocating sliding. *Wear*, 271:802–816, 2011.

[18] D. Nowell, D. Dini, and D. A. Hills. Recent developments in the understanding of fretting fatigue. *Engineering Fracture Mechanics*, 73:207–222, 2006.

[19] M. E. Kartal, D. M. Mulvihill, D. Nowell, and D. A. Hills. Measurements of pressure and area dependent tangential contact stiffness between rough surfaces using digital image correlation. *Tribology International*, 44:1188–1198, 2011.

[20] M. E. Kartal, D. M. Mulvihill, D. Nowell, and D. A. Hills. Determination of the frictional properties of titanium and nicekl alloys using the digital image correlation method. *Experimental Mechanics*, 51:359–371, 2011.

[21] K. L. Johnson. *Contact Mechanics*. Cambridge University Press, Cambridge, UK, 1985.

[22] R. L. Jackson and I. Green. A finite element study of elasto-plastic hemispherical contact against a rigid flat. *ASME Journal of Tribology*, 127:343–354, 2005.

[23] L. Kogut and I. Etsion. A static friction model for elastic-plastic contacting rough surfaces. *ASME Journal of Tribology*, 126: 34–40, 2004.

[24] M. R. W. Brake. An analytical elastic plastic contact model with strain hardening and frictional effects for normal and oblique impacts. *International Journal of Solids and Structures*, 62:104–123, 2015.

[25] M. R. Brake. The role of epistemic uncertainty of contact models in the design and optimization of mechanical systems with aleatoric uncertainty. *Nonlinear Dynamics*, 77:899–922, 2014.

[26] M. R. W. Brake, editor. *The Mechanics of Jointed Structures*. Springer, 2017.

[27] M. R. W. Brake. A reduced Iwan model that includes pinning for bolted joint mechanics. *Nonlinear Dynamics*, 87:1335–1349, 2017.

[28] R. Murthy, B. K. Choi, X. Q. Wang, M. C. Sipperley, M. P. Mignolet, et al. Maximum entropy modeling of discrete uncertain properties with application to friction. *Probabilistic Engineering Mechanics*, 44:128–137, 2016.

[29] N. Peyret, J. L. Dion, G. Chevallier, and P. Argoul. Micro slip induced damping in planar contact under constant and uniform normal stress. *International Journal of Applied Mechanics*, 2:281–304, 2010.

[30] D. J. Segalman. A four-parameter Iwan model for lap-type joints. *ASME Journal of Applied Mechanics*, 72:752–760, 2005.

[31] L. Gaul and R. Nitsche. The role of friction in mechanical joints. *ASME Applied Mechanics Reviews*, 54:93–110, 2001.

[32] S. Zucca, C. M. Firrone, and M. M. Gola. Modeling underplatform dampers for turbine blades: A refined approach in the frequency domain. *Journal of Vibration and Control*, 19:1087–1102, 2013.

[33] M. Krack, L. Panning-von Scheidt, J. Wallaschek, A. Hartung, and C. Siewert. Reduced order modeling based on complex nonlinear modal analysis and its application to bladed disks with shroud contact. *ASME Journal of Engineering for Gas Turbines and Power*, 135:102502/1–8, 2013.

[34] L. Gaul, J. Roseira, and J. Becker. Structural damping with friction beams. *Shock and Vibration*, 15:291–298, 2008.

[35] I. A. Sever. Experimental and numerical investigation of rotating bladed disk forced response using underplatform friction dampers. *ASME Journal of Engineering for Gas Turbines and Power*, 130:042503, 2008.

[36] E. P. Petrov and D. J. Ewins. State-of-the-art dynamic analysis for non-linear gas turbine structures. *Proceedings of the Institution of Mechanical Engineers, Part G: Journal of Aerospace Engineering*, 218:199–211, 2004.

[37] E. P. Petrov and D. J. Ewins. Generic friction models for time-domain vibration analysis of bladed disks. *ASME Journal of Turbomachinery*, 126:184–192, 2004.

[38] E. P. Petrov and D. J. Ewins. Analytical formulation of friction interface elements for analysis of nonlinear multiharmonic vibrations of bladed discs. *ASME Journal of Turbomachinery*, 125:364–371, 2002.

[39] Z. Kappassov, J.-A. Corrales, and V. Perdereau. Tactile sensing in dexterous robot hands - review. *Robotics and Autonomous Systems*, 74:195–220, 2015.

[40] A. Chatterjee, A. Rodriguez, and A. Bowling. Analytic solution for planar indeterminate impact problems using an energy constraint. *Multibody System Dynamics*, 42:347–379, 2018.

[41] A. Chatterjee, H. Ghaednia, A. Bowling, and M. R. W. Brake. Estimation of impact forces during multi-point collisions involving small deformations. *Multibody System Dynamics*, May 2020:1–46, 2020.

[42] M. Long and H. J. Rack. Titanium alloys in total joint replacement - a materials science perspective. *Biomaterials*, 19: 1621–1639, 1998.

[43] D. Zhao, S. A. Banks, K. H. Mitchell, D. D. D'Lima, C. W. Colwell Jr, et al. Correlation between the knee adduction torque and medial contact force for a variety of gait patterns. *Journal of Orthopaedic Research*, 25:789–797, 2007.

[44] D. Y. Li, A. Becker, K. A. Shorter, T. Bretl, and E. T. Hsiao-Wecksler. Estimating system state during human walking with a powered ankle-foot orthosis. *IEEE/ASME Transactions on Mechatronics*, 16:835–844, 2011.

[45] B. J. Fregly, T. F. Besier, D. G. Lloyd, S. L. Delp, S. A. Banks, et al. Grand challenge competition to predict in vivo knee loads. *Journal of Orthopaedic Research*, 30:503–513, 2012.

[46] M. I. Tiwana, S. J. Redmond, and N. H. Lovell. A review of tactile sensing technologies with applications in biomedical engineering. *Sensors and Actuators A: Physical*, 179:17–31, 2012.

[47] F. L. Litvin, A. Fuentes, and K. Hayasaka. Design, manufacture, stress analysis, and experimental tests of low-noise high endurance spiral bevel gears. *Mechanism and Machine Theory*, 41:83–118, 2006.

[48] N. Tala-Ighil, P. Maspeyrot, M. Fillon, and A. Bounif. Effects of surface texture on journal-bearing characteristics under steady-state operating conditions. *Proceedings of the Institution of Mechanical Engineers, Par J: Journal of Engineering Tribology*, 221:623–633, 2007.

[49] G. Han, U. Boz, L. Liu, C. Henak, and M. Eriten. Indenter-foam dampers inspired by cartilage: Dynamic mechanical analyses and design. *ASME Journal of Vibration and Acoustics*, 142:051113, 2020.

[50] J. R. Barber, A. Klarbring, and M. Ciavarella. Shakedown in frictional contact problems for the continuum. *Comptes Rendus Mécanique*, 336:34–41, 2008.

[51] J. R. Barber, M. Davies, and D. A. Hills. Frictional elastic contact with periodic loading. *International Journal of Solids and Structures*, 48:2041–2047, 2011.

[52] A. Thaitirarot, R. C. Flicek, D. A. Hills, and J. R. Barber. The use of static reduction in the finite element solution of two-dimensional frictional contact problems. *Proceedings of the Institution of Mechanical Engineers Part C: Journal of Mechanical Engineering Science*, 228:1474–1487, 2013.

[53] H. M. Hilber, T. J. R. Hughes, and R. L. Taylor. Improved numerical dissipation for time integration algorithms in structural dynamics. *Earthquake Engineering and Structural Dynamics*, 5:283–292, 1977.

[54] M. R. Brake. *IMEX-a: An Adaptive, Fifth Order Implicit-Explicit Integration Scheme*. SAND2013-4299. Sandia National Laboratories, Albuquerque, NM, 2013.

[55] E. P. Petrov. A high-accuracy model reduction for analysis of nonlinear vibrations in structures with contact interfaces. *ASME Journal of Engineering for Gas Turbines and Power*, 133:102503, 2011.

[56] C. M. Firrone, S. Zucca, and M. M. Gola. The effect of underplatform dampers on the forced response of bladed disks by a coupled static/dynamic harmonic balance method. *International Journal of Non-Linear Mechanics*, 46:363–375, 2011.

[57] M. Krack, L. Panning-von Scheidt, and J. Wallaschek. A high-order harmonic balance method for systems with distinct states. *Journal of Sound and Vibration*, 332:5476–5488, 2013.

[58] D. Süß and K. Willner. Investigation of a jointed friction oscillator using the multiharmonic balance method. *Mechanical Systems and Signal Processing*, 52-53:73–87, 2015.

[59] M. Krack. Nonlinear modal analysis of nonconservative systems: Extension of the periodic motion concept. *Computers & Structures*, 154:59–71, 2015.

[60] J. J. Hollkamp and R. W. Gordon. Reduced-order models for nonlinear response prediction: Implicit condensation and expansion. *Journal of Sound and Vibration*, 318:1139–1153, 2008.

[61] H. Festjens, G. Chevallier, and J.-L. Dion. A numerical tool for the design of assembled structures under dynamic loads. *International Journal of Mechanical Sciences*, 75:170–177, 2013.

[62] R. M. Lacayo and M. S. Allen. Updating structural models containing nonlinear Iwan joints using quasi-static modal analysis. *Mechanical Systems and Signal Processing*, 114:413–438, 2019.

[63] N. N. Balaji and M. R. W. Brake. An efficient quasi-static non-linear modal analysis procedure generalizing Rayleigh quotient stationarity for non-conservative dynamical systems. *Computers and Structures*, 230:106184, 2020.

[64] B. Cappella and G. Dietler. Force-distance curves by atomic force microscopy. *Surface Science Reports*, 34:1–104, 1999.

[65] H.-J. Butt, B. Cappella, and M. Kappl. Force measurements with the atomic force microscope: Technique, interpretation and applications. *Surface Science Reports*, 59:1–152, 2005.

[66] Y. Lu, Y. Ganesan, and J. Lou. A multi-step method for in situ mechanical characterization of 1-d nanostructures using a novel micromechanical device. *Experimental Mechanics*, 50:47–54, 2010.

[67] P. Zhang, L. Ma, F. Fan, Z. Zeng, C. Peng, et al. Fracture toughness of graphene. *Nature Communications*, 5:1–7, 2014.

[68] J.-H. Lee, D. Veysset, J. P. Singer, M. Retsch, G. Saini, et al. High strain rate deformation of layered nanocomposites. *Nature Communications*, 3:1–9, 2012.

[69] J.-H. Lee, P. E. Loya, J. Lou, and E. L. Thomas. Dynamic mechanical behavior of multilayer graphene via supersonic projectile penetration. *Science*, 346:1092–1096, 2014.

[70] S. A. Joyce and J. E. Houston. A new force sensor incorporating force-feedback control for interfacial force microscopy. *Review of Scientific Instruments*, 62:710–715, 1990.

[71] T. A. Michalske and J. E. Houston. Dislocation nucleation at nano-scale mechanical contacts. *Acta Materialia*, 46:391–396, 1998.

[72] L. Sirghi and F. Rossi. Adhesion and elasticity in nanoscale indentation. *Applied Physics Letters*, 89:243118, 2006.

[73] B. V. Derjaguin, V. M. Muller, and Y. P. Toporov. Effect of contact deformations on the adhesion of particles. *Journal of Colloid and Interface Science*, 53:314–326, 1975.

[74] K. L. Johnson, K. Kendall, and A. D. Roberts. Surface energy and the contact of elastic solids. *Proceedings of the Royal Society of London A*, 324:301–313, 1971.

[75] D. Maugis. Adhesion of spheres: The JKR-DMT transition using a Dugdale model. *Journal of Colloid and Interface Science*, 150:243–269, 1992.

[76] Y.-P. Zhao, L. S. Wang, and T. X. Yu. Mechanics of adhesion in MEMS – a review. *Journal of Adhesion Science and Technology*, 17:519–546, 2003.

[77] F. Yang. Effect of adsorption on nanoindentation test. *Applied Physics Letters*, 80:959–961, 2002.

[78] K. L. Johnson and J. A. Greenwood. An adhesion map for the contact of elastic spheres. *Journal of Colloid and Interface Science*, 192:326–333, 1997.

[79] B. Bhushan. Adhesion and stiction: Mechanisms, measurement techniques, and methods for reduction. *Journal of Vacuum Science & Technology B: Microelectronics and Nanometer Structures Processing, Measurement, and Phenomena*, 21:2262–2296, 2003.

[80] R. G. Budynas and K. Nisbett. *Shigley's Mechanical Engineering Design*. McGraw Hill, 10th edition, 2014.

[81] N. N. Balaji, W. Chen, and M. R. W. Brake. Traction-based multi-scale nonlinear dynamic modeling of bolted joints: Formulation, application, and trends in micro-scale interface evolution. *Mechanical Systems and Signal Processing*, 139:106615, 2020.

[82] B. Luan and M. O. Robbins. The breakdown of continuum models for mechanical contacts. *Nature*, 435:929–932, 2005.

[83] H. Ghaednia, X. Wang, S. Saha, Y. Xu, A. Sharma, et al. A review of elastic-plastic contact mechanics. *Applied Mechanics Reviews*, 69:060804, 2017.

[84] A. C. Fischer-Cripps. Critical review of analysis and interpretation of nanoindentation test data. *Surface & Coatings Technology*, 200:4153–4165, 2006.

[85] B. Merle, W. H. Higgins, and G. M. Pharr. Extending the range of constant strain rate nanoindentation testing. *Journal of Materials Research*, 35:343–352, 2020.

[86] P. S. Phani, W. C. Oliver, and G. M. Pharr. Understanding and modeling plasticity error during nanoindentation with continuous stiffness measurement. *Materials and Design*, 194:108923, 2020.

[87] P. S. Phani, W. C. Oliver, and G. M. Pharr. An experimental assessment of methods for mitigating plasticity error during nanoindentation with continuous stiffness measurement. *Materials and Design*, 194:108924, 2020.

[88] E. S. Berkovich. Three-faceted diamond pyramid for micro-hardness testing. *Industrial Diamond Review*, 11:129–132, 1951.

[89] E. Broitman. Indentation hardness measurements at macro-, micro-, and nanoscale: A critical overview. *Tribology Letters*, 65: 23, 2017.

[90] A. Gouldstone, H.-J. Koh, K.-Y. Zeng, A. E. Giannakopoulos, and S. Suresh. Discrete and continuous deformation during nanoindentation of thin films. *Acta Materialia*, 48:2277–2295, 2000.

[91] H. Hertz. Über die berührung fester elastischer körper (On the contact of elastic solids). *Journal fur die Reine und Andgewandte Mathematik*, 92:156–171, 1882.

[92] ASTM. Standard hardness conversion tables for metals relationship among Brinell hardness, Vickers hardness, Rockwell hardness, superficial hardness, Knoop hardness, and scleroscope hardness. Technical Report ASTM E 140-07, American Society for Testing and Materials, 2010.

[93] A. Bolshakov and G. M. Pharr. Influences of pileup on the measurement of mechanical properties by load and depth sensing indentation techniques. *Journal of Materials Research*, 13:1049–1058, 1998.

[94] G. M. Pharr, E. G. Herbert, and Y. F. Gao. The indentation size effect: A critical examination of experimental observations and mechanistic interpretations. *Annual Review of Materials Research*, 40:271–292, 2010.

[95] J. Musil, F. Kunc, H. Zeman, and H. Poláková. Relationships between hardness, Young's modulus and elastic recovery in hard nanocomposite coatings. *Surface and Coatings Technology*, 154:304–313, 2002.

[96] S. Vepřek. Recent search for new superhard materials: Go nano! *Journal of Vacuum Science & Technology A*, 31:050822, 2013.

[97] S. D. Antolovich and R. W. Armstrong. Plastic strain localization in metals: Origins and consequences. *Progress in Materials Science*, 59:1–160, 2014.

[98] M. Dao, L. Lu, R. J. Asaro, J. T. M. De Hosson, and E. Ma. Toward a quantitative understanding of mechanical behavior of nanocrystalline metals. *Acta Materialia*, 55:4041–4065, 2007.

[99] Z. C. Cordero, B. E. Knight, and C. A. Schuh. Six decades of the Hall-Petch effect - a survey of grain-size strengthening studies on pure metals. *International Materials Reviews*, 61:495–512, 2016.

[100] K. D. Ralston and N. Birbilis. Effect of grain size on corrosion: A review. *Corrosion*, 66:075005, 2010.

[101] R. Valiev. Nanostructuring of metals by severe plastic deformation for advanced properties. *Nature Materials*, 3:511–516, 2004.

[102] R. Song, D. Ponge, D. Raabe, J. G. Speer, and D. K. Matlock. Overview of processing, microstructure and mechanical properties of ultrafine grained bcc steels. *Materials Science and Engineering A*, 441:1–17, 2006.

[103] I. A. Ovid'ko, R. Z. Valiev, and Y. T. Zhu. Review on superior strength and enhanced ductility of metallic nanomaterials. *Progress in Materials Science*, 94:462–540, 2018.

[104] W. D. Nix and H. Gao. Indentation size effects in crystalline materials: A law for strain gradient plasticity. *Journal of the Mechanics and Physics of Solids*, 46:411–425, 1998.

[105] Y. Huang, F. Zhang, K. C. Hwang, W. D. Nix, G. M. Pharr, et al. A model of size effects in nano-indentation. *Journal of the Mechanics and Physics of Solids*, 54:1668–1686, 2006.

[106] J. G. Swadener, E. P. George, and G. M. Pharr. The correlation of the indentation size effect measured with indenters of various shapes. *Journal of the Mechanics and Physics of Solids*, 50:681–694, 2002.

[107] A. Gouldstone, N. Chollacoop, M. Dao, J. Li, A. M. Minor, et al. Indentation across size scales and disciplines: Recent developments in experimentation and modeling. *Acta Materialia*, 55:4015–4039, 2007.

[108] S. M. Walley. Historical origins of indentation hardness testing. *Materials Science and Technology*, 28:1028–1044, 2012.

[109] E. Meyer. Untersuchen über härteprüfung und härte brinell methoden (Studies on hardness testing and the Brinell hardness method). *Zeitschrift des Vereines Deutscher Ingenieure*, 52:645–654, 1908.

[110] P. Ludwik, editor. *Die Kegelprobe. Ein neues Verfahren zur Härtebestimmung von Materialien. (The Cone Test - A New Way to Determine the Hardness of Materials)*. Springer-Verlag, 1908.

[111] J. Brinell. Sätt att bestämma kroppars hårdhet jämte några tillämpningar of detsamma (Ways to determine hardness along with applications). *Teknisk Tidskrift*, 30:69–87, 1900.

[112] S. Biwa and B. Storakers. An analysis of fully plastic Brinell indentation. *Journal of the Mechanics and Physics of Solids*, 43: 1303–1333, 1995.

[113] F. Knoop, C. G. Peters, and W. B. Emerson. A sensitive pyramidal-diamond tool for indentation measurements. *Journal of Research of the National Beureau of Standards*, 23:39–61, 1939.

[114] E. A. Baxevani and A. E. Giannakopoulos. The modified Rockwell test: A new probe for mechanical properties of metals. *Experimental Mechanics*, 49:371–382, 2009.

[115] R. L. Smith and G. E. Sandland. An accurate method of determining the hardness of metals, with particular reference to those of a high degree of hardness. *Proceedings of the Institution of Mechanical Engineers*, 102:623–641, 1922.

[116] J. T. Despard, H. Ghaednia, and M. R. W. Brake. Improved parameter estimation for nanoindentation measurements. In *2019 STLE Annual Meeting*, Nashville, TN, May 2019.

[117] J. T. Despard. *A New Tool for Investigating Mesoscale Contact*. Masters Dissertation. Rice University, Houston, TX., 2020.

[118] Y. Y. Lim and M. M. Chaudhri. The effect of the indenter load on the nanohardness of ductile metals: An experimental study on polycrystalline work-hardened and annealed oxygen-free copper. *Philosophical Magazine A*, 79:2979–3000, 1999.

[119] J. Gupta, J. Hure, B. Tanguy, L. Laffont, M.-C. Lafont, et al. Characterization of ion irradiation effects on the microstructure, hardness, deformation and crack initiation behavior of austenitic stainless steel: Heavy ions vs protons. *Journal of Nuclear Materials*, 501:45–58, 2018.

[120] K. Mao, H. Wang, Y. Wu, V. Tomar, and J. P. Wharry. Microstructure-property relationship for AISI 304/308L stainless steel laser weldment. *Materials Science & Engineering A*, 721:234–243, 2018.

[121] L. Qian, M. Li, Z. Zhou, H. Yang, and X. Shi. Comparison of nano-indentation hardness to microhardness. *Surface & Coatings Technology*, 195:264–271, 2006.

[122] N. Ye and K. Komvopoulos. Indentation analysis of elastic-plastic homogeneous and layered media. *Journal of Tribology*, 125:685–691, 2003.

[123] L. Kogut and K. Komvopoulos. Analysis of the spherical indentation cycle for elastic-perfectly plastic solids. *Journal of Materials Research*, 19:3641–3653, 2004.

[124] E. O'Neill. *Investigating the Effects of the Relative Radius of Curvature in Elastic-Plastic Spherical Contact*. Masters Dissertation. William Marsh Rice University, Houston, TX, 2020.

[125] A. Chatterjee, A. A. Polycarpou, J. R. Abelson, and P. Bellon. Nanoscratch study of hard $HfB_2$ thin films using experimental and finite element techniques. *Wear*, 268:677–685, 2010.

[126] F. Ren, S. N. Arshad, P. Bellon, R. S. Averback, M. Pouryazdan, et al. Sliding wear-induced chemical nanolayering in Cu-Ag, and its implications for high wear resistance. *Acta Materialia*, 72:148–158, 2014.

[127] R. Madhavan, P. Bellon, and R. S. Averback. Wear resistance of Cu/Ag multilayers: A microscopic study. *ACS Applied Materials & Interfaces*, 10:15288–15297, 2018.

[128] S. Vepřek. The search for novel, superhard materials. *Journal of Vacuum Science & Technology A*, 17:2401–2420, 1999.

[129] T. Zhu and J. Li. Ultra-strength materials. *Progress in Materials Science*, 55:710–757, 2010.

[130] Z. Zhao, B. Xu, and Y. Tian. Recent advances in superhard materials. *Annual Review of Materials Research*, 46:383–406, 2016.

[131] S. Vepřek and M. J. G. Vepřek-Heijman. Industrial applications of superhard nanocomposite coatings. *Surface & Coatings Technology*, 202:5063–5073, 2008.

[132] P. H. Mayrhofer, C. Mitterer, L. Hultman, and H. Clemens. Microstructural design of hard coatings. *Progress in Material Science*, 51:1032–1114, 2006.

[133] H. Spikes. The history and mechanisms of ZDDP. *Tribology Letters*, 17:469–489, 2004.

[134] M. A. Nicholls, T. Do, P. R. Norton, M. Kasrai, and G. M. Bancroft. Review of the lubrication of metallic surfaces by zinc dialkyl-dithiophosphates. *Tribology International*, 38:15–39, 2005.

[135] N. N. Gosvami, J. A. Bares, F. Mangolini, A. R. Konicek, D. G. Yablon, et al. Mechanisms of antiwear tribofilm growth revealed in situ by single-asperity sliding contacts. *Science*, 348:102–106, 2015.

[136] J. Zhang and H. Spikes. On the mechanism of ZDDP antiwear film formation. *Tribology Letters*, 63:24, 2016.

[137] A. Akchurin and R. Bosman. A deterministic stress-activated model for tribo-film growth and wear simulation. *Tribology Letters*, 65:59, 2017.

[138] J. Schiøtz, F. D. Di Tolla, and K. W. Jacobsen. Softening of nanocrystalline metals at very small grain sizes. *Nature*, 391: 561–563, 1998.

[139] M. A. Meyers, A. Mishra, and D. J. Benson. Mechanical properties of nanocrystalline materials. *Progress in Materials Science*, 51:427–556, 2006.

[140] D. Wolf, V. Yamakov, S. R. Phillpot, A. Mukherjee, and H. Gleiter. Deformation of nanocrystalline materials by molecular-dynamics simulation: Relationship to experiments? *Acta Materialia*, 53:1–408, 2005.

[141] K. Lu. Nanocrystalline metals crystallized from amorphous solids: Nanocrystallization, structure, and properties. *Materials Science and Engineering*, R16:161–221, 1996.

[142] H. Gleiter. Nanostructured materials: Basic concepts and microstructure. *Acta Materialia*, 48:1–29, 2000.

[143] F. Roters, P. Eisenlohr, L. Hantcherli, D. D. Tjahjanto, T. R. Bieler, et al. Overview of constitutive laws, kinematics, homogenization and multiscale methods in crystal plasticity finite-element modeling: Theory, experiments, applications. *Acta Materialia*, 58:1152–1211, 2010.

[144] R. W. Armstrong, W. L. Elban, and S. M. Walley. Elastic, plastic, cracking aspects of the hardness of materials. *International Journal of Modern Physics B*, 27:1330004, 2013.

[145] K. S. Kumar, H. Van Swygenhoven, and S. Suresh. Mechanical behavior of nanocrystalline metals and alloys. *Acta Materialia*, 51:5743–5774, 2003.

[146] N. Hansen. Hall-Petch relation and boundary strengthening. *Scripta Materialia*, 51:801–806, 2004.

[147] F. Louchet, J. Weiss, and T. Richeton. Hall-Petch law revisited in terms of collective dislocation dynamics. *Physical Review Letters*, 97:075504, 2006.

[148] S. N. Naik and S. M. Walley. The Hall-Petch and inverse Hall-Petch relations and the hardness of nanocrystalline metals. *Journal of Materials Science*, 55:2661–2681, 2020.

[149] J. R. Trelewicz and C. A. Schuh. The Hall-Petch breakdown in nanocrystalline metals: A crossover to glass-like deformation. *Acta Materialia*, 55:5948–5958, 2007.

[150] D. Tabor. A simple theory of static and dynamic hardness. *Proceedings of the Royal Society of London, Series A*, 192: 247–274, 1948.

[151] R. W. Siegel and G. E. Fougere. Mechanical properties of nanophase metals. *NanoStructured Materials*, 6:205–216, 1995.

[152] R. S. Mishra and Z. Y. Ma. Friction stir welding and processing. *Materials Science & Engineering R-Reports*, 50:1–78, 2005.

[153] S. J. Eder, M. Rodriguez Ripoll, U. Cihak-Bayr, D. Dini, and C. Gachot. Unraveling and mapping the mechanisms for near-surface microstructure evolution in CuNi alloys under sliding. *ACS Applied Materials & Interfaces*, 12:32197–32208, 2020.

[154] T. J. Rupert and C. A. Schuh. Sliding wear of nanocrystalline Ni-W: Structural evolution and the apparent breakdown of Archard scaling. *Acta Materialia*, 58:4137–4148, 2010.

[155] N. Argibay, T. A. Furnish, B. L. Boyce, B. G. Clark, and M. Chandross. Stress-dependent grain size evolution of nanocrystalline Ni-W and its impact on friction behavior. *Scripta Materialia*, 123:26–29, 2016.

[156] Y. Shi and I. Szlufarska. Wear-induced microstructural evolution of nanocrystalline aluminum and the role of zirconium dopants. *Acta Materialia*, 200:432–441, 2020.

[157] T. J. Rupert, W. Cai, and C. A. Schuh. Abrasive wear response of nanocrystalline Ni-W alloys across the Hall-Petch breakdown. *Wear*, 298-299:120–126, 2013.

[158] Y. Liu, T. W. Liskiewicz, and B. D. Beake. Dynamic changes of mechanical properties induced by friction in the Archard wear model. *Wear*, 428-429:366–375, 2019.

[159] H. A. Padilla, B. L. Boyce, C. C. Battaile, and S. V. Prasad. Frictional performance and near-surface evolution of nanocrystalline Ni-Fe as governed by contact stress and sliding velocity. *Wear*, 297:860–871, 2013.

[160] W. G. Sawyer, N. Argibay, D. L. Burris, and B. A. Krick. Mechanistic studies in friction and wear of bulk materials. *Annual Review of Materials Research*, 44:395–427, 2014.

[161] J. F. Panzarino and T. J. Rupert. Concurrent transitions in wear rate and surface microstructure in nanocrystalline Ni-W. *Materialia*, 4:38–46, 2018.

[162] Z. Shan, E. A. Stach, J. M. K. Wiezorek, J. A. Knapp, D. M. Follstaedt, et al. Grain boundary-mediated plasticity in nanocrystalline nickel. *Science*, 30:654–657, 2004.

[163] C. Greiner, Z. Liu, R. Schneider, L. Pastewka, and P. Gumbsch. The origin of surface microstructure evolution in sliding friction. *Scripta Materialia*, 153:63–67, 2018.

[164] S. C. Lim and M. F. Ashby. Wear-mechanism maps. *Acta Metallurgica*, 35:1–24, 1987.

[165] I. Petrov, P. B. Bama, L. Hultman, and J. E. Greene. Microstructural evolution during film growth. *Journal of Vacuum Science & Technology A*, 21:S117, 2003.

[166] S. C. Tjong and H. Chen. Nanocrystalline materials and coatings. *Materials Science and Engineering R-Reports*, 45:1–88, 2004.

[167] G. M. Pharr and W. C. Oliver. Measurement of thin-film mechanical-properties using nanoindentation. *MRS Bulletin*, 17: 28–33, 1992.

[168] J. Mehta, V. K. Mittal, and P. Gupta. Role of thermal spray coatings on wear, erosion and corrosion behavior: A review. *Journal of Applied Science and Engineering*, 20:445–452, 2017.

[169] J. Mencik, D. Munz, E. Quandt, E. R. Weppelmann, and M. V. Swain. Determination of elastic modulus of thin layers using nanoindentation. *Journal of Materials Research*, 12:2475–2484, 1997.

[170] A. M. Korsunsky, M. R. McGurk, S. J. Bull, and T. F. Page. On the hardness of coated systems. *Surface and Coatings Technology*, 99:171–183, 1998.

[171] J. R. Greer, W. C. Oliver, and W. D. Nix. Size dependence of mechanical properties of gold at the micron scale in the absence of strain gradients. *Acta Materialia*, 53:1821–1830, 2005.

[172] A. Misra, J. P. Hirth, and R. G. Hoagland. Length-scale-dependent deformation mechanisms in incoherent metallic multilayered composites. *Acta Materialia*, 53:4817–4824, 2005.

[173] C. A. Schuh, J. K. Mason, and A. C. Lund. Quantitative insight into dislocation nucleation from high-temperature nanoindentation experiments. *Nature Materials*, 4:617–621, 2005.

[174] K. Sangwal. Indentation size effect, indentation cracks and microhardness measurement of brittle crystalline solids - some basic concepts and trends. *Crystal Research and Technology: Journal of Experimental and Industrial Crystallography*, 44: 1019–1037, 2009.

[175] D. Jiang. Recent progresses in the phenomenological description for the indentation size effect in microhardness testing of brittle ceramics. *Journal of Advanced Ceramics*, 1:38–49, 2012.

[176] H. Ghaednia, M. R. W. Brake, M. Berryhill, and R. L. Jackson. Strain hardening from elastic-perfectly plastic to perfectly elastic flattening single asperity contact. *ASME Journal of Tribology*, 141:031402, 2019.

[177] H. Ghaednia, G. Mifflin, P. Lunia, E. O. O'Neill, and M. R. W. Brake. Strain hardening from elastic-perfectly plastic to perfectly elastic indentation single asperity contact. *Frontiers in Mechanical Engineering, Tribology*, 6:60, 2020.

[178] S. Vepřek, R. F. Zhang, M. J. G. Vepřek-Heijman, S. H. Sheng, and A. S. Argon. Superhard nanocomposites: Origin of hardness enhancement, properties and applications. *Surface & Coatings Technology*, 204:1898–1906, 2010.

[179] J. Wang and A. Misra. An overview of interface-dominated deformation mechanisms in metallic multilayers. *Current Opinion in Solid State and Materials Science*, 15:20–28, 2011.

[180] J.-H. Lee, Y. F. Gao, K. E. Johanns, and G. M. Pharr. Cohesive interface simulations of indentation cracking as a fracture toughness measurement method for brittle materials. *Acta Materialia*, 60:5448–5467, 2012.

[181] D. B. Marshall, R. F. Cook, N. P. Padture, M. L. Oyen, A. Pajares, et al. The compelling case for indentation as a functional exploratory and characterization tool. *Journal of the American Ceramic Society*, 98:2671–2680, 2015.

[182] M. Sebastiani, K. E. Johanns, E. G. Herbert, and G. M. Pharr. Measurement of fracture toughness by nanoindentation methods: Recent advances and future challenges. *Current Opinion in Solid State and Materials Science*, 19:324–333, 2015.

[183] B. R. Lawn, A. G. Evans, and D. B. Marshall. Elastic/plastic indentation damage in ceramics: The median/radial crack system. *Journal of the American Ceramic Society*, 63:574–581, 1980.

[184] K. Nihara. A fracture mechanics analysis of indentation-induced Palmqvist crack in ceramics. *Journal of Materials Science Letters*, 2:221–223, 1983.

[185] B. A. Mound and G. M. Pharr. Nanoindentation of fused quartz at loads near the cracking threshold. *Experimental Mechanics*, 59:369–380, 2019.

[186] S. Bruns, K. E. Johanns, H. ur Rehman, G. M. Pharr, and K. Durst. Constitutive modeling of indentation cracking in fused silica. *Journal of the American Ceramic Society*, 100:1928–1940, 2017.

[187] W. J. Sames, F. A. List, S. Pannala, R. R. Dehoff, and S. S. Babu. The metallurgy and processing science of metal additive manufacturing. *International Materials Reviews*, 61:315–360, 2016.

[188] H. Shu, S. A. Smith, and M. R. W. Brake. The influence of additively manufactured nonlinearities on the dynamic response of assembled structures. *ASME Journal of Vibration and Acoustics*, 142:011019, 2020.

[189] T. DebRoy, H. L. Wei, J. S. Zuback, T. Mukherjee, J. W. Elmer, et al. Additive manufacturing of metallic components - process, structure and properties. *Progress in Materials Science*, 92:112–224, 2018.

[190] G. M. Karthik and H. S. Kim. Heterogeneous aspects of additive manufactured metallic parts: A review. *Metals and Materials International*, 27:1–39, 2021.

[191] T. G. Spears and S. A. Gold. In-process sensing in selective laser melting (SLM) additive manufacturing. *Integrating Materials and Manufacturing Innovation*, 5:16–40, 2016.

[192] V. Manvatkar, A. De, and T. DebRoy. Spatial variation of melt pool geometry, peak temperature and solidification parameters during laser assisted additive manufacturing process. *Materials Science and Technology*, 31:924–930, 2015.

[193] L. E. Murr. Metallurgy of additive manufacturing: Examples from electron beam melting. *Additive Manufacturing*, 5:40–53, 2015.

[194] S. K. Everton, M. Hirsch, P. Stravroulakis, R. K. Leach, and A. T. Clare. Review of in-situ process monitoring and in-situ metrology for metal additive manufacturing. *Materials and Design*, 95:431–445, 2016.

[195] A. Yadollahi and N. Shamsaei. Additive manufacturing of fatigue resistant materials: Challenges and opportunities. *International Journal of Fatigue*, 98:14–31, 2017.

[196] C. Kantzos, J. Pausa, R. Cunningham, S. P. Narra, J. Beuth, et al. An investigation of process parameter modifications on additively manufactured inconel 718 parts. *Journal of Materials Engineering and Performance*, 28:620–626, 2019.

[197] R. M. Mahamood, E. T. Akinlabi, M. Shukla, and S. Pityana. Scanning velocity influence on microstructure, microhardness and wear resistance performance of laser deposited Ti6Al4V/TiC composite. *Materials and Design*, 50:656–666, 2013.

[198] A. Yadollahi, M. J. Mahtabi, A. Khalili, H. R. Doude, and J. C. Newman Jr. Fatigue life prediction of additively manufactured material: Effects of surface roughness, defect size, and shape. *Fatigue & Fracture of Engineering Materials & Structures*, 41: 1602–1614, 2018.

[199] C. Cai, C. Radoslaw, J. Zhang, Q. Yan, S. Wen, et al. In-situ preparation and formation of TiB/Ti-6Al-4V nanocomposite via laser additive manufacturing: Microstructure evolution and tribological behavior. *Powder Technology*, 342:73–84, 2019.

[200] S. R. Sales de Mello, M. E. H. Maia da Costa, C. M. Menezes, C. D. Boeira, F. L. Freire Jr, et al. On the phonon dissipation contribution to nanoscale friction by direct contact. *Scientific Reports*, 7:1–8, 2017.

[201] P. Sahoo and S. K. Das. Tribology of electroless nickel coatings - a review. *Materials and Design*, 32:1760–1775, 2011.

[202] J. Musil. Hard nanocomposite coatings: Thermal stability, oxidation resistance and toughness. *Surface & Coatings Technology*, 207:50–65, 2012.

[203] D. Berman, A. Erdemir, and A. V. Sumant. Few layer graphene to reduce wear and friction on sliding steel surfaces. *Carbon*, 54:454–459, 2013.

[204] C. Gachot, A. Rosenkranz, S. M. Hsu, and H. L. Costa. A critical assessment of surface texturing for friction and wear improvement. *Wear*, 372-373:21–41, 2017.

[205] P. G. Grützmacher, F. J. Profito, and A. Rosenkranz. Multi-scale surface texturing in tribology – current knowledge and future perspectives. *Lubricants*, 7:95, 2019.

[206] A. K. Sharma, A. K. Tiwari, and A. R. Dixit. Effects of minimum quantity lubrication (mql) in machining processes using conventional and nanofluid based cutting fluids: A comprehensive review. *Journal of Cleaner Production*, 127:1–18, 2016.

[207] K. Bobzin. High-performance coatings for cutting tools. *CIRP Journal of Manufacturing Science and Technology*, 18:1–9, 2017.

[208] P. S. M. Dougherty, R. Pudjoprawoto, and C. F. Higgs, III. Bit cutter-on-rock tribometry: Analyzing friction and rate-of-penetration for deep well drilling substrates. *Tribology International*, 77:178–185, 2014.

[209] L. Mattei, F. Di Puccio, B. Piccigallo, and E. Ciulli. Lubrication and wear modelling of artificial hip joints: A review. *Tribology International*, 44:532–549, 2011.

[210] F. Di Puccio and L. Mattei. Biotribology of artificial hip joints. *World Journal of Orthopedics*, 6:77–94, 2015.

[211] L. Kunčická, R. Kocich, and T. C. Lowe. Advances in metals and alloys for joint replacement. *Progress in Materials Science*, 88:232–2804, 2017.

[212] M. N. Kotzalas and G. L. Doll. Tribological advancements for reliable wind turbine performance. *Philosophical Transactions of the Royal Society A*, 368:4829–4850, 2010.

[213] M.-H. Evans. White structure flaking (WSF) in wind turbine gearbox bearings: Effects of 'butterflies' and white etching cracks (WECs). *Materials Science and Technology*, 28:3–22, 2012.

[214] M. Javidani and D. Larouche. Application of cast Al-Si alloys in internal combustion engine components. *International Materials Reviews*, 59:132–158, 2014.

[215] V. W. Wong and S. C. Tung. Overview of automotive engine friction and reduction trends - effects of surface, material, and lubricant-additive technologies. *Friction*, 4:1–28, 2016.

[216] H. K. D. H. Bhadeshia. Steels for bearings. *Progress in Materials Science*, 57:268–435, 2012.

[217] K. Holmberg and P. A. A. Erdemir. Global energy consumption due to friction in passenger cars. *Tribology International*, 47: 221–234, 2012.

[218] K. Holmberg and A. Erdemir. Influence of tribology on global energy consumption, costs and emissions. *Friction*, 5:263–284, 2017.

[219] N. N. Balaji and M. R. W. Brake. The surrogate system hypothesis for joint mechanics. *Mechanical Systems and Signal Processing*, 126:42–64, 2019.

[220] B. Seeger, P. Butaud, F. Du, V. Baloglu, M. R. W. Brake, et al. In situ measurements of interfacial contact pressure during impact hammer tests. In *36rd International Modal Analysis Conference (IMAC XXXVI)*, Orlando, FL, February 2018.

[221] T. Dreher, M. R. W. Brake, B. Seeger, and M. Krack. In situ, real-time measurements of contact pressure internal to jointed interfaces during dynamic excitation of an assembled structure. *Mechanical Systems and Signal Processing*, 149:107859, 2021.

[222] V. Eswaraiah, V. Sankaranarayanan, and S. Ramaprabhu. Graphene-based engine oil nanofluids for tribological applications. *Applied Materials & Interfaces*, 3:4221–42275, 2011.

[223] T. W. Scharf and S. V. Prasad. Solid lubricants: A review. *Journal of Materials Science*, 48:511–531, 2013.

[224] W. Dai, B. Kheireddin, H. Gao, and H. Liang. Roles of nanoparticles in oil lubrication. *Tribology International*, 102:88–98, 2016.

[225] M. H. Müser, W. B. Dapp, R. Bugnicourt, P. Sainsot, N. Lesaffre, et al. Meeting the contact-mechanics challenge. *Tribology Letters*, 65:1–18, 2017.

[226] B. Bhushan, J. N. Israelachvili, and U. Landman. Nanotribology: Friction, wear and lubrication at the atomic scale. *Nature*, 374:607–616, 1995.

[227] G. G. Adams and M. Nosonovsky. Contact modeling - forces. *Tribology International*, 33:431–442, 2000.

[228] T. Baumberger and C. Caroli. Solid friction from stick-slip down to pinning and aging. *Advances in Physics*, 55:279–348, 2006.

[229] A. A. G. Bruzzone, H. L. Costa, P. M. Lonardo, and D. A. Lucca. Advances in engineered surfaces for functional performance. *CIRP Annals - Manufacturing Technology*, 57:750–7690, 2008.

[230] I. Szlufarska, M. Chandross, and R. W. Carpick. Recent advances in single-asperity nanotribology. *Journal of Physics D: Applied Physics*, 41:123001, 2008.

[231] A. I. Vakis, V. A. Yastrebov, J. Scheibert, L. Nicola, D. Dini, et al. Modeling and simulation in tribology across scales: An overview. *Tribology International*, 125:169–199, 2018.

[232] B. R. Lawn. Indentation of ceramics with spheres: A century after Hertz. *Journal of the American Ceramic Society*, 81: 1977–1944, 1998.

[233] N. K. Myshkin, M. I. Petrokovets, and A. V. Kovalev. Tribology of polymers: Adhesion, friction, wear, and mass-transfer. *Tribology International*, 38:910–921, 2005.

[234] S. P. Timoshenko and J. N. Goodier. *Theory of Elasticity*. McGraw-Hill Book Company, New York, NY, 1951.

[235] Y. Tatara. Extensive theory of force-approach relations of elastic spheres in compression and in impact. *ASME Journal of Engineering Materials and Technology*, 111:163–168, 1989.

[236] Y. Tatara. On compression of rubber elastic sphere over a large range of displacements – part 1: Theoretical study. *ASME Journal of Engineering Materials and Technology*, 113:285–291, 1991.

[237] Y. Tatara, S. Shima, and J. C. Lucero. On compression of rubber elastic sphere over a large range of displacements – part 2: Comparison of theory and experiment. *ASME Journal of Engineering Materials and Technology*, 113:292–295, 1991.

[238] Y. Tatara. Large deformations of a rubber sphere under diametral compression (part 1: Theoretical analysis of press approach, contact radius and lateral extension). *JSME International Journal*, 36:190–196, 1993.

[239] S. Shima, Y. Tatara, M. Iio, C. Shu, and J. C. Lucero. Large deformations of a rubber sphere under diametral compression (part 2: Experiments on many rubber materials and comparisons of theories with experiments). *JSME International Journal*, 36: 197–205, 1993.

[240] K. K. Liu, D. R. Williams, and B. J. Briscoe. The large deformation of a single micro-elastomeric sphere. *Journal of Physics D: Applied Physics*, 31:294–303, 1998.

[241] A. Agarwal and M. Gonzalez. Contact radius and curvature corrections to the nonlocal contact formulation accounting for multi-particle interactions in elastic confined granular systems. *International Journal of Engineering Science*, 133:26–46, 2018.

[242] J. Jamari and D. J. Schipper. An elastic-plastic contact model of ellipsoid bodies. *Tribology Letters*, 21:262–271, 2006.

[243] J. Jamari and D. J. Schipper. Plastic deformation and contact area of an elastic-plastic contact of ellipsoid bodies after unloading. *Tribology International*, 40:1311–1318, 2007.

[244] J. C. Chung. Elastic-plastic contact analysis of an ellipsoid and a rigid flat. *Tribology International*, 43:491–502, 2010.

[245] L. C. Hale. *Principles and Techniques for Designing Precision Machines*. Doctoral Dissertation. Massachusetts Institute of Technology, Cambridge, MA, 1999.

[246] L. P. Lin and J. F. Lin. An elliptical elastic-plastic microcontact model developed for an ellipsoid in contact with a smooth rigid flat. *ASME Journal of Tribology*, 129:772–782, 2007.

[247] V. Becker and M. Kamlah. A theoretical model for the normal contact force of two elastoplastic ellipsoidal bodies. *ASME Journal of Applied Mechanics*, 88:031006, 2021.

[248] R. Hill. *The Mathematical Theory of Plasticity*. Oxford University Press, New York, 1950.

[249] C. Thornton. Coefficient of restitution for collinear collisions of elastic-perfectly plastic spheres. *ASME Journal of Applied Mechanics*, 64:383–386, 1997.

[250] L. Vu-Quoc and X. Zhang. An elasto-plastic contact force-displacement model in the normal direction: Displacement-driven version. *Proceedings of the Royal Society of London, Series A*, 455:4013–4044, 1999.

[251] L. Vu-Quoc, X. Zhang, and L. Lesburg. A normal force-displacement model for contacting spheres accounting for plastic deformation: Force-driven formulation. *ASME Journal of Applied Mechanics*, 67:363–371, 2000.

[252] W. J. Stronge. *Impacts in Mechanical Systems: Analysis and Modelling*, volume 551, chapter Contact Problems for Elasto-Plastic Impact in Multi-Body Systems, pages 189–234. Springer, 2000.

[253] Y. Du and S. Wang. Energy dissipation in normal elastoplastic impact between two spheres. *ASME Journal of Applied Mechanics*, 76:061010–1–8, 2009.

[254] C.-Y. Wu, C. Thornton, and L.-Y. Li. A semi-analytical model for oblique impacts of elastoplastic spheres. *Proceedings of the Royal Society of London, Series A*, 465:937–960, 2010.

[255] M. R. Brake. An analytical elastic-perfectly plastic contact model. *International Journal of Solids and Structures*, 49: 3129–3141, 2012.

[256] P. S. Follansbee and G. B. Sinclair. Quasi-static normal indentation of an elasto-plastic half-space by a rigid sphere - i analysis. *International Journal of Solids and Structures*, 20:81–91, 1984.

[257] G. B. Sinclair, P. S. Follansbee, and K. L. Johnson. Quasi-static normal indentation of an elasto-plastic half-space by a rigid sphere - ii results. *International Journal of Solids and Structures*, 21:865–888, 1985.

[258] L. Kogut and I. Etsion. Elastic-plastic contact analysis of a sphere and a rigid flat. *ASME Journal of Applied Mechanics*, 69: 657–662, 2002.

[259] I. Etsion, Y. Kligerman, and Y. Kadin. Unloading of an elastic-plastic loaded spherical contact. *International Journal of Solids and Structures*, 42:3716–3729, 2005.

[260] R. L. Jackson, I. Chusoipin, and I. Green. A finite element study of the residual stress and deformation in hemispherical contacts. *ASME Journal of Tribology*, 127:484–493, 2005.

[261] R. L. Jackson and L. Kogut. A comparison of flattening and indentation approaches for contact mechanics modeling of single asperity contacts. *ASME Journal of Tribology*, 128:209–212, 2006.

[262] A. E. Giannakopoulos and S. Suresh. Determination of elastoplastic properties by instrumented sharp indentation. *Scripta Materialia*, 40:1191–1198, 1999.

[263] B. Taljat and G. M. Pharr. Development of pile-up during spherical indentation of elastic-plastic solids. *International Journal of Solids and Structures*, 41:3891–3904, 2004.

[264] J. F. Archard. Elastic deformation and the laws of friction. *Proceedings of the Royal Society of London, Series A*, 243: 190–205, 1957.

[265] J. A. Greenwood and J. B. P. Williamson. Contact of nominally flat surfaces. *Proceedings of the Royal Society of London, Series A*, 295:300–319, 1966.

[266] A. W. Bush, R. D. Gibson, and T. R. Thomas. The elastic contact of a rough surface. *Wear*, 35:87–111, 1975.

[267] J. A. Greenwood and J. J. Wu. Surface roughness and contact: An apology. *Meccanica*, 36:617–630, 2001.

[268] D. J. Whitehouse and J. F. Archard. The properties of random surfaces of significance in their contact. *Proceedings of the Royal Society of London A*, 316:97–121, 1970.

[269] E. J. Abbott and F. A. Firestone. Specifying surface quality: A method based on accurate measurement and comparison. *Mechanical Engineering*, 55:569–572, 1933.

[270] B. N. J. Persson, F. Bucher, and B. Chiaia. Elastic contact between randomly rough surfaces: Comparison of theory with numerical results. *Physical Review B*, 65:184106, 2002.

[271] K. Zhang, G. Li, J. Z. Gong, and M. Zhang. Normal contact stiffness of rough surfaces considering oblique asperity contact. *Advances in Mechanical Engineering*, 11:1–14, 2019.

[272] R. L. Jackson and J. L. Streator. A multi-scale model for contact between rough surfaces. *Wear*, 261:1337–1347, 2006.

[273] X. Wang, B. An, Y. Xu, and R. L. Jackson. The effect of resolution on the deterministic finite element elastic-plastic rough surface contact under combined normal and tangential loading. *Tribology International*, 144:106141, 2020.

[274] W. R. Chang, I. Etsion, and D. B. Bogy. An elastic-plastic model for the contact of rough surfaces. *ASME Journal of Tribology*, 109:257–263, 1987.

[275] H. So and D. C. Liu. An elastic-plastic model for the contact of anisotropic rough surfaces. *Wear*, 146:201–218, 1991.

[276] J. H. Horng. An elliptic-elastic-plastic asperity microcontact model for rough surfaces. *ASME Journal of Tribology*, 120: 82–88, 1998.

[277] Y. Zhao, D. M. Maietta, and L. Chang. An asperity microcontact model incorporating the transition from elastic deformation to fully plastic flow. *ASME Journal of Tribology*, 122:86–93, 2000.

[278] J. Abdo and K. Farhang. Elastic-plastic contact model for rough surfaces based on plastic asperity concept. *International Journal of Non-linear Mechanics*, 40:495–506, 2005.

[279] R. L. Jackson and I. Green. A statistical model of elasto-plastic asperity contact between rough surfaces. *Tribology International*, 39:906–914, 2006.

[280] Y.-R. Jeng and P.-Y. Wang. An elliptical microcontact model considering elastic, elastoplastic, and plastic deformation. *ASME Journal of Tribology*, 125:232–240, 2003.

[281] A. Majumdar and B. Bhushan. Fractal model of elastic-plastic contact between rough surfaces. *ASME Journal of Tribology*, 113:1–11, 1991.

[282] B. Bhushan and A. Majumdar. Elastic-plastic contact model for bifractal surfaces. *Wear*, 153:53–64, 1992.

[283] T. L. Warren and D. Krajcinovic. Fractal models of elastic-perfectly plastic contact of rough surfaces based on the cantor set. *International Journal of Solids and Structures*, 32:2907–2922, 1995.

[284] W. Yan and K. Komvopoulos. Contact analysis of elastic-plastic fractal surfaces. *Journal of Applied Physics*, 84:3617–3624, 1998.

[285] J. L. Liou and J. F. Lin. A new microcontact model developed for variable fractal dimension, topothesy, density of asperity, and probability density function of asperity heights. *ASME Journal of Applied Mechanics*, 74:603–613, 2007.

[286] L. Kogut and R. L. Jackson. A comparison of contact modeling utilizing statistical and fractal approaches. *ASME Journal of Tribology*, 128:213–217, 2006.

[287] L. Pastewka and M. O. Robbins. Contact area of rough speres: Large scale simulations and simple scaling laws. *Applied Physics Letters*, 108:221601, 2016.

[288] N. Prodanov, W. B. Dapp, and M. H. Müser. On the contact area and mean gap of rough, elastic contacts: Dimensional analysis, numerical corrections, and reference data. *Tribology Letters*, 53:433–448, 2014.

[289] P. Sainsot and A. A. Lubrecht. Efficient solution of the dry contact of rough surfaces: A comparison of fast Fourier transform and multigrid methods. *Proceedings of the Institution of Mechanical Engineers, Part J: Journal of Engineering Tribology*, 225: 441–448, 2011.

[290] R. Bugnicourt, P. Sainsot, N. Lesaffre, and A. A. Lubrecht. Transient frictionless contact of a rough rigid surface on a viscoelastic half-space. *Tribology International*, 113:279–285, 2017.

[291] R. Bugnicourt, P. Sainsot, D. Dureisseix, C. Gauthier, and A. A. Lubrecht. FFT-based methods for solving a rough adhesive contact: Description and convergence study. *Tribology Letters*, 66:29, 2018.

[292] S. Solhjoo and A. I. Vakis. Single asperity nanocontacts: Comparison between molecular dynamics simulations and continuum mechanics models. *Computational Materials Science*, 99:209–220, 2015.

[293] S. Solhjoo and A. I. Vakis. Continuum mechanics at the atomic scale: Insights into non-adhesive contacts using molecular dynamics simulations. *Journal of Applied Physics*, 120:215102, 2016.

[294] A. I. Bennett, K. L. Harris, K. D. Schulze, J. M. U. na, A. J. McGhee, et al. Contact measurements of randomly rough surfaces. *Tribology Letters*, 65:134, 2017.

[295] M. R. W. Brake, P. L. Reu, and D. S. Aragon. A comprehensive set of impact data for common aerospace metals. *ASME Journal of Computational and Nonlinear Dynamics*, 12:061011, 2017.

[296] R. L. Jackson, I. Green, and D. B. Marghitu. Predicting the coefficient of restitution of impacting elastic-perfectly plastic spheres. *Nonlinear Dynamics*, 60:217–229, 2010.

[297] M. M. Chaudhri, I. M. Hutchings, and P. L. Makin. Plastic compression of spheres. *Philosophical Magazine A - Physics of Condensed Matter Structure Defects and Mechanical Properties*, 49:493–503, 1984.

[298] A. Ovcharenko, G. Halperin, G. Verberne, and I. Etsion. In situ investigation of the contact area in elastic-plastic spherical contact during loading-unloading. *Tribology Letters*, 25:153–160, 2007.

[299] O. Bartier, X. Hernot, and G. Mauvoisin. Theoretical and experimental analysis of contact radius for spherical indentation. *Mechanics of Materials*, 42:640–656, 2010.

[300] J. Alcalá, A. E. Giannakopoulos, and S. Suresh. Continuous measurements of load-penetration curves with spherical microindenters and the estimation of mechanical properties. *Journal of Materials Research*, 13:1390–1400, 1998.

[301] J. Alcalá and D. Esqué-de los Ojos. Reassessing spherical indentation: Contact regimes and mechanical property extraction. *International Journal of Solids and Structures*, 47:2714–2732, 2010.

[302] J. Jamari and D. J. Schipper. Experimental investigation of fully plastic contact of a sphere against a hard flat. *ASME Journal of Tribology*, 128:230–235, 2006.

[303] J. Jamari and D. J. Schipper. Deformation due to contact between a rough surface and a smooth ball. *Wear*, 262:138–145, 2007.

[304] J. Jamari, M. B. de Rooij, and D. J. Schipper. Plastic derministic contact of rough surfaces. *ASME Journal of Tribology*, 129: 957–962, 2007.

[305] Y. Tatara and N. Moriwaki. Study on impact of equivalent two bodies (coefficients of restitution of spheres of brass, lead, glass, porcelain and agate, and the material properties). *Bulletin of the JSME*, 25:631–637, 1982.

[306] A. H. Kharaz and D. A. Gorham. A study of the restitution coefficient in elastic-plastic impact. *Philosophical Magazine A - Physics of Condensed Matter Structure Defects and Mechanical Properties*, 80:549–559, 2000.

[307] H. Minamoto and S. Kawamura. Effects of material strain rate sensitivity in low speed impact between two identical spheres. *International Journal of Impact Engineering*, 36:680–686, 2009.

[308] H. Minamoto and S. Kawamura. Moderately high speed impact of two identical spheres. *International Journal of Impact Engineering*, 38:123–129, 2011.

[309] J. P. Nobre, A. M. Dias, and R. Gras. A study on elasto-plastic impact friction. *Wear*, 230:133–145, 1999.

[310] D. A. Gorham and A. H. Kharaz. The measurement of particle rebound characteristics. *Powder Technology*, 112:193–202, 2000.

[311] H. Ghaednia, O. Cermik, and D. B. Marghitu. Experimental and theoretical analysis of the elasto-plastic oblique impact of a rode with a flat. *International Journal of Impact Engineering*, 86:307–317, 2015.

[312] P. Müller, M. Heckel, A. Sack, and T. Pöschel. Complex velocity dependence of the coefficient of restitution of a bouncing ball. *Physical Review Letters*, 110:254301, 2013.

[313] J. M. Boac, M. E. Casada, R. G. Maghirang, and J. P. Harner III. Material and interaction properties of selected grains and oilseeds for modeling discrete particles. *Transactions of the ASABE*, 53:1201–1216, 2010.

[314] C. González-Montellano, J. M. Fuentes, E. Ayuga-Téllez, and F. Ayuga. Determination of the mechanical properties of maize grains and olives required for use in DEM simulations. *Journal of Food Engineering*, 111:553–562, 2012.

[315] J. Hlosta, D. Žurovec, J. Rozbroj, A. Ramírez-Gómez, J. Nečas, et al. Experimental determination of particle-particle restitution coefficient via double pendulum method. *Chemical Engineering Research and Design*, 135:222–233, 2018.

[316] R. Sondergaard, K. Chaney, and C. E. Brennen. Measurements of solid spheres bouncing off flat plates. *ASME Journal of Applied Mechanics*, 57:694–699, 1990.

[317] A. H. Kharaz, D. A. Gorham, and A. D. Salman. An experimental study of the elastic rebound of spheres. *Powder Technology*, 120:281–291, 2001.

[318] H. Dong and M. H. Moys. Measurement of impact behaviour between balls and walls in grinding mills. *Minearls Engineering*, 16:543–550, 2003.

[319] A. B. Stevens and C. M. Hrenya. Comparison of soft-sphere models to measurements of collision properties during normal impacts. *Powder Technology*, 154:99–109, 2005.

[320] H. Dong and M. H. Moys. Experimental study of oblique impacts with initial spin. *Powder Technology*, 161:22–31, 2006.

[321] A. Aryaei, K. Hashemnia, and K. Jafarpur. Experimental and numerical study of ball size effect on restitution coefficient in low velocity impacts. *International Journal of Impact Engineering*, 37:1037–1044, 2010.

[322] M. C. Marinack, Jr., R. E. Musgrave, and C. F. Higgs III. Experimental investigations on the coefficient of restitution of single particles. *Tribology Transactions*, 56:572–580, 2013.

[323] D. Patil, M. C. Marinack, Jr., C. DellaCorte, and C. F. Higgs III. Experimental investigations of the superelastic impact performance of Nitinol 60. *Tribology Transactions*, 60:615–620, 2017.

[324] D. Patil and C. F. Higgs III. Experimental investigations on the coefficient of restitution for sphere-thin plate elastoplastic impact. *ASME Journal of Tribology*, 140:011406, 2018.

[325] K. Hashemnia. Experimental study of the effect of temperature on the coefficient of restitution of steel balls impact to some industrial metal sheets at elevated temperatures. *Powder Technology*, 368:170–177, 2020.

[326] C. S. Sandeep, K. Senetakis, D. Cheung, C. E. Choi, Y. Wang, et al. Experimental study on the coefficient of restitution of grain against block interfaces for natural and engineered materials. *Canadian Geotechnical Journal*, 58:35–48, 2021.

[327] G. Amontons. De la résistance causée dans les machines. *Mémoires de l'Académie Royale, A*, pages 257–282, 1699.

[328] C. A. Coulomb. *Théorie Des Machines Simples*. Bachelier, Paris, 1821.

[329] F. P. Bowden and D. Tabor. The mechanism of metallic friction. *Nature*, 150:197–199, 1942.

[330] B. Armstrong-Hélouvry, P. Dupont, and C. Canudas de Wit. A survey of models, analysis tools and compensation methods for the control of machines with friction. *Automatica*, 30:1083–1138, 1994.

[331] M. Urbakh, J. Klafter, D. Gourdon, and J. Israelachvili. The nonlinear nature of friction. *Nature*, 430:525–528, 2004.

[332] B. N. J. Persson, O. Albohr, U. Tartaglino, A. I. Volokitin, and E. Tosatti. On the nature of surface roughness with application to contact mechanics, sealing, rubber friction and adhesion. *Journal of Physics: Condensed Matter*, 17:R1–R62, 2005.

[333] N. S. Tambe and B. Bhushan. Friction model for the velocity dependence of nanoscale friction. *Nanotechnology*, 16: 2309–2324, 2005.

[334] Y. Mo, K. T. Turner, and I. Szlufarska. Friction laws at the nanoscale. *Nature*, 457:1116–1119, 2009.

[335] Y. Dong, Q. Li, and A. Martini. Molecular dynamics simulation of atomic friction: A review and guide. *Journal of Vacuum Science & Technology A*, 31:030801, 2013.

[336] E. Rabinowicz. Friction coefficients of noble metals over a range of loads. *Wear*, 159:89–94, 1992.

[337] M. Otsuki and H. Matsukawa. Systematic breakdown of Amontons' law of friction for an elastic object locally obeying Amontons' law. *Scientific Reports*, 3:1–6, 2013.

[338] A. Erdemir. Genesis of superlow friction and wear in diamondlike carbon films. *Tribology International*, 37:1005–1012, 2004.

[339] T. W. Scharf, S. V. Prasad, M. T. Dugger, P. G. Kotula, R. S. Goeke, et al. Growth, structure, and tribological behavior of atomic layer-deposited tungsten disulphide solid lubricant coatings with applications to MEMS. *Acta Materialia*, 54:4731–4743, 2006.

[340] T. W. Scharf, P. G. Kotula, and S. V. Prasad. Friction and wear mechanisms in $MoS_2/Sb_2O_3/Au$ nanocomposite coatings. *Acta Materialia*, 58:4100–4109, 2010.

[341] B. D. Beake, V. M. Vishnyakov, and A. J. Harris. Relationship between mechanical properties of thin nitride-based films and their behaviour in nano-scratch tests. *Tribology International*, 44:468–475, 2011.

[342] A. T. Mathis, N. N. Balaji, R. J. Kuether, A. R. Brink, M. R. W. Brake, et al. A review of damping models for structures with mechanical joints. *Applied Mechanics Reviews*, 72:040802, 2020.

[343] J. R. Rice, N. Lapusta, and K. Ranjith. Rate and state dependent friction and the stability of sliding between elastically deformable solids. *Journal of the Mechanics and Physics of Solids*, 49:1865–1898, 2001.

[344] L. Zhang and H. Tanaka. Towards a deeper understanding of wear and friction on the atomic scale - a molecular dynamics analysis. *Wear*, 211:44–53, 1997.

[345] J. A. Hurtado and K.-S. Kim. Scale effects in friction of single-asperity contacts. I. from concurrent slip to single-dislocation-assisted slip. *Proceedings of the Royal Society of London, A*, 455:3363–3384, 1999.

[346] B. Bhushan and M. Nosonovsky. Scale effects in friction using strain gradient plasticity and dislocation-assisted sliding (microslip). *Acta Materialia*, 51:4331–4345, 2003.

[347] V. S. Deshpande, A. Needleman, and E. Van der Giessen. Discrete dislocation plasticity analysis of static friction. *Acta Materialia*, 52:3135–3149, 2004.

[348] D. S. Balint, V. S. Deshpande, A. Needleman, and E. Van der Giessen. Discrete dislocation plasticity analysis of the wedge indentation of films. *Journal of the Mechanics and Physics of Solids*, 54:2281–2303, 2006.

[349] A. Ghatak, K. Vorvolakos, H. She, D. L. Malotky, and M. K. Chaudhury. Interfacial rate processes in adhesion and friction. *The Journal of Physical Chemistry B*, 104:4018–4030, 2000.

[350] E. Gerde and M. Marder. Friction and fracture. *Nature*, 413:285–288, 2001.

[351] H. Kawamura, T. Hatano, N. Kato, S. Biswas, and B. K. Chakrabarti. Statistical physics of fracture, friction, and earthquakes. *Reviews of Modern Physics*, 84:839–884, 2012.

[352] G. Straffelini. A simplified approach to the adhesive theory of friction. *Wear*, 249:79–85, 2001.

[353] C. Lee, Q. Li, W. Kalb, X.-Z. Liu, H. Berger, et al. Frictional characteristics of atomically thin sheets. *Science*, 328:76–80, 2010.

[354] H. N. G. Wadley, C. B. Scruby, and J. H. Speake. Acoustic emission for physical examination of metals. *International Metals Reviews*, 2:41–64, 1980.

[355] H. N. G. Wadley and R. Mehrabian. Acoustic emission for materials processing: a review. *Materials Science and Engineering*, 65:245–263, 1984.

[356] R. E. Williams. Acoustic emission characteristics of abrasive flow machining. *ASME Journal of Manufacturing Science and Engineering*, 120:264–271, 1998.

[357] A. Akay. Acoustics of friction. *The Journal of the Acoustical Society of America*, 111:1525–1548, 2002.

[358] X. Li. A brief review: Acoustic emission method for tool wear monitoring during turning. *International Journal of Machine Tools & Manufacture*, 42:157–165, 2002.

[359] S. Hannel, S. Fouvry, P. Kapsa, and L. Vincent. The fretting sliding transition as a criterion for electrical contact performance. *Wear*, 249:761–770, 2001.

[360] L. Kogut and K. Komvopoulos. Electrical contact resistance theory for conductive rough surfaces. *Journal of Applied Physics*, 94:3151–3162, 2003.

[361] Z. L. Wang. Triboelectric nanogenerators as new energy technology for self-powered systems and as active mechanical and chemical sensors. *ACS Nano*, 7:9533–9557, 2013.

[362] Z. L. Wang, J. Chen, and L. Lin. Progress in triboelectric nanogenerators as a new energy technology and self-powered sensors. *Energy & Environmental Science*, 8:2250–2282, 2015.

[363] Z. L. Wang. On Maxwell's displacement current for energy and sensors: The origin of nanogenerators. *Materials Today*, 20: 74–82, 2017.

[364] C. Wu, A. C. Wang, W. Ding, H. Guo, and Z. L. Wang. Triboelectric nanogenerator: A foundation of the energy for the new era. *Advanced Energy Materials*, 9:1802906, 2019.

[365] A. F. Diaz and R. M. Felix-Navarro. A semi-quantitative tribo-electric series for polymeric materials: The influence of chemical structures and properties. *Journal of Electrostatics*, 62:277–290, 2004.

[366] S. Matsusaka, H. Maruyama, T. Matsuyama, and M. Ghadiri. Triboelectric charging of powders: A review. *Chemcial Engineering Science*, 65:5781–5807, 2010.

[367] F.-R. Fan, Z.-Q. Tian, and Z. L. Wang. Flexible triboelectric generator. *Nano Energy*, 1:328–334, 2012.

[368] H. Zou, Y. Zhang, L. Guo, P. Wang, X. He, et al. Quantifying the triboelectric series. *Nature Communications*, 10:1427, 2019.

[369] R. Hinchet, H.-J. Yoon, H. Ryu, M.-K. Kim, E.-K. Choi, et al. Transcutaneous ultrasound energy harvesting using capacitive triboelectric technology. *Science*, 365:491–494, 2019.

[370] A. I. Volokitin and B. N. J. Persson. Near-field radiative heat transfer and noncontact friction. *Reviews of Modern Physics*, 79:1291–1329, 2007.

[371] G. P. Ostermeyer and M. Müller. Dynamic interaction of friction and surface topography in brake systems. *Tribology International*, 39:370–380, 2006.

[372] M. Müller and G. P. Ostermeyer. Cellular automata method for macroscopic surface and friction dynamics in brake systems. *Tribology International*, 40:942–952, 2007.

[373] M. Müller and G. P. Ostermeyer. A cellular automation model to describe the three-dimensional friction and wear mechanism of brake systems. *Wear*, 263:1175–1188, 2007.

[374] K. Bode and G. P. Ostermeyer. A comprehensive approach for the simulation of heat and heat-induced phenomena in friction materials. *Wear*, 311:47–56, 2014.

[375] C. G. Camara, J. V. Escobar, J. R. Hird, and S. J. Putterman. Correlation between nanosecond X-ray flashes and stick-slip friction in peeling tape. *Nature*, 455:1089–1092, 2008.

[376] H. Dankowicz. On the modeling of dynamic friction phenomena. *ZAMM-Journal of Applied Mathematics and Mechanics/Zeitschrift für Angewandte Mathematik und Mechanik: Applied Mathematics and Mechanics*, 79:399–409, 1999.

[377] I.-H. Sung, H.-S. Lee, and D.-E. Kim. Effect of surface topography on the frictional behavior at the micr/nano-scale. *Wear*, 254:1019–1031, 2003.

[378] W. Chen, M. Jin, I. G. Lawal, M. R. W. Brake, and H. Song. Measurement of slip and separation in jointed structures with non-flat interfaces. *Mechanical Systems and Signal Processing*, 134:106325, 2019.

[379] U. Landman, W. D. Luedtke, and J. Gao. Atomic-scale issues in tribology: Interfacial junctions and nano-elastohydrodynamics. *Langmuir*, 12:4514–4528, 1996.

[380] G. G. Adams and S. Müftü. A scale-dependent model for multi-asperity contact and friction. *ASME Journal of Tribology*, 125: 700–708, 2003.

[381] K. L. Johnson. Contact mechanics and the wear of metals. *Wear*, 190:162–170, 1995.

[382] L. Li, I. Etsion, and F. E. Talke. Contact area and static friction of rough surfaces with high plasticity index. *ASME Journal of Tribology*, 132:031401, 2010.

[383] P. Berthoud, T. Baumberger, C. G'Sell, and J.-M. Hiver. Physical analysis of the state- and rate-dependent friction law: Static friction. *Physical Review B*, 59:14313–14327, 1999.

[384] A. Fantetti, L. R. Tamatam, M. Volvert, I. Lawal, L. Liu, et al. The impact of fretting wear on structural dynamics: Experiment and simulation. *Tribology International*, 138:111–124, 2019.

[385] G. P. Ostermeyer. On the dynamics of the friction coefficient. *Wear*, 254:852–858, 2003.

[386] G. P. Ostermeyer and M. Graf. Influence of wear on thermoelastic instabilities in automotive brakes. *Wear*, 308:113–120, 2013.

[387] K. Kato. Classification of wear mechanisms/models. *Proceedings of the Institution of Mechanical Engineers, Part J: Journal of Engineering Tribology*, 218:199–211, 2004.

[388] A. Zmitrowicz. Wear patterns and laws of wear - a review. *Journal of Theoretical and Applied Mechanics*, 44:219–253, 2006.

[389] H. C. Meng and K. C. Ludema. Wear models and predictive equations: Their form and content. *Wear*, 181-183:443–457, 1995.

[390] M. G. Gee and S. Owen-Jones. *Wear Testing Methods and Their Relevance to Industrial Wear Problems*. The National Physical Laboratory Report CMMT (A) 92, 1997.

[391] G. Ahmadi and X. Xia. A model for mechanical wear and abrasive particle adhesion during the chemical mechanical polishing process. *Journal of the Electrochemical Society*, 148:G99–G109, 2001.

[392] E. Rabinowicz. *Friction and Wear of Materials*. John Wiley & Sons, New York, NY, 1965.

[393] E. Rabinowicz. The least wear. *Wear*, 100:533–541, 1984.

[394] J.-F. Molinari, R. Aghababaei, T. Brink, L. Frérot, and E. Milanese. Adhesive wear mechanisms uncovered by atomistic simulations. *Friction*, 6:245–259, 2018.

[395] R. Aghababaei, D. H. Warner, and J.-F. Molinari. Critical length scale controls adhesive wear mechanisms. *Nature Communications*, 7:11816, 2016.

[396] D. K. Dwivedi. Adhesive wear behaviour of cast aluminium-silicon alloys: Overview. *Materials and Design*, 31:2517–2531, 2010.

[397] R. Aghababaei, D. H. Warner, and J.-F. Molinari. On the debris-level origins of adhesive wear. *Proceedings of the National Academy of Sciences*, 114:7935–7940, 2017.

[398] P. Sahoo and S. K. R. Chowdhury. A fractal analysis of adhesive wear at the contact between rough solids. *Wear*, 253: 942–934, 2002.

[399] X. Yin and K. Komvopoulos. An adhesive wear model of fractal surfaces in normal contact. *International Journal of Solids and Structures*, 47:912–921, 2010.

[400] A. Gåård, N. Hallbäck, P. Krakhmalev, and J. Bergström. Temperature effects on adhesive wear in dry sliding contacts. *Wear*, 268:968–975, 2010.

[401] D. Markov and D. Kelly. Mechanisms of adhesion-initiated catastrophic wear: Pure sliding. *Wear*, 239:189–210, 2000.

[402] G. A. Fontalvo, R. Humer, C. Mitterer, K. Sammt, and I. Schemmel. Microstructural aspects determining the adhesive wear of tool steels. *Wear*, 260:1028–1034, 2006.

[403] N. Fillot, I. Iordanoff, and Y. Berthier. Modelling third body flows with a discrete element method - a tool for understanding wear with adhesive particles. *Tribology International*, 40:973–981, 2007.

[404] L. Rapoport, A. Moshkovich, V. Perfilyev, A. Gedanken, Y. Koltypin, et al. Wear life and adhesion of solid lubricant films on laser-textured steel surfaces. *Wear*, 267:1203–1207, 2009.

[405] R. I. Trezona, D. N. Allsopp, and I. M. Hutchings. Transitions between two-body and three-body abrasive wear: Influence of test conditions in the microscale abrasive wear test. *Wear*, 225-229:205–214, 1999.

[406] G. B. Stachowiak and G. W. Stachowiak. The effects of particle characteristics on three-body abrasive wear. *Wear*, 249: 201–207, 2001.

[407] R. L. Deuis, C. Subramanian, and J. M. Yellup. Abrasive wear of aluminium composites - a review. *Wear*, 201:132–144, 1996.

[408] M. F. Buchely, J. C. Gutierrez, L. M. Léon, and A. Toro. The effect of microstructure on abrasive wear of hardfacing alloys. *Wear*, 259:52–61, 2005.

[409] E. Gnecco, R. Bennewitz, and E. Meyer. Abrasive wear on the atomic scale. *Physical Review Letters*, 88:215501, 2002.

[410] K. Holmberg, H. Ronkainen, A. Laukkanen, and K. Wallin. Friction and wear of coated surfaces - scales, modelling and simulation of tribomechanisms. *Surface & Coatings Technology*, 202:1034–1049, 2007.

[411] A. V. Olver. The mechanism of rolling contact fatigue: An update. *Proceedings of the Institution of Mechanical Engineers Part J: Journal of Engineering Tribology*, 219:313–330, 2005.

[412] F. Sadeghi, B. Jalalahmadi, T. S. Slack, N. Raje, and N. K. Arakere. A review of rolling contact fatigue. *ASME Journal of Tribology*, 131:041403, 2009.

[413] J. Halme and P. Andersson. Rolling contact fatigue and wear fundamentals for rolling bearing diagnostics - state of the art. *Proceedings of the Institution of Mechanical Engineers, Part J: Journal of Engineering Tribology*, 224:377–393, 2009.

[414] X. Liu, P. K. Chu, and C. Ding. Surface modification of titanium, titanium alloys, and related materials for biomedical applications. *Materials Science and Engineering R*, 47:49–121, 2004.

[415] Q. Chen and G. A. Thouas. Metallic implant biomaterials. *Materials Science and Engineering R*, 87:1–57, 2015.

[416] H. A. Padilla and B. L. Boyce. A review of fatigue behavior in nanocrystalline metals. *Experimental Mechanics*, 50:5–231, 2010.

[417] M. M. Stack. Bridging the gap between tribology and corrosion: From wear maps to Pourbaix diagrams. *International Materials Reviews*, 50:1–17, 2005.

[418] D. Landolt. Electrochemical and materials aspects of tribocorrosion systems. *Journal of Physics D: Applied Physics*, 39: 3121–3127, 2006.

[419] A. Ayyagari, V. Hasannaeimi, H. S. Grewal, H. Arora, and S. Mukherjee. Corrosion, erosion and wear behavior of complex concentrated alloys: A review. *Metals*, 8:603, 2018.

[420] B. T. Lu and J. L. Lou. Synergism of electrochemical and mechanical factors in erosion-corrosion. *Journal of Physical Chemistry B*, 110:4217–4231, 2006.

[421] S. Mischler. Triboelectrochemical techniques and interpretation methods in tribocorrosion: A comparative evaluation. *Tribology International*, 41:573–578, 2008.

[422] R. J. K. Wood. Tribo-corrosion of coatings: A review. *Journal of Physics D: Applied Physics*, 40:5502–5521, 2007.

[423] M. V. Prozhega, N. A. Tatus, S. V. Samsonov, O. Y. Kolyuzhni, and N. N. Smirnov. Experimental study of erosion-corrosion wear of materials: A review. *Journal of Friction and Wear*, 35:155–160, 2014.

[424] R. J. K. Wood. Erosion-corrosion interactions and their effect on marine and offshore materials. *Wear*, 261:1012–1023, 2006.

[425] D. Landolt, S. Mischler, and M. Stemp. Electrochemical methods in tribocorrosion: A critical appraisal. *Electrochimica Acta*, 46:3913–3929, 2001.

[426] G. Kear, B. D. Barker, and F. C. Walsh. Electrochemical corrosion of unalloyed copper in chloride media - a critical review. *Corrosion Science*, 46:109–135, 2004.

[427] J. C. Hoogvliet, M. Dijksma, B. Kamp, and W. P. van Bennekom. Electrochemical pretreatment of polycrystalline gold electrodes to produce a reproducible surface roughness for self-assembly: A study in phosphate buffer pH 7.4. *Analytical Chemistry*, 72:2016–2021, 2000.

[428] D. Landolt, P.-F. Chauvy, and O. Zinger. Electrochemical micromachining, polishing and surface structuring of metals: Fundamental aspects and new developments. *Electrochimica Acta*, 48:3185–3201, 2003.

[429] P. Ponthiaux, F. Wenger, D. Drees, and J. P. Celis. Electrochemical techniques for studying tribocorrosion processes. *Wear*, 256:459–468, 2004.

[430] G. Bregliozzi, A. Di Schino, S. I.-U. Ahmed, J. M. Kenny, and H. Haefke. Cavitation wear behaviour of austenitic stainless steels with different grain sizes. *Wear*, 258:503–510, 2005.

[431] J. F. Santa, L. A. Espitia, J. A. Blanco, S. A. Romo, and A. Toro. Slurry and cavitation erosion resistance of thermal spray coatings. *Wear*, 267:160–167, 2009.

[432] P. Kumar and R. P. Saini. Study of cavitation in hydro turbines - a review. *Renewable and Sustainable Energy Reviews*, 14: 374–383, 2010.

[433] Y. Qiu and M. M. Khonsari. Experimental investigation of tribological performance of laser textured stainless steel rings. *Tribology International*, 44:635–644, 2010.

[434] D. Gropper, L. Wang, and T. J. Harvey. Hydrodynamic lubrication of textured surfaces: A review of modeling techniques and key findings. *Tribology International*, 94:509–529, 2016.

[435] A. Ramalho and J. C. Miranda. The relationship between wear and dissipated energy in sliding systems. *Wear*, 260:361–367, 2006.

[436] R. A. Miller. Thermal barrier coatings for aircraft engines: History and directions. *Journal of Thermal Spray Technology*, 6: 35–42, 1997.

[437] P. Fauchais, A. Vardelle, and B. Dussoubs. Quo vadis thermal spraying. *Journal of Thermal Spray Technology*, 10:44–66, 2001.

[438] Z. Wang, A. Kulkarni, S. Deshpande, T. Nakamura, and H. Herman. Effects of pores and interfaces on effective properties of plasma sprayed zirconia coatings. *Acta Materialia*, 51:5319–5334, 2003.

[439] D. R. Clarke, M. Oechsner, and N. P. Padture. Thermal-barrier coatings for more efficient gas-turbine engines. *MRS Bulletin*, 37:891–898, 2012.

[440] M. R. W. Brake, A. C. Hall, and J. D. Madison. Designing energy dissipation properties via thermal spray coatings. *Surface and Coatings Technology*, 310:70–78, 2017.

[441] R. S. Lima, J. Karthikeyan, C. M. Kay, J. Lindemann, and C. C. Berndt. Microstructural characteristics of cold-sprayed nanostructured WC-Co coatings. *Thin Solid Films*, 416:129–135, 2002.

[442] H. Assadi, F. Gärtner, T. Stoltenhoff, and H. Kreye. Bonding mechanism in cold gas spraying. *Acta Materialia*, 51:4379–4394, 2003.

[443] J. T. Despard, E. O'Neill, S. Ahadzie, and M. R. W. Brake. Overview of tribology in tribomechadynamics: A need for in-situ testing. In *Tribomechadynamics 2019*, Houston, TX, August 2019.

[444] B. Bhattacharya and B. Ellingwood. A new CDM-based appraoch to structural deterioration. *International Journal of Solids and Structures*, 36:1757–1779, 1999.

[445] M. D. Bryant, M. M. Khonsari, and F. F. Ling. On the thermodynamics of degradation. *Proceedings of the Royal Society A*, 464:2001–2014, 2008.

[446] L. A. Sosnovskiy and S. S. Sherbakov. A model of mechanothermodynamic entropy in tribology. *Entropy*, 19:115, 2017.

[447] M. Amiri and M. Modarres. An entropy-based damage characterization. *Entropy*, 16:6434–6463, 2014.

[448] A. Beheshti and M. M. Khonsari. A thermodynamic approach for prediction of wear coefficient under unlubricated sliding condition. *Tribology Letters*, 38:347–354, 2010.

[449] A. B. Aghdam and M. M. Khonsari. On the correlation between wear and entropy in dry sliding contact. *Wear*, 270:781–790, 2011.

[450] D. A. Hills. Mechanics of fretting fatigue. *Wear*, 175:107–113, 1994.

[451] M. P. Szolwinski and T. N. Farris. Mechanics of fretting fatigue crack formation. *Wear*, 198:93–107, 1996.

[452] E. Sauger, S. Fouvry, L. Ponsonnet, P. Kapsa, J. M. Martin, et al. Tribologically transformed structure in fretting. *Wear*, 245: 39–52, 2000.

[453] R. Rajendran. Gas turbine coatings - an overview. *Engineering Failure Analysis*, 26:355–369, 2012.

[454] N. A. Bhatti, K. Pereira, and M. A. Wahab. Effect of stress gradient and quadrant averaging on fretting fatigue crack initiation angle and life. *Tribology International*, 131:212–221, 2019.

[455] Z.-B. Cai, Z.-Y. Li, M.-G. Yin, M.-H. Zhu, and Z.-R. Zhou. A review of fretting study on nuclear power equipment. *Tribology International*, 144:106095, 2020.

[456] T. Guo, Z. Liu, J. Correia, and A. M. P. de Jesus. Experimental study on fretting-fatigue of bridge cable wires. *International Journal of Fatigue*, 131:105321, 2020.

[457] J. Hintikka, A. Mäntylä, J. Vaara, T. Frondelius, and A. Lehtovaara. Stable and unstable friction in fretting contacts. *Tribology International*, 131:73–82, 2019.

[458] M. Varenberg, G. Halperin, and I. Etsion. Different aspects of the role of wear debris in fretting wear. *Wear*, 252:902–910, 2004.

[459] A. L. Greer, K. L. Rutherford, and I. M. Hutchings. Wear resistance of amorphous alloys and related materials. *International Materials Reviews*, 47:87–112, 2002.

[460] J. J. Madge, S. B. Leen, I. R. McColl, and P. H. Shipway. Contact-evolution based prediction of fretting fatigue life: Effect of slip amplitude. *Wear*, 262:1159–1170, 2007.

[461] T. Dursun and C. Soutis. Recent developments in advanced aircraft aluminium alloys. *Materials and Design*, 56:862–871, 2014.

[462] G. H. Majzoobi, A. Azadikhah, and J. Nemati. The effects of deep rolling and shot peening on fretting fatigue resistance of aluminum-7075-T6. *Materials Science and Engineering A*, 516:235–247, 2009.

[463] T. N. Chakherlou, M. Shakouri, A. Akbari, and A. B. Aghdam. Effect of cold expansion and bolt clamping on fretting fatigue behavior of Al 2024-T3 in double shear lap joints. *Engineering Failure Analysis*, 25:29–41, 2012.

[464] J. Vázquez, C. Navarro, and J. Domínguez. Experimental results in fretting fatigue with shot and laser peened Al 7075-T651 specimens. *International Journal of Fatigue*, 40:143–153, 2012.

[465] A. K. Gujba and M. Medraj. Laser peening process and its impact on materials properties in comparison with shot peening and ultrasonic impact peening. *Materials*, 7925-7974:509–529, 2014.

[466] F. Lai, S. Qu, R. Lewis, T. Slatter, W. Fu, et al. The influence of ultrasonic surface rolling on the fatigue and wear properties of 23-8N engine valve steel. *International Journal of Fatigue*, 125:299–313, 2019.

[467] W. Zhao, D. Liu, X. Zhang, Y. Zhou, R. Zhang, et al. Improving the fretting and corrosion fatigue performance of 300M ultra-high strength steel using the ultrasonic surface rolling process. *International Journal of Fatigue*, 121:30–38, 2019.

[468] J. Yang, D. Liu, Z. Zhang, M. Liu, W. Zhao, et al. The effect of ultrasonic surface rolling process on the fretting fatigue property of GH4169 superalloy. *International Journal of Fatigue*, 133:105373, 2020.

[469] Y. Fu, J. Wei, and A. W. Batchelor. Some considerations on the mitigation of fretting damage by the application of surface-modification technologies. *Jouranl of Materials Processing Technology*, 99:231–245, 2000.

[470] A. Amanov, I.-S. Cho, D.-E. Kim, and Y.-S. Pyun. Fretting wear and friction reduction of CP titanium and Ti-6Al-4V alloy by ultrasonic nanocrystalline surface modification. *Surfaces & Coatings Technology*, 207:135–142, 2012.

[471] R. H. Oskouei and R. N. Ibrahim. Improving fretting fatigue behaviour of Al 7075-T6 bolted plates using electroless Ni-P coatings. *International Journal of Fatigue*, 44:157–167, 2012.

[472] A. A. D. Sarhan, E. Zalnezhad, and M. Hamdi. The influence of higher surface hardness on fretting fatigue life of hard anodized aerospace AL7075-T6 alloy. *Materials Science & Engineering A*, 560:377–387, 2013.

[473] J. D. Lemm, A. R. Warmuth, S. R. Pearson, and P. H. Shipway. The influence of surface hardness on the fretting wear of steel pairs - its role in debris retention in the contact. *Tribology International*, 81:258–266, 2015.

[474] A. Amanov and R. Umarov. The effects of ultrasonic nanocrystal surface modification temperature on the mechanical properties and fretting wear resistance of Inconel 690 alloy. *Applied Surface Science*, 441:515–529, 2018.

[475] W. Zhai, W. Lu, P. Zhang, J. Wang, X. Liu, et al. Wear-triggered self-healing behavior on the surface of nanocrystalline nickel aluminum bronze/Ti3SiC2 composites. *Applied Surface Science*, 436:1038–1049, 2018.

[476] L. Ma, K. Eom, J. Geringer, T.-S. Jun, and K. Kim. Literature review on fretting wear and contact mechanics of tribological coatings. *Coatings*, 9:501, 2019.

[477] M. Niinomi. Mechanical biocompatibilities of titanium alloys for biomedical applications. *Journal of Materials Science Lettersthe Mechanical Behavior of Biomedical Materials*, 1:30–42, 2008.

[478] X. Zhang, Y. Chen, and J. Hu. Recent advances in the development of aerospace materials. *Progress in Aerospace Sciences*, 97:22–34, 2018.

[479] S. Fouvry, P. Duó, and P. Perruchaut. A quantitative approach of Ti-6Al-4V fretting damage: Friction, wear and crack nucleation. *Wear*, 257:916–929, 2004.

[480] O. Jin and S. Mall. Effects of slip on fretting behavior: Experiments and analyses. *Wear*, 256:671–684, 2004.

[481] S. Fouvry, V. Fridrici, C. Langlade, P. Kapsa, and L. Vincent. Palliatives in fretting: A dynamical approach. *Tribology International*, 39:1005–1015, 2006.

[482] Z. R. Zhou, K. Nakazawa, M. H. Zhu, N. Maruyama, P. Kapsa, et al. Progress in fretting maps. *Tribology International*, 39: 1068–1073, 2006.

[483] K. J. Kubiak, T. G. Mathia, and S. Fouvry. Interface roughness effect on friction map under fretting contact conditions. *Tribology International*, 43:1500–1507, 2010.

[484] S. Garcin, S. Fouvry, and S. Heredia. A FEM fretting map modeling: Effect of surface wear on crack nucleation. *Wear*, 330-331:145–159, 2015.

[485] M. H. Zhu and Z. R. Zhou. On the mechanisms of various fretting wear modes. *Tribology International*, 44:1378–1388, 2011.

[486] R. Rajasekaran and D. Nowell. Fretting fatigue in dovetail blade roots: Experiment and analysis. *Tribology International*, 39: 1277–1285, 2006.

[487] L. Bohórquez and J. Domínguez. Characterization of the contact between a punch and a half-infinite substrate in a fretting situation. *International Journal of Mechanical Sciences*, 49:608–621, 2007.

[488] R. C. Flicek. *Analysis of Complete Contacts Subject to Fatigue*. Doctoral Dissertation. University of Oxford, Oxford, UK, 2014.

[489] T. D. B. Jacobs and R. W. Carpick. Nanoscale wear as a stress-assisted chemical reaction. *Nature Nanotechnology*, 8: 108–112, 2013.

[490] J. F. Archard. Contact and rubbing of flat surfaces. *Journal of Applied Physics*, 24:981–988, 1953.

[491] I. R. McColl, J. Ding, and S. B. Leen. Finite element simulation and experimental validation of fretting wear. *Wear*, 256: 1114–1127, 2004.

[492] D. H. Jeong, F. Gonzalez, G. Palumbo, K. T. Aust, and U. Erb. The effect of grain size on the wear properties of electrodeposited nanocrystalline nickel coatings. *Scripta Materialia*, 44:493–499, 2001.

[493] Y. S. Zhang, Z. Han, K. Wang, and K. Lu. Friction and wear behaviors of nanocrystalline surface layer of pure copper. *Wear*, 260:942–948, 2006.

[494] P. Flores. Modeling and simulation of wear in revolute clearance joints in multibody systems. *Mechanism and Machine Theory*, 44:1211–1222, 2009.

[495] S. Fouvry, T. Liskiewicz, P. Kapsa, S. Hannel, and E. Sauger. An energy description of wear mechanisms and its application to oscillating sliding contacts. *Wear*, 255:287–298, 2003.

[496] C. A. Schuh, T. G. Nieh, and T. Yamasaki. Hall-Petch breakdown manifested in abrasive wear resistance of nanocrystalline nickel. *Scripta Materialia*, 46:735–740, 2002.

[497] A. Dasari, Z.-Z. Yu, and Y.-W. Mai. Fundamental aspects and recent progress on wear/scratch damage in polymer nanocomposites. *Materials Science and Engineering R*, 63:31–80, 2009.

[498] Q. Tian, P. Flores, and H. M. Lankarani. A comprehensive survey of the analytical, numerical and experimental methodologies for dynamics of multibody mechanical systems with clearance or imperfect joints. *Mechanism and Machine Theory*, 122:1–57, 2018.

[499] E. Y. A. Wornyoh, V. K. Jasti, and C. F. Higgs, III. A review of dry particulate lubrication: Powder and granular materials. *ASME Journal of Tribology*, 129:438–449, 2007.

[500] E. R. M. Gelinck and D. J. Schipper. Calculation of Stribeck curves for line contact. *Tribology International*, 33:175–181, 2000.

[501] X. Lu, M. M. Khonsari, and E. R. M. Gelinck. The Stribeck curve: Experimental results and theoretical prediction. *ASME Journal of Tribology*, 128:789–794, 2006.

[502] M. Woydt and R. Wäsche. The history of the Stribeck curve and ball bearing steels: The role of Adolf Martens. *Wear*, 268: 1542–1546, 2010.

[503] H. Zhang, M. Hua, G.-N. Dong, D.-Y. Zhang, and K.-S. Chin. A mixed lubrication model for studying tribological behaviors of surface texturing. *Tribology International*, 93:583–592, 2016.

[504] P. M. Lugt and G. E. Morales-Espejel. A review of elasto-hydrodynamic lubrication theory. *Tribology Transactions*, 54: 470–496, 2011.

[505] A. Rostami and J. L. Streator. Study of liquid-mediated adhesion betweeen 3d rough surfaces: A spectral approach. *Tribology International*, 84:36–47, 2015.

[506] A. Kovalchenko, O. Ajayi, A. Erdemir, G. Fenske, and I. Etsion. The effect of laser surface texturing on transitions in lubrication regimes during unidirectional sliding contact. *Tribology International*, 38:219–225, 2005.

[507] M. Wakuda, Y. Yamauchi, S. Kanzaki, and Y. Yasuda. Effect of surface texturing on friction reduction between ceramic and steel materials under lubricated sliding contact. *Wear*, 254:356–363, 2003.

[508] I. Etsion. State of the art in laser surface texturing. *ASME Journal of Tribology*, 127:248–253, 2005.

[509] U. Pettersson and S. Jacobson. Influence of surface texture on boundary lubricated sliding contacts. *Tribology International*, 36:857–864, 2003.

[510] U. Sudeep, N. Tandon, and R. K. Pandey. Performance of lubricated rolling/sliding concentrated contacts with surface textures: A review. *ASME Journal of Tribology*, 137:031501, 2015.

[511] C. F. Higgs, III and J. Tichy. Granular flow lubrication: Continuum modeling of shear behavior. *ASME Journal of Tribology*, 126:499–510, 2004.

[512] E. J. Terrell and C. F. Higgs, III. A particle-augmented mixed lubrication modeling approach to predicting chemical mechanical polishing. *ASME Journal of Tribology*, 131:012201, 2009.

[513] N. V. Queipo, R. T. Haftka, W. Shyy, T. Goel, R. Vaidyanathan, et al. Surrogate-based analysis and optimization. *Progress in Aerospace Sciences*, 41:1–28, 2005.

[514] T. Goel, R. T. Haftka, W. Shyy, and N. V. Queipo. Ensemble of surrogates. *Structural and Multidisciplinary Optimization*, 33: 199–216, 2007.

[515] A. I. J. Forrester and A. J. Keane. Recent advances in surrogate-based optimization. *Progress in Aerospace Sciences*, 45: 50–79, 2009.

[516] F. A. C. Viana, T. W. Simpson, V. Balabanov, and V. Toropov. Metamodeling in multidisciplinary design optimization: How far have we really come? *AIAA Journal*, 52:670–690, 2014.

[517] G. Carleo, I. Cirac, K. Cranmer, L. Daudet, M. Schuld, et al. Machine learning and the physical sciences. *Reviews of Modern Physics*, 91:045002, 2019.

[518] R. Ramprasad, R. Batra, G. Pilania, A. Mannodi-Kanakkithodi, and C. Kim. Machine learning in materials informatics: Recent applications and prospects. *NPJ Computational Materials*, 3:1–13, 2017.

[519] K. T. Butler, D. W. Davies, H. Cartwright, O. Isayev, and A. Walsh. Machine learning for molecular and materials science. *Nature*, 559:547–555, 2018.

[520] B. Sanchez-Lengeling and A. Aspuru-Guzik. Inverse molecular design using machine learning: Generative models for matter engineering. *Science*, 361:360–365, 2018.

[521] J. Schmidt, M. R. G. Marques, S. Botti, and M. A. L. Marques. Recent advances and applications of machine learning in solid-state materials science. *NPJ Computational Materials*, 5:1–36, 2019.

[522] E. W. Bucholz, C. S. Kong, K. R. Marchman, W. G. Sawyer, S. R. Phillpot, et al. Data-driven model for estimation of friction coefficient via informatics methods. *Tribology Letters*, 47:211–221, 2012.

[523] T. Thankachan, K. S. Prakash, and M. Kamarthin. Optimizing the tribological behavior of hybrid copper surface composites using statistical and machine learning techniques. *ASME Journal of Tribology*, 140:0316107, 2018.

[524] A. Borjali, K. Monson, and B. Raeymaekers. Predicting the polyethylene wear rate in pin-on-disc experiments in the context of prosthetic hip implants: Deriving a data-driven model using machine learning methods. *Tribology International*, 133:101–110, 2019.

[525] G. Boidi, M. Rodrigues da Silva, F. J. Profito, and I. F. Machado. Using machine learning radial basis function (rbf) method for predicting lubricated friction on textured and porous surfaces. *Surface Topography: Metrology and Properties*, 8:044002, 2020.

[526] T. Gurgenc, O. Altay, M. Ulas, and C. Ozel. Extreme learning machine and support vector regression wear loss predictions for magnesium alloys coated using various spray coating methods. *Journal of Applied Physics*, 127:185103, 2020.

[527] J. Fang, G. Sun, N. Qiu, N. H. Kim, and Q. Li. On design optimization for structural crashworthiness and its state of the art. *Structural and Multidisciplinary Optimization*, 55:1091–1119, 2017.

[528] G. Gilardi and I. Sharf. Literature survey of contact dynamics modelling. *Mechanism and Machine Theory*, 37:1213–1239, 2002.

[529] M. K. Bhardwaj, R. K. Kapania, E. Reichenbach, and G. P. Guruswamy. Computational fluid dynamics/computational structural dynamics interaction methodology for aircraft wings. *AIAA Journal*, 36:2179–2186, 1998.

[530] S. Oberst and J. C. S. Lai. Nonlinear transient and chaotic interactions in disc brake squeal. *Journal of Sound and Vibration*, 342:272–289, 2015.

[531] R. Rengarajan, S. Noll, and R. Singh. Explanation for variability in lower frequency structure-borne noise and vibration: Roles of rear subframe dynamics and right-left spindle phasing. *SAE International Journal of Vehicle Dynamics, Stability, and NVH*, 2:27–40, 2018.

[532] T. A. Laursen and I. Stanciulescu. An algorithm for incorporation of frictional sliding conditions within a steady state rolling framework. *Communications in Numerical Methods in Engineering*, 22:301–318, 2006.

[533] I. Stanciulescu and T. A. Laursen. On the interaction of frictional formulations with bifurcation phenomena in hyperelastic steady state rolling calculations. *International Journal of Solids and Structures*, 43:2959–2988, 2006.

[534] H. Wang, I. L. Al-Qadi, and I. Stanciulescu. Simulation of tyre-pavement interaction for predicting contact stresses at static and various rolling conditions. *International Journal of Pavement Engineering*, 13:310–321, 2012.

[535] H. Wang, I. L. Al-Qadi, and I. Stanciulescu. Effect of surface friction on tire-pavement contact stresses during vehicle maneuvering. *Journal of Engineering Mechanics*, 140:04014001, 2014.

[536] K. M. Salerno, D. S. Bolintineanu, G. S. Grest, J. B. Lechman, S. J. Plimpton, et al. Effect of shape and friction on the packing and flow of granular materials. *Physical Review E*, 98:050901, 2018.

[537] A. Fernandez del Rincon, F. Viadero, M. Iglesias, P. García, A. de-Juan, et al. A model for the study of meshing stiffness in spur gear transmissions. *Mechanism and Machine Theory*, 61:30–58, 2013.

[538] H. Cao, L. Niu, S. Xi, and X. Chen. Mechanical model development of rolling bearing-rotor systems: A review. *Mechanical Systems and Signal Processing*, 102:37–58, 2018.

[539] R. G. Parker, V. Agashe, and S. M. Vijayakar. Dynamic response of a planetary gear system using a finite element/contact mechanics model. *ASME Journal of Mechanical Design*, 122:304–310, 2000.

[540] S. Theodossiades and S. Natsiavas. Non-linear dynamics of gear-pair systems with periodic stiffness and backlash. *Journal of Sound and Vibration*, 229:287–310, 2000.

[541] A. MacLeod, N. Peckham, G. Serrancoli, I. Rombach, P. Hourigan, et al. Personalized high tibial osteotomy has mechanical safety equivalent to generic device in a case-control in silico clinical trial. *Communications Medicine*, 1:1–9, 2021.

[542] Y. A. Khulief. Modeling of impact in multibody systems: An overview. *ASME Journal of Computational and Nonlinear Dynamics*, 8:021012, 2013.

[543] M. R. Brake, P. L. Reu, D. J. VanGoethem, M. V. Bejarano, and A. Sumali. Experimental validation of an elastic-plastic contact model. In *ASME 2011 International Mechanical Engineering Congress and Exposition*, Denver, CO, November 11-17 2011.

[544] R. Seifried, W. Schiehlen, and P. Eberhard. The role of the coefficient of restitution on impact problems in multi-body dynamics. *Proceedings of the Institution of Mechanical Engineers, Part K: Journal of Multi-body Dynamics*, 224:279–306, 2010.

[545] W. J. Stronge. Smooth dynamics of oblique impact with friction. *International Journal of Impact Engineering*, 51:36–49, 2013.

[546] G. Pietrzak and A. Curnier. Large deformation frictional contact mechanics: Continuum formulation and augmented lagrangian treatment. *Computer Methods in Applied Mechanics and Engineering*, 177:351–381, 1999.

[547] J. R. Barber. *Contact Mechanics*. Springer, Cham, Switzerland, 2018.

[548] M. R. Brake. The effect of the contact model on the impact-vibration response of continuous and discrete systems. *Journal of Sound and Vibration*, 332:3849–3878, 2013.

[549] D. J. Wagg. A note on coefficient of restitution models including the effects of impact induced vibration. *Journal of Sound and Vibration*, 300:1071–1078, 2007.

[550] D. J. Wagg, G. Karpodinis, and S. R. Bishop. An experimental study of the impulse response of a vibro-impacting cantilever beam. *Journal of Sound and Vibration*, 228:243–264, 1999.

[551] K. H. Hunt and F. R. E. Crossley. Coefficient of restitution interpreted as damping in vibroimpact. *ASME Journal of Applied Mechanics*, 42:440–445, 1975.

[552] M. Rodrigues da Silva, F. Marques, M. Tavares da Silva, and P. Flores. A compendium of contact force models inspired by Hunt and Crossley's cornerstone work. *Mechanism and Machine Theory*, 167:104501, 2022.

[553] J. Dundurs and M. Stippes. Role of elastic constants in certain contact problems. *ASME Journal of Applied Mechanics*, 37: 965–970, 1970.

[554] A. Persson. *On the Stress Distribution of Cylindrical Elastic Bodies in Contact*. Doctoral Dissertation. Chalmers University of Technology, Gothenburg, Sweden, 1964.

[555] M. Ciavarella and P. Decuzzi. The state of stress induced by the plane frictionless cylindrical contact. I. the case of elastic similarity. *International Journal of Solids and Structures*, 38:4507–4523, 2001.

[556] L. M. Keer, J. Dundurs, and K. C. Tsai. Problems involving receding contact between a layer and a half space. *ASME Journal of Applied Mechanics*, 39:1115–1120, 1972.

[557] J. J. Kauzlarich and J. A. Greenwood. Contact between a centrally loaded plate and a rigid or elastic base, with application to pivoted pad bearings. *Proceedings of the Institution of Mechanical Engineers Part C: Journal of Mechanical Engineering Science*, 215:623–628, 2001.

[558] Y. J. Ahn and J. R. Barber. Response of frictional receding contact problems to cyclic loading. *International Journal of Mechanical Sciences*, 50:1519–1525, 2008.

[559] S. Karuppanan and D. A. Hills. Frictional complete contacts between elastically similar bodies subject to normal and shear loads. *International Journal of Solids and Structures*, 45:4662–4675, 2008.

[560] D. A. Hills, , and D. Dini. Common edge contacts: Effect of interface line orientation. *International Journal of Mechanical Sciences*, 81:73–76, 2014.

[561] Z. Clark, R. Ramesh, and D. A. Hills. Edge slip zone size of misaligned common edge contacts. *The Journal of Strain Analysis for Engineering Design*, 52:450–454, 2017.

[562] M. Ciavarella and G. Macina. New results for the fretting-induced stress concentration on Hertzian and flat rounded contacts. *International Journal of Mechanical Sciences*, 45:449–467, 2003.

[563] A. Sackfield, D. Dini, and D. A. Hills. The finite and semi-infinite tilted, flat but rounded punch. *International Journal of Solids and Structures*, 42:4988–5009, 2005.

[564] T. Zhang, P. E. McHugh, and S. B. Leen. Computational study on the effect of contact geometry on fretting behavior. *Wear*, 271:1462–1480, 2011.

[565] S. El-Borgi, R. Abdelmoula, and L. Keer. A receding contact plane problem between a functionally graded layer and a homogeneous substrate. *International Journal of Solids and Structures*, 43:658–674, 2006.

[566] G. Feng, W. D. Nix, Y. Yoon, and C. J. Lee. A study of the mechanical properties of nanowires using nanoindentation. *Journal of Applied Physics*, 99:074304, 2006.

[567] S. R. Bishop. Impact oscillators. *Philosophical Transactions of the Royal Society of London A*, 347:347–351, 1994.

[568] J. M. T. Thompson and H. B. Stewart. *Nonlinear Dynamics and Chaos*. John Wiley and Sons, Ltd., 2002.

[569] B. Blazejczyk-Okolewska, K. Czolczynski, and T. Kapitaniak. Classification principles of types of mechanical systems with impacts - fundamental assumptions and rules. *European Journal of Mechanics A - Solids*, 23:517–537, 2004.

[570] M. Y. Louge and M. E. Adams. Anomalous behavior of normal kinematic restitution in the oblique impacts of a hard sphere on an elastoplastic plate. *Physical Review E*, 65:021303, 2002.

[571] D. B. Marghitu and Y. Hurmuzlu. Nonlinear dynamics of an elastic rod with frictional impact. *Nonlinear Dynamics*, 10: 187–201, 1996.

[572] M. Dupac and D. B. Marghitu. Nonlinear dynamics of a flexible mechanism with impact. *Journal of Sound and Vibration*, 289: 952–966, 2006.

[573] B. Blazejczyk-Okolewska, K. Czolczynski, and T. Kapitaniak. Dynamics of a two-degree-of-freedom cantilever beam with impacts. *Chaos, Solitons and Fractals*, 40:1991–2006, 2009.

[574] T. Chaise, J. Li, D. Nélias, R. Kubler, S. Taheri, et al. Modelling of multiple impacts for the prediction of distortions and residual stresses induced by ultrasonic shot peening (USP). *Journal of Materials Processing Technology*, 212:2080–2090, 2012.

[575] Y. Fu, H. Ouyang, and R. B. Davis. Triboelectric energy harvesting from the vibro-impact of three cantilevered beams. *Mechanical Systems and Signal Processing*, 121:509–531, 2019.

[576] L. A. Wood and K. P. Byrne. Analysis of a random repeated impact process. *Journal of Sound and Vibration*, 78:329–345, 1981.

[577] P. J. Holmes. The dynamics of repeated impacts with a sinusoidally vibrating table. *Journal of Sound and Vibration*, 84: 173–189, 1982.

[578] P. J. Holmes and F. C. Moon. Strange attractors and chaos in nonlinear mechanics. *ASME Journal of Applied Mechanics*, 50:1021–1032, 1983.

[579] N. Popplewell, C. N. Bapat, and K. McLachlan. Stable periodic vibroimpacts of an oscillator. *Journal of Sound and Vibration*, 87:41–59, 1983.

[580] F. C. Moon and S. W. Shaw. Chaotic vibrations of a beam with non-linear boundary conditions. *International Journal of Non-Linear Mechanics*, 18:465–477, 1983.

[581] S. W. Shaw and P. J. Holmes. A periodically forced piecewise linear oscillator. *Journal of Sound and Vibration*, 90:129–155, 1983.

[582] S. W. Shaw and P. J. Holmes. A periodically forced impact oscillator with large dissipation. *ASME Journal of Applied Mechanics*, 50:849–857, 1983.

[583] S. W. Shaw and P. J. Holmes. Periodically forced linear oscillator with impacts: Chaos and long-period motions. *Physical Review Letters*, 51:623–626, 1983.

[584] J. M. T. Thompson. Complex dynamics of compliant off-shore structures. *Proceedings of the Royal Society of London, Series A*, 387:407–427, 1983.

[585] J. M. T. Thompson, A. R. Bokaian, and R. Ghaffari. Subharmonic resonances and chaotic motions of a bilinear oscillator. *IMA Journal of Applied Mathematics*, 31:207–234, 1983.

[586] S. W. Shaw. Forced vibrations of a beam with one-sided amplitude constraint: Theory and experiment. *Journal of Sound and Vibration*, 99:199–212, 1985.

[587] S. W. Shaw. The dynamics of a harmonically excited system having rigid amplitude constraints part 1: Subharmonic motions and local bifurcations. *ASME Journal of Applied Mechanics*, 52:453–458, 1985.

[588] S. W. Shaw. The dynamics of a harmonically excited system having rigid amplitude constraints part 2: Chaotic motions and global bifurcations. *ASME Journal of Applied Mechanics*, 52:459–464, 1985.

[589] A. Muszynska. Rotor-to-stationary element rub-related vibration phenomena in rotating machinery – literature survey. *Shock and Vibration Digest*, 21:3–11, 1989.

[590] K. Popp. Non-smooth mechanical systems - an overview. *Forschung im Ingenieurwesen*, 64:223–229, 1998.

[591] L. Půst, F. Peterka, G. Stépán, G. R. Tomlinson, and A. Tondl. Nonlinear oscillations in machines and mechanisms theory. *Mechanism and Machine Theory*, 34:1237–1253, 1999.

[592] J. Jerrelind and A. Stensson. Nonlinear dynamics of parts in engineering systems. *Chaos, Solitons and Fractals*, 11: 2413–2428, 2000.

[593] M. di Bernardo, C. J. Budd, A. R. Champneys, P. Kowalczyk, A. B. Nordmark, et al. Bifurcations in nonsmooth dynamical systems. *SIAM Review*, 50:629–701, 2008.

[594] S. Natsiavas. Analytical modeling of discrete mechanical systems involving contact, impact, and friction. *Applied Mechanics Reviews*, 71:050802, 2019.

[595] G. S. Whiston. Global dynamics of a vibro-impacting linear oscillator. *Journal of Sound and Vibration*, 118:395–429, 1987.

[596] G. W. Blankenship and A. Kahraman. Steady state forced response of a mechanical oscillator with combined parametric excitation and clearance type non-linearity. *Journal of Sound and Vibration*, 185:743–765, 1995.

[597] S. W. Shaw and R. H. Rand. The transition to chaos in a simple mechanical system. *International Journal of Non-Linear Mechanics*, 24:41–56, 1989.

[598] S. Natsiavas. On the dynamics of oscillators with bi-linear damping and stiffness. *International Journal of Non-Linear Mechanics*, 25:535–554, 1990.

[599] S. Natsiavas. Stability and bifurcation analysis for oscillators with motion limiting constraints. *Journal of Sound and Vibration*, 141:97–102, 1990.

[600] M. F. Heertjes, M. J. G. van de Molengraft, J. J. Kok, A. de Kraker, and D. H. van Campen. Manifold based feedback linearization of a 1-DOF beam with one-sided spring. *Nonlinear Dynamics*, 16:91–102, 1998.

[601] A. B. Nordmark. Non-periodic motion caused by grazing incidence in an impact oscillator. *Journal of Sound and Vibration*, 145:279–297, 1991.

[602] J. P. Cusumano and B.-Y. Bai. Period-infinity periodic motions, chaos and spatial coherence in a 10 degree of freedom impact oscillator. *Chaos, Solitons and Fractals*, 3:515–536, 1993.

[603] L. Zuo and A. Curnier. Non-linear real and complex modes of conewise linear systems. *Journal of Sound and Vibration*, 174: 289–313, 1994.

[604] S. Foale and S. R. Bishop. Transient response of a constrained beam subjected to narrow-band random excitation. *Journal of Sound and Vibration*, 185:723–733, 1995.

[605] M. Wiercigroch. Modelling of dynamical systems with motion dependent discontinuities. *Chaos, Solitons and Fractals*, 11: 2429–2442, 2000.

[606] Y. Zhang and I. Sharf. Validation of nonlinear viscoelastic contact force models for low speed impact. *ASME Journal of Applied Mechanics*, 76:051002, 2009.

[607] H. Wang, X. Yin, X. Qi, Q. Deng, B. Yu, et al. Experimental and theoretical analysis of the elastic-plastic normal repeated impacts of a sphere on a beam. *International Journal of Solids and Structures*, 109:131–142, 2017.

[608] D. J. Segalman, D. L. Gregory, M. J. Starr, B. R. Resor, M. D. Jew, et al. *Handbook on Dynamics of Jointed Structures*. Technical Report SAND2009-4164. Sandia National Laboratories, Albuquerque, NM, 2009.

[609] R. M. Lacayo, L. Pesaresi, J. Groß, D. Fochler, J. Armand, et al. Nonlinear modeling of structures with bolted joints: a comparison of two approaches based on a time-domain and frequency-domain solver. *Mechanical Systems and Signal Processing*, 114:413–438, 2019.

[610] J. H. Porter, N. N. Balaji, C. R. Little, and M. R. W. Brake. A quantitative assessment of the model form error of friction models across different interface representations for jointed structures. *Mechanical Systems and Signal Processing*, 163:108163, 2022.

[611] J. H. Porter, N. N. Balaji, and M. R. W. Brake. A non-masing microslip rough contact modeling framework for spatially and cyclically varying normal pressure. In *39th International Modal Analysis Conference (IMAC XXXIX)*, Online, February 2021.

[612] M. Krack, L. Salles, and F. Thouverez. Vibration prediction of bladed disks coupled by friction joints. *Archives of Computational Methods in Engineering*, 24(3):589–636, 2017.

[613] S. Bograd, P. Reuß, A. Schmidt, L. Gaul, and M. Mayer. Modeling the dynamics of mechanical joints. *Mechanical Systems and Signal Processing*, 25:2801–2826, 2011.

[614] N. N. Balaji, T. Dreher, M. Krack, and M. R. W. Brake. Reduced order modeling for the dynamics of jointed structures through hyper-reduced interface representation. *Mechanical Systems and Signal Processing*, 149:107249, 2021.

[615] D. R. Roettgen and M. S. Allen. Nonlinear characterization of a bolted, industrial structure using a modal framework. *Mechanical Systems and Signal Processing*, 84:152–170, 2017.

[616] C. W. Schwingshackl, D. Di Maio, I. Sever, and J. S. Green. Modeling and validation of the nonlinear dynamic behavior of bolted flange joints. *ASME Journal of Engineering for Gas Turbines and Power*, 135:122504–1–8, 2013.

[617] L. Pesaresi, L. Salles, J. S. Green, and C. W. Schwingshackl. Modelling the nonlinear behaviour of an underplatform damper test rig for turbine applications. *Mechanical Systems and Signal Processing*, 85:662–679, 2017.

[618] A. R. Brink, R. J. Kuether, M. D. Fronk, B. L. Witt, and B. L. Nation. Contact stress and lienarized modal predictions of as-built preloaded assembly. *ASME Journal of Vibration and Acoustics*, 142:051106, 2020.

[619] J. H. Porter and M. R. W. Brake. A high resolution rough contact model for bolted joints and its sensitivity to topology and material properties. In *40th International Modal Analysis Conference (IMAC XL)*, Orlando, FL, February 2022.

[620] D. J. Segalman. *A Modal Approach to Modeling Spatially Distributed Vibration Energy Dissipation*. Technical Report SAND2010-4763. Sandia National Laboratories, Albuquerque, NM, 2010.

[621] M. A. Guthrie. *Application of the Modal Iwan Damping Approach to a Beam Damping System*. Technical Report SAND2012-3178P. Sandia National Laboratories, Albuquerque, NM, 2012.

[622] B. Deaner. *Modeling the Nonlinear Damping of Jointed Structures Using Modal Models*. Masters Dissertation. University of Wisconsin-Madison, Madison, WI., 2013.

[623] B. J. Deaner, M. S. Allen, M. J. Starr, D. J. Segalman, and H. Sumali. Application of viscous and Iwan modal damping models to experimental measurements from bolted structures. *ASME Journal of Vibration and Acoustics*, 137:021012, 2015.

[624] R. M. Lacayo, B. J. Deaner, and M. S. Allen. A numerical study on the limitations of modal Iwan models for impulsive excitations. *Journal of Sound and Vibration*, 390:118–140, 2017.

[625] M. S. Allen, R. L. Mayes, and E. J. Bergman. Experimental modal substructuring to couple and uncouple substructres with flexible fixtures and multi-point connections. *Journal of Sound and Vibration*, 329:4891–4906, 2010.

[626] M. S. Allen, D. C. Kammer, and R. L. Mayes. Metrics for diagnosing negative mass and stiffness when uncoupling experimental and analytical substructures. *Journal of Sound and Vibration*, 331:5435–5448, 2012.

[627] D. Krattiger, L. Wu, M. Zacharczuk, M. Buck, R. J. Kuether, et al. Interface reduction for Hurty/Craig-Bampton substructured models: Review and improvements. *Mechanical Systems and Signal Processing*, 114:579–603, 2019.

[628] M. Brøns, T. A. Kasper, G. Chauda, S. W. B. Klaassen, C. W. Schwingshackl, et al. Experimental investigation of local dynamics in bolted lap joints using digital image correlation. *ASME Journal of Vibration and Acoustics*, 142:051114, 2020.

[629] W. Chen, D. Jana, A. Singh, M. Jin, M. Cenedese, et al. Nonlinear identification of a jointed structure using full-field data part I - experimental investigation. *Mechanical Systems and Signal Processing*, 166:108401, 2022.

[630] M. Jin, G. Kosova, M. Cenedese, W. Chen, A. Singh, et al. Nonlinear identification of a jointed structure using full-field data part II - analysis. *Mechanical Systems and Signal Processing*, 166:108402, 2022.

[631] M. R. W. Brake, C. W. Schwingshackl, and P. Reuß. Observations of variability and repeatability in jointed structures. *Mechanical Systems and Signal Processing*, 129:282–307, 2019.

[632] M. Pau, B. Leban, and A. Baldi. Experimental analysis of contact for the indentation of a flat rounded punch. *International Journal of Solids and Structures*, 43:7959–7965, 2006.

[633] L. Pesaresi, A. Fantetti, F. Cegla, L. Salles, and C. W. Schwingshackl. On the use of ultrasound waves to monitor the local dynamics of friction joints. *Experimental Mechanics*, 60:129–141, 2020.

[634] M. Ruan. *The Variability of Strains in Bolts and the Effecton on Preload in Jointed Structures*. Masters Dissertation. Rice University, Houston, TX., 2019.

[635] M. Eriten, A. A. Polycarpou, and L. A. Bergman. Surface roughness effects on energy dissipation in fretting contact of nominally flat surfaces. *ASME Journal of Applied Mechanics*, 78:Art. 021011, 2011.

[636] M. Eriten, A. A. Polycarpou, and L. A. Bergman. Physics-based modeling for fretting behavior of nominally flat rough surfaces. *International Journal of Solids and Structures*, 48:1436–1450, 2011.

[637] S. A. Smith, M. R. W. Brake, and C. W. Schwingshackl. On the characterization of nonlinearities in assembled structures. *ASME Journal of Vibration and Acoustics*, 142:051105, 2020.

[638] M. R. W. Brake. Bolted joints and tribomechadynamics. In *36th International Modal Analysis Conference (IMAC XXXVI)*, Orlando, FL, January 2018.

[639] B. A. Miller and I. Green. Numerical formulation for the dynamic analysis of spiral-grooved gas face seals. *ASME Journal of Tribology*, 123:395–403, 2001.

[640] I. Green. A transient dynamic analysis of mechanical seals including asperity contact and face deformation. *Tribology Transactions*, 45:284–293, 2002.

[641] J. Armand, L. Salles, C. W. Schwingshackl, D. Süß, and K. Willner. On the effects of roughness on the nonlinear dynamics of a bolted joint: A multiscale analysis. *European Journal of Mechanics / A Solids*, 70:44–57, 2018.

[642] F. Pichler, W. Witteveen, and L. Koller. Efficient virtual tribomechadynamics by means of joint modes for detailed investigation of complex local stick and slip behavior inside a joint. *ASME Journal of Vibration and Acoustics*, 142:051108, 2020.

[643] D. Shetty and M. Allen. Fast simulation of a single degree-of-freedom system consisting of an Iwan element using the method of averaging. *ASME Journal of Vibration and Acoustics*, 142:051107, 2020.

[644] D. A. Najera-Flores and R. J. Kuether. A study of whole joint model calibration using quasi-static modal analysis. *ASME Journal of Vibration and Acoustics*, 142:051109, 2020.

[645] Y. D. Wu, M. J. Leamy, and M. Varenberg. Schallamach waves in rolling: Belt drives. *Tribology International*, 119:354–358, 2018.

[646] Y. D. Wu, M. Varenberg, and M. J. Leamy. Schallamach wave-induced instabilities in a belt-drive system. *ASME Journal of Applied Mechanics*, 86:031002, 2019.

[647] Y. D. Wu, M. J. Leamy, and M. Varenberg. Belt-drive mechanics: Friction in the absence of sliding. *ASME Journal of Applied Mechanics*, 86:101001, 2019.

[648] Y. D. Wu, M. Varenberg, and M. J. Leamy. Detachment waves and self-oscillation in a belt-drive system incorporating tensile cords. *ASME Journal of Vibration and Acoustics*, 142:051101, 20120.

[649] Y. D. Wu, M. J. Leamy, and M. Varenberg. Minimizing self-oscillation in belt drives: Surface texturing. *Tribology International*, 145:106157, 2020.

[650] J. Armand, L. Pesaresi, L. Salles, and C. W. Schwingshackl. A multiscale approach for nonlinear dynamic response predictions with fretting wear. *ASME Journal of Engineering for Gas Turbines and Power*, 139:022505, 2017.

[651] A. Fantetti, C. Gastaldi, and T. M. Berruti. Modeling and testing friction flexible dampers: Challenges and peculiarities. *Experimental Techniques*, 42:407–419, 2018.

[652] C. Gastaldi, T. M. Berruti, and M. M. Gola. The relevance of damper pre-optimization and its effectiveness on the forced response of blades. *ASME Journal of Engineering for Gas Turbines and Power*, 140:062505, 2018.

[653] C. Gastaldi, T. M. Berruti, and M. M. Gola. Best practices for underplatform damper designers. *Proceedings of the Institution of Mechanical Engineers Part C: Journal of Mechanical Engineering Science*, 232:1221–1235, 2018.

[654] C. Gastaldi, S. Zucca, and B. I. Epureanu. Jacobian projection reduced-order models for dynamic systems with contact nonlinearities. *Mechanical Systems and Signal Processing*, 100:550–569, 2018.

[655] L. Pesaresi, J. Armand, C. W. Schwingshackl, L. Salles, and C. Wong. An advanced underplatform damper modelling approach based on a microslip contact model. *Journal of Sound and Vibration*, 436:327–340, 2018.

[656] J. Armand, L. Pesaresi, L. Salles, C. Wong, and C. W. Schwingshackl. A modelling approach for the nonlinear dynamics of assembled structures undergoing fretting wear. *Proceedings of the Royal Society A*, 475:20180731, 2019.

[657] M. Umer, C. Gastaldi, and D. Botto. Friction damping and forced-response of vibrating structures: An insight into model validation. *International Journal of Solids and Structures*, 202:521–531, 2020.

[658] Y. Sun, J. Yuan, L. Pesaresi, E. Denimal, and L. Salles. Parametric study and uncertainty quantification of the nonlinear modal properties of frictional dampers. *ASME Journal of Vibration and Acoustics*, 142:051102, 2020.

[659] C. Gastaldi, T. M. Berruti, and M. M. Gola. The effect of surface finish on the proper functioning of underplatform dampers. *ASME Journal of Vibration and Acoustics*, 142:051103, 2020.

[660] C. Gastaldi and T. M. Berruti. Direct measurement of the damping and stiffening capabilities of cylindrical underplatform dampers. *Mechanical Systems and Signal Processing*, 139:106632, 2020.

[661] C. Gastaldi, T. M. Berruti, and M. M. Gola. A novel test rig for friction parameters measurement on underplatform dampers. *International Journal of Solids and Structures*, 185-186:170–181, 2020.

[662] C. Gastaldi, J. Gross, M. Scheel, T. M. Berruti, and M. Krack. Modeling complex contact conditions and their effect on blade dynamics. *ASME Journal of Engineering for Gas Turbines and Power*, 143:011007, 2021.

[663] E. Denimal, C. Wong, L. Salles, and L. Pesaresi. On the efficiency of a conical underplatform damper for turbines. *ASME Journal of Engineering for Gas Turbines and Power*, 143:021020, 2021.

[664] J. Yuan, A. Fantetti, E. Denimal, S. Bhatnagar, L. Pesaresi, et al. Propagation of friction parameter uncertainties in the nonlinear dynamic response of turbine blades with underplatform dampers. *Mechanical Systems and Signal Processing*, 156: 107673, 2021.

[665] O. Akar and K. Willner. Investigation of the Helmholtz motion of a violin string: A finite element approach. *ASME Journal of Vibration and Acoustics*, 142:051112, 2020.

[666] L. Koller, W. Witteveen, F. Pichler, and P. Fischer. Semihyper-reduction for finite element structures with nonlinear surface loads on the basis of stress modes. *ASME Journal of Computational and Nonlinear Dynamics*, 15:081004, 2020.

[667] L. Koller, W. Witteveen, F. Pichler, and P. Fischer. A general hyper-reduction strategy for finite element structures with nonlinear surface loads based on the calculus of variations and stress modes. *Computer Methods in Applied Mechanics and Engineering*, 379:113744, 2021.

[668] M. K. Mahdiabadi, A. Bartl, D. Xu, P. Tiso, and D. J. Rixen. An augmented free-interface-based modal substructuring for nonlinear structural dynamics including interface reduction. *Journal of Sound and Vibration*, 462:114915, 2019.

[669] M. K. Mahdiabadi, P. Tiso, A. Brandt, and D. J. Rixen. A non-intrusive model-order reduction of geometrically nonlinear structural dynamics using modal derivatives. *Mechanical Systems and Signal Processing*, 147:107126, 2021.

[670] B. Peherstorfer, D. Butnaru, K. Wilcox, and H.-J. Bungartz. Localized discrete empirical interpolation method. *SIAM Journal on Scientific Computing*, 36:A168–A192, 2014.

[671] T. Daniel, F. Casenave, N. Akkari, and D. Ryckelynck. Model order reduction assisted by deep neural networks (ROM-net). *Advanced Modeling and Simulation in Engineering Sciences*, 7:16, 2020.

[672] H. Launay, J. Besson, D. Ryckelynck, and F. Willot. Hyper-reduced arc-length algorithm for stability analysis in elastoplasticity. *International Journal of Solids and Structures*, 208-209:167–180, 2021.

[673] W. Witteveen and F. Pichler. Separate time integration based on the Hilber, Hughes, Taylor scheme for flexible bodies with a large number of modes. *ASME Journal of Computational and Nonlinear Dynamics*, 15:061001, 2020.

[674] T. J. R. Hughes. *The Finite Element Method; Linear Static and Dynamic Finite Element Analysis*. Dover Publications, Inc., 2000.

[675] J. Oliver, A. E. Huespe, and J. C. Cante. An implicit/explicit integration scheme to increase computability of non-linear material and contact/friction problems. *Computer Methods in Applied Mechanics and Engineering*, 197:1865–1889, 2008.

[676] C. Studer, R. I. Leine, and C. Glocker. Step size adjustment and extrapolation for time-stepping schemes in non-smooth dynamics. *International Journal for Numerical Methods in Engineering*, 76:1747–1781, 2008.

[677] P. Flores and J. Ambrósio. On the contact detection for contact-impact analysis in multibody systems. *Multibody System Dynamics*, 24:103–122, 2010.

[678] P. Flores, R. Leine, and C. Glocker. Application of the nonsmooth dynamics approach to model and analysis of the contact-impact events in cam-follower systems. *Nonlinear Dynamics*, 69:2117–2133, 2012.

[679] S. Natsiavas, P. Passas, and E. Paraskevopoulos. A time-stepping method for multibody systems with frictional impacts based on a return map and boundary layer theory. *International Journal of Non-Linear Mechanics*, 131:103683, 2021.

[680] C. Hesch and P. Betsch. Transient 3d contact problems – NTS method: Mixed methods and conserving integration. *Computational Mechanics*, 48:437–449, 2011.

[681] V. Acary. Energy conservation and dissipation properties of time-integration methods for nonsmooth elastodynamics with contact. *ZAMM-Journal of Applied Mathematics and Mechanics/Zeitschrift für Angewandte Mathematik und Mechanik: Applied Mathematics and Mechanics*, 96:585–603, 2016.

[682] L. Charroyer, O. Chiello, and J.-J. Sinou. Self-excited vibrations of a non-smooth contact dynamical system with planar friction based on the shooting method. *International Journal of Mechanical Sciences*, 144:90–101, 2018.

[683] M. Lavella and D. Botto. Fretting wear characterization by point contact of nickel superalloy interfaces. *Wear*, 271:1543–1551, 2011.

[684] C. W. Schwingshackl, E. P. Petrov, and D. J. Ewins. Measured and estimated friction interface parameters in a nonlinear dynamic analysis. *Mechanical Systems and Signal Processing*, 28:574–584, 2012.

[685] M. Lavella, D. Botto, and M. M. Gola. Design of a high-precision, flat-on-flat fretting test apparatus with high temperature capability. *Wear*, 302:1073–1081, 2013.

[686] D. Botto and M. Lavella. High temperature tribological study of cobalt-based coatings reinforced with different percentages of alumina. *Wear*, 318:89–97, 2014.

[687] M. Lavella and D. Botto. Fretting wear of alloy steels at the blade tip of steam turbines. *Wear*, 426-427:735–740, 2019.

[688] Z. B. Riley, R. A. Perez, G. W. Bartram, S. M. Spottswood, B. P. Smarslok, et al. Aerothermoelastic experimental design for the AEDC/VKF tunnel c: Challenges associated with measuring the response of flexible panels in high-temperature, high-speed wind tunnels. *Journal of Sound and Vibration*, 441:96–105, 2019.

[689] M. Freydin, E. H. Dowell, S. M. Spottswood, and R. A. Perez. Nonlinear dynamics and flutter of plate and cavity in response to supersonic wind tunnel start. *Nonlinear Dynamics*, 103:3019–3036, 2021.

[690] N. N. Balaji, S. A. Smith, and M. R. W. Brake. Evolution of the dynamics of jointed structures over pro-longed testing. In *40th International Modal Analysis Conference (IMAC XL)*, Orlando, FL, February 2022.

[691] E. Melan. *Theorie Statisch Unbestimmter Systeme Aus Ideal-Plastischem Baustoff*. Hölder-Pichler-Tempsky in Komm., 1936.

[692] A. R. S. Ponter and M. Engelhardt. Shakedown limits for a general yield condition: Implementation and application for a Von Mises yield condition. *European Journal of Mechanics / A Solids*, 19:423–445, 2000.

[693] J. W. Ringsberg, M. Loo-Morrey, B. L. Josefson, A. Kapoor, and J. H. Beynon. Prediction of fatigue crack initiation for rolling contact fatigue. *International Journal of Fatigue*, 22:205–215, 2000.

[694] G. Kang, Q. Kan, J. Zhang, and Y. Sun. Time-dependent ratchetting experiments experiments of SS304 stainless steel. *International Journal of Plasticity*, 22:858–894, 2006.

[695] A. Klarbring, M. Ciavarella, and J. R. Barber. Shakedown in elastic contact problems with Coulomb friction. *International Journal of Solids and Structures*, 44:8355–8365, 2007.

[696] J. R. Barber. Frictional systems subjected to oscillating loads. *Annals of Solid and Structural Mechanics*, 2:45–55, 2011.

[697] R. L. Munisamy, D. A. Hills, and D. Nowell. Static axisymmetric Hertzian contacts subject to shearing forces. *ASME Journal of Applied Mechanics*, 61:278–283, 1994.

[698] S. Fouvry, P. Kapsa, and L. Vincent. An elastic-plastic shakedown analysis of fretting wear. *Wear*, 247:41–54, 2001.

[699] D. Dini, A. Sackfield, and D. A. Hills. Comprehensive bounded asymptotic solutions for incomplete contacts in partial slip. *Journal of Mechanics and Physics of Solids*, 53:437–454, 2005.

[700] R. C. Flicek, D. A. Hills, J. R. Barber, and D. Dini. Determination of the shakedown limit for large, discrete frictional systems. *European Journal of Mechanics A - Solids*, 49:242–250, 2015.

[701] R. C. Flicek, M. R. W. Brake, and D. A. Hills. Predicting a contact's sensitivity to initial conditions using metrics of frictional coupling. *Tribology International*, 108:95–110, 2017.

[702] R. W. Neu. Progress in standardization of fretting fatigue terminology and testing. *Tribology International*, 44:1371–1377, 2011.

[703] K. Holmberg, A. Matthews, and H. Ronkainen. Coatings tribology - contact mechanisms and surface design. *Tribology International*, 31:107–120, 1998.

[704] F. W. Gayle and M. Goodway. Precipitation hardening in the first aerospace aluminum alloy: The Wright *Flyer* crankcase. *Science*, 266:1015–1017, 1994.